A Study of Nanofilled Silicone Dielectrics for Outdoor Insulation

by

Isaías Ramírez Vázquez

A thesis
presented to the University of Waterloo
in fulfillment of the
thesis requirement for the degree of
Doctor of Philosophy
in
Electrical and Computer Engineering

Waterloo, Ontario, Canada, 2009

AUTHOR'S DECLARATION

I hereby declare that I am the sole author of this thesis. This is a true copy of the thesis, including any required final revisions, as accepted by my examiners.

I understand that my thesis may be made electronically available to the public.

Abstract

Polymeric insulators are now a common replacement for conventional porcelain and glass string insulators on overhead distribution and transmission lines. The use of this mature technology represents many advantages to the utilities; however, in polluted environments and those with high moisture levels in the environment, electrical discharges will develop on the surface of the insulation. In the long term, electrical discharges cause degradation of the polymer insulation in the form of electrical tracking and material erosion, and both are detrimental to the life of the insulation. Inorganic fillers are added to polymer materials to make the insulation more resistant to discharges, and at the same time, to lower the cost of the insulation. However, there is a limit to the amount of filler that can be added as the processability of the polymer compound becomes extremely difficult and expensive. Microfillers are extensively used to modify the physical properties of the polymeric matrix, and the properties of these composites are well known. On the other hand, nanofillers are being used in some insulating composites for reinforcement of mechanical properties; their electrical characteristics have shown inconsistency in the literature, and this is attributable to the non-uniformity of the filler dispersion. Most researchers agree that particle dispersion is critical in the development of nanocomposites for electrical insulation applications. If the nanoparticles are well dispersed, the electrical properties of these materials will be significantly improved.

The main problem in using nanofillers is that the nanoparticles agglomerate easily because of their high surface energy, such that conventional mixing techniques are unable to break apart the nanoparticle aggregates. A secondary problem is the incompatibility of the hydrophobic polymer with the hydrophilic nanoparticles which results in poor interfacial interactions.

In this thesis, the reinforcement of a silicone rubber matrix is successfully accomplished with the combination of microfiller, nanofiller, and a commercial surfactant.

To improve particle dispersion, several techniques are available apart from mixing. This includes surface modification of the nanoparticles by chemical and physical methods by using surfactants. While surfactants are commonly applied to liquids, their use to disperse

nanoparticles in compositions forming solid dielectric materials has not yet been reported. The findings in this thesis have shown that Triton™ X-100, a common surfactant, significantly aids in the dispersion of nanosilica and nanoalumina in silicone rubber. The main advantage of the surfactant is that it lowers the surface energy and the interfacial tension of the nanoparticles. This reduces agglomeration and facilitates the separation of the particles during mixing, thereby allowing improved dispersion of the nanofillers, as observed through Scanning Electron Microscopy (SEM). However, also shown in the thesis is that Triton™ X-100 cannot interact efficiently with all types of nanofillers.

A high concentration of surfactant can also compromise the adsorption of the matrix polymer chains on the filler particles, so it is necessary to establish a balance between matrix adsorption and the dispersion of the particles. Mechanical properties such as the tensile strength, elongation at break, and hardness may also suffer from the use of excess surfactant. In addition, excess surfactant can lead to surface wetting properties different from composites containing none. Better wetting due to the migration of excess surfactant to the surface of the silicone may favour arcing in a wet environment.

The current investigation shows that for a specific filler and concentration, an optimal concentration of surfactant provides good erosion resistance without adversely affecting the mechanical characteristics of the nanocomposite. Stress–strain and hardness measurements are done to investigate the surfactant's effect on the mechanical properties of the composites. The effect of the surfactant on the surface of the composites is analyzed with static contact angle measurements.

The heat resistance of nanofilled silicone rubber is explored using an infrared laser simulating the heat developed by dry-band arcing. Also, several industry standard test methods such as salt fog and inclined plane tests are used to evaluate the erosion resistance of the filled composites. The results of all three tests confirm that the combination of microfiller and nanofiller with surfactant results in composites with improved erosion resistance to dry band arcing, with the exception of the case where calcinated filler is used in the formulation.

In this thesis, the thermal conductivity is measured using a standard ASTM method and calculated using several theoretical, semi-theoretical, and empirical models. A thermal model developed in COMSOL Multiphysics™ and solved using a finite element method (FEM)

shows a temperature distribution in the modelled nanocomposites which is comparable to the temperature distribution measured with an infrared camera under laser heating.

In addition, this investigation aims to define the mechanism by which the nanofillers improve the heat and erosion resistance of the silicone composites. In order to understand this mechanism, nano fumed silica, nano natural silica, and nano alumina are used in a silicone rubber (SiR) matrix in order to study the thermally decomposed silicone and the residual char that is formed during laser ablation tests.

The white residue remaining after laser ablation on the surface of composites with fumed silica, natural silica, and alumina is analyzed in a number of ways. Scanning Electron Microscopy, Energy Dispersive X-ray analysis (EDAX), and X-ray diffraction (XRD) techniques are used to analyze the thermally decomposed silicone residue after laser heating indicating that the protective mechanism of the three analyzed nanofillers – fumed silica, natural silica, and alumina – appears to be the same. The formation of a continuous layer on the surface behaves as a thermal insulator protecting the material underneath from further decomposition.

Acknowledgements

I appreciate deeply the continuous support of my supervisors Dr Shesha Jayaram and Dr Edward Cherney; their guidance, suggestions, and advice throughout my research are highly valued.

I also like to thank to Dr Mario Gauthier for his great support in the development of this work. Our discussions were essential in understanding this interesting topic.

I would like to express my sincere gratitude to Dr. Juan Francisco Pérez Robles from CINVESTAV-Querétaro for his useful advice. His recommendations definitely changed the course of this research. Also, I give my appreciation to all members of my PhD Committee and also to Dr Carlos Romualdo Torres for their constructive comments and suggestions.

My gratefulness is due to Dr. Fermín Espino Cortés for giving my family their first home in this amazing country, Canada. Our transition period ran smoothly with Laura and Laurita's help. Not only as a friend, but also as a professional he must be acknowledged for the useful discussions we had and by his help in the thermal modelling.

Thanks to my friends in the High Voltage Group for the moments we spent together. Also, I would like to thank all my friends in different Departments of the University of Waterloo for the coffee-discussion times; these moments were unforgettable.

My gratefully appreciation to our families and friends in México; their support and communications made our sojourn in Canada easygoing. I also acknowledge those who are not here physically in this world, but their memories still are in my heart.

The patience and continuous support of Ma. Elena, Jezabel, and Karen were fundamental in this adventure; this experience will be unforgettable in our lives.

The financial support provided by NSERC of Canada is appreciated. Thanks are due to IEEE-DEIS Society for the received Fellowship.

I acknowledge the Instituto de Investigaciones Eléctricas (IIE) for a study leave, FICYDET for the mortgage bank loan, and the Consejo Nacional de Ciencia y Tecnología (CONACYT) for the financial support of my graduate studies.

Dedication

To my lovely wife Ma. Elena,

and my adorable daughters Jezabel Alejandra and Karen Citlali .

Table of Contents

List of Tables

List of Figures

Chapter 1

Introduction

Numerous investigations have explored the addition of micron-sized fillers to solid dielectric materials in order to form composites for use as electrical insulation in high voltage applications. These fillers serve to improve the thermal properties of the composite material, thereby facilitating the removal of damaging heat from high voltage phenomena such as dry band arcing. Further improvements to materials using micron-sized fillers are not likely at this time because mixing of the viscous compositions has reached the limitations of current processing technology.

The first commercial application of nanomaterials, developed by Toyota, was the synthesis of an intercalated compound of montmorillonite and 6-Polyamide to take advantage of improved mechanical properties. This was later followed by research to enhance the electrical properties of materials [1]. One of the advantages of nanometric fillers is their large specific surface area when compared with micron-sized fillers; consequently, interfacial effects dominate over volume effects present in microfilled materials [2].

Researchers' findings on nano-sized particle (nanoparticle) filled dielectrics show similar property improvements for considerably reduced filler additions compared to a higher amount of micron-sized fillers. Until now, nanofillers have not been considered for commercial outdoor insulation; however, the promise of further improvements to dielectric materials is an interesting field of study and is the objective of this thesis.

1.1 Composite Insulators for High Voltage

Since the mid 1970's, the use of polymeric insulators has increased so dramatically that today ceramic insulators are rarely used. Electrical companies started using polymeric insulators at distribution voltages, and then gradually, at low voltage transmission, now at 765 kV ac and 500 kV dc, and soon at 1000 kV [3]. The insulators are classified according to the way that they are used, for example, post and suspension types. The suspension type is most common, supporting an energized conductor from an overhead structure, such as a tower. Post insulators are commonly used in distribution lines and substations.

The composite suspension insulator, as illustrated in Figure 1.1, consists of three components; namely, a fibreglass core, an end attachment hardware (end fittings) connected to the core, and a protective housing with weathersheds for the core. The core provides the mechanical function of the insulator; the hardware allows the insulator to be attached to an overhead tower and to an energized conductor. The core by itself is inappropriate for use outdoors, since moisture and voltage cause electrical tracking on the core and result in mechanical failure. Therefore, a housing is moulded onto the core, protecting the core from electrical tracking, and the design of the housing provides the electrical strength under wet and polluted conditions.

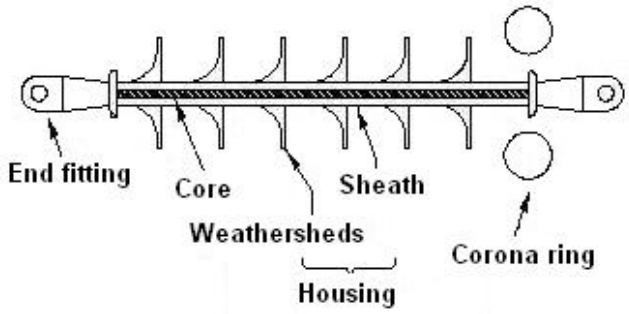

Figure 1.1 Components of a composite suspension insulator.

For outdoor insulation, two materials are commonly used for the housing: ethylene propylene diene monomer (EPDM) rubber and silicone rubber (SiR). Although both materials are used, SiR is preferred due to its characteristic hydrophobicity and its good performance in polluted environments.

This study is concerned only with the SiR housing material and its ability to perform in polluted environments.

1.1.1 Outdoor Insulator Service Environment

The outdoor service environment consists of moisture in the form of rain, fog, dew, and direct spray, pollutants from the sea and roads that are salted during winter months in cold climates, and chemicals from industry, as well as other forms of pollution. In addition, the housing material is subjected to ultraviolet radiation, temperature extremes, overvoltages due to switching and lightning surges, and mechanical loads due to wind and ice.

Typically, SiR insulators are considered for polluted environments because such insulators perform better than ceramic insulators in highly polluted conditions with or without preventive maintenance. Also, room temperature vulcanizing (RTV) silicone coatings are applied on apparatus bushings, surge arresters, and porcelain station posts as an alternative to replacement. The main advantage of SiR insulation is its low life cycle cost. Not only are the purchase and installation costs lower, but the maintenance costs over the life of the insulators are also lower. Electrical companies have preferred the installation of SiR polymeric insulators in sea coast areas and industrial areas, even though tracking and erosion degradation have been observed in some extremely polluted environments. These insulators have also been used in desert areas and in regions with a high incidence of vandalism

(shooting). The reduced number of metallic parts in this kind of insulator makes it suitable for saline areas, where the corrosion of the hardware is a significant issue; insulation is often damaged by the corrosion of the metallic parts.

1.1.2 Classification of Silicone Rubber Used in Outdoor Insulation

Silicone is the general term to describe the family of organo-silicon compounds based on a molecular chain of alternating silicon and oxygen atoms. The viscosity of the compound depends upon the length of the chain and the organic groups attached to the silicon atoms [4].

The silicon-oxygen linkage in the silicone polymer chain is the same as that in sand, quartz, and glass. This bond is responsible for the good high temperature stability of the silicones and their resistance to weathering, corona discharge, and oxidation by ozone. An illustration of the polymer chain is depicted in Figure 1.2.

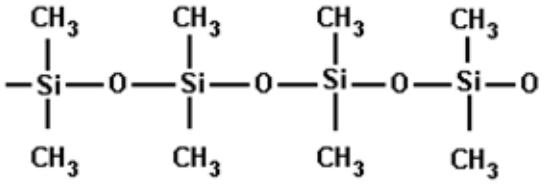

Figure 1.2 Silicon-oxygen linkage in the silicone polymer chain [4].

Although the dimethylsiloxane unit is the basis of silicone polymers, it is common for some of the methyl groups to be substituted with other groups in very small ratios (e.g. 0.1%) to achieve improved crosslinking and other desirable properties.

Thus the addition of phenyl groups ($-C_6H_5$) improves the low temperature properties of silicones (down to 173 K or even lower). The addition of vinyl groups ($-CH=CH_2$) improves the vulcanization characteristics and the compression resistance of the vulcanizate. If a

combination of properties is desired, both phenyl and vinyl groups can be substituted for the methyl groups along the siloxane chain.

As summarized in Table 1.1, the ASTM D1418-05 standard denotes the main classes of silicone rubbers [5]. The Q class represents the silicon and oxygen in the polymer chain, and M preceding Q indicates that methyl is one of the substituent groups on the polymer chain. MQ is preceded by V when vinyl side groups are present. Type VMQ is commonly used for insulators.

One of the most interesting aspects of SiR has been the liquid compound known as RTV (Room Temperature Vulcanizing) silicone rubber. RTV silicone rubber exhibits almost the same outstanding properties as regular heat curing silicone rubbers, namely, thermal stability, ozone resistance, and electrical characteristics. However, the mechanical properties of RTV differ from the heat curing silicone rubbers.

Table 1.1 Silicone rubber classification according to ASTM D1418-05.

Class type	Description	Use
MQ	Silicone rubbers with only methyl groups on the polymer chain such as dimethyl polysiloxane.	RTV silicone rubber coatings.
VMQ	Silicone rubbers having both methyl and vinyl substituent groups on the polymer chain.	Heat cured rubber. Liquid silicone rubber.

The most common base polymer for the housing in outdoor insulation is VMQ, composed of organic methyl groups ($-CH_3$), vinyl groups ($-CH=CH_2$), and a linear silicon-oxygen backbone. Various fillers such as fumed silica and alumina trihydrate, pigments, crosslinker,

antioxidant, adhesion promoter, and process aids (for example silicone fluid) are added to the base material and mixed, forming a compound for injection moulding of insulator housings [6]. Short chain cyclic compounds, often referred to as low molecular weight fluid, are present in the base material that are not locked in by vulcanization and are free to diffuse to the surface of the cured rubber and are responsible for the hydrophobicity in silicones.

1.1.3 Hydrophobicity in Silicone Composites

The most important property of SiR is its hydrophobicity, caused by the low molecular weight (LMW) fluid [7]. Due to this property, the insulating surface prevents water filming, i.e., on a hydrophobic surface, the water forms discrete droplets. Electrical activity is the primary reason for the loss of hydrophobicity and after some time aging. Aging is due to multiple phenomena such as UV, temperature, pollutants, and moisture. However, hydrophobicity is also lost naturally due to the rain or artificially by washing the insulating surface. Fortunately, the hydrophobicity is recovered after a few hours at normal temperatures through the diffusion of the LMW fluid from the bulk to the surface, as well as through a minor effect due to reorientation of the hydrophobic methyl groups at the surface [7].

1.1.4 Role of Fillers in SiR Insulation

Inorganic fillers are essential in the formulation of SiR outdoor insulation. Their inclusion improves tracking and erosion degradation resistance, as well as the insulation's mechanical properties. Fillers have both desirable and undesirable effects on electrical aging and the recovery of the hydrophobicity in SiR.

Some of the desirable effects of fillers follow.

a) Improved thermal conductivity of the compound, thereby improving heat dissipation and hence preventing the development of excessive hot spots.

b) Reduced organic material exposure to heat from dry band arcing, thus decreasing the weight loss of the compound subsequent to aging.

One undesirable effect of the fillers is that they act as a "diffusion barrier" for the LMW fluid and slow down the recovery process. Moreover, the presence of fillers reduces the amount of silicone material available, thereby reducing the amount of LMW fluid for hydrophobicity [7]. However, some researchers have argued that with increased filler content, the recovery is faster [8]. Thus, for a given formulation, the quantity and type of filler included in the formulation is critical.

Micro silica is classified as semi-reinforcing filler, which improves the physical properties of silicone compositions through molecular bonding with the silicone polymer. Consequently, micro silica has been studied extensively as filler in outdoor insulation applications [9].

1.2 Introduction to Nanofillers

Traditionally, SiR as the base material with the addition of microfillers is used in the manufacturing of outdoor insulation, and extensive research has been done in relation to the use of microfillers in SiR. The fillers for these materials are micron-sized (hereafter referred to as micro), with a particle size of 1-50 μm. Currently, the industry is using 30% to 65%, by weight (hereafter referred to as wt%), of fillers to achieve the required resistance to dry band arcing. Recently, a great deal of attention has been paid to the application of nanofillers, with particle sizes between 1 and 100 nm, in the field of electrical insulating materials [10]. The

key advantage of nanocomposites is their larger specific area as compared with micro materials. As reported in the literature, the use of nanoparticles in the matrix of polymeric materials can improve the mechanical and electrical properties of polymeric composites. A range of studies have been reported that compare the performances of nano to micro sized particle-filled composites; these studies are discussed in the next section.

1.3 Literature Review

1.3.1 Use of Nanofillers and Microfillers in Insulation Applications

Rätzke *et al.* [11] first demonstrated how nanofillers and microfillers in an HTV (high temperature vulcanizing) silicone elastomer affect the resistance to arcing. In their work the best dispersion was obtained for nanosilica; on the other hand, large agglomerates were found to be formed by nanoalumina. The results of the arcing tests demonstrated longer test time duration with increased filler concentrations of silica and alumina. The authors found that the thermal conductivity rose in an approximately linear fashion with the filler concentration and that the higher thermal conductivity improved the resistance to erosion. However, it is not known whether the percolation limit for these formulations was reached. Enhanced resistance to arcing with nanosilica is achieved only at a high concentration of filler, approximately 40% wt; however, most of the technical literature suggests that improvements in the material properties are evident at low filler concentrations (1% to 10% wt). The strong interfacial bonding and small inter-filler spacing of the nanodielectrics restricts material degradation. Also, it has been suggested that stronger interfacial bonding should mitigate the pyrolysis of the polymer chains.

In the research of Lei *et al*. [12] two kinds of nanomaterials were adopted to modify the properties of RTV SiR under conditions of corona discharge; namely, nanosilica and nanolayered silicate (at 2 and 5% wt concentrations). After aging with corona, nanofilled RTV performed much better than the virgin RTV material. It was concluded that nanofilled RTV has a superior corona aging performance as compared to the virgin RTV material. However, it was obvious that any virgin material exhibited a worse performance than a matrix with any amount of nanofiller.

According to Dengke *et al*. [13, 14], the addition of a small amount (2 to 5 %wt) of inorganic nanofillers to polymers should be sufficient for mechanical and thermal stability and performance improvement. They selected nanosilica because it is a commercial nanoscale material. Although the hydrophobicity of all the composites decreased after corona aging, hydrophobicity was recovered after a few hours. However, the authors did not explain why they did not employ higher concentrations of nanofiller.

Formulations of RTV SiR with nanosilica versus RTV SiR with micro silica have been tested by El-Hag *et al*. [15], who found that the erosion resistance increased in direct proportion to the amount of filler used. Contrary to the research done by Rätzke's group, the authors did not find any significant improvement in terms of thermal conductivity between nanofilled and unfilled SiR at the filler concentrations used. Possibly, the percolation limit was not reached because of the low nanofiller concentration (10% wt), and consequently the thermal conductivity did not improve. It was apparent that clusters resulting from the agglomeration of nanoparticles (12 nm) were present in the submicron range. As a result, the inclined plane test confirmed that the nanofilled SiR composites with as low as 10% wt of

nanofillers displayed a significant improvement in resistance to erosion as compared with microfilled SiR composites [15].

In other research, Meyer *et al*. [16] showed that RTV SiR filled with nanosilica, when compared with RTV SiR filled with micro silica, demonstrated a higher tracking and erosion resistance, lower roughness, and slightly lower hydrophobicity. The concentrations used in this work were 5% and 10% wt for nano and micro silica, respectively, and nanosilica had higher tracking and erosion resistance than micro silica.

Polyamide films tested by Irwin *et al*. [17] displayed significant improvements to elongation, scratch hardness, and strength. Fuse *et al*. [18] studied polyamide with layered silicate nanofillers from 1 to 5% wt. They found that the conduction current decreased with the addition of nanofillers, and the dielectric strength was almost independent of the nanofiller content for impulse, dc, and ac voltages. These researchers did not see an improvement with the use of nanofillers as they performed these tests.

The work of Imai *et al*. [19] in epoxy resin included the mixing of nano, micro, and the combination of nano and microcomposites (NMMC). It was evident that microfilled epoxy and NMMC maintained a far smaller erosion depth than the base epoxy resin. For the lifetime tests, the base epoxy resin required less time to break down than the nanofilled formulation, followed by microfilled epoxy, and finally, significantly longer time for the NMMC formulation. The insulation breakdown strength exhibited the same behaviour as time to breakdown. Imai *et al*. assumed that an increase in particle concentration in nano and micro filler mixtures prevented treeing from propagating efficiently. From these results it was evident that the NMMC mixture displayed improved electrical insulation properties; hence, the formulation with the combination of micro and nanofillers it is a good option. Full scale

trials were molded by Imai *et al.* [20], but the main problem found in the use of nanofillers was the dispersion.

According to Roy *et al*. [21], the voltage endurance behaviour of cross-linked polyethylene (XLPE) was significantly improved with the inclusion of treated nanoparticles (aminosilane-treated nanosilica, vinylsilane-treated nanosilica). This difference was attributed to the chemical treatment of the nanosilica. All the nanoscale fillers were characterized by a significantly improved breakdown strength and endurance over the base resin. In this work, nanofillers showed an improvement, yet for Fuse *et al*. [18] the nanofillers did not improve the dielectric strength, contrary to other researchers.

Another controversial point is the result obtained by Santanu *et al*. [22], who noted a difference in dielectric strength depending on the processing or mixing techniques used. The highest breakdown strength, with the inclusion of nanofillers, was observed when the dispersion was carried out with mechanical mixing, followed by ultrasonic agitation. However, a higher dielectric strength was obtained for formulations with microfillers, rather than the formulations with nanofillers [22].

1.4 Particle Dispersion

The main problem facing the use of nanoparticles as fillers in organic materials (nanocomposites) is their dispersion. Most researchers agree that uniform mixing and particle dispersion are critical in the development of nanocomposites [11-16]. The electrical properties of these materials can be improved if the nanoparticles are well dispersed [21]. One of the problems is that the nanoparticles agglomerate easily because of their high surface energy, such that conventional mixing techniques are unable to break apart the nanoparticle

aggregates. The dispersion rate seems to be linear on a short mixing time scale and exponential over a long mixing time interval, depending on the type of mixer used. Another problem is the incompatibility of the hydrophobic polymer with hydrophilic nanoparticles, resulting in poor interfacial interactions.

To improve particle dispersion, several techniques are available apart from mixing [23,24]. They include surface modification of the nanoparticles by various physical and chemical methods. Another technique to improve particle dispersion is calcination. These techniques are discussed in the following sections.

1.4.1 Mixing

Various types of mixers incorporating a high shear mixing blade have been used to disperse nanofillers in materials. In general, these mixers have not provided optimum results in dispersing nano-sized particles into host materials [22].

To determine the feasibility of the mixing process for highly cohesive nanoparticles, it is necessary to estimate the forces generated during mixing and to demonstrate that these forces are larger than the cohesive or adhesive forces acting on the powder particles. Interparticle forces can be of the van der Waals type (inversely proportional to the distance between the particles), electrostatic and magnetic attraction, and chemical bonding.

The mixing of particles with a size ranging between a few nanometres and 100 nanometres is extremely difficult since the interparticle forces are much stronger than for particles with a size greater than 1 μm. In the research by Dongguang *et al*. [23], the results have proven that solvent-based methods (with ethanol and hexane) are most effective. Followed by that, with a lower efficiency, was a mixing process consisting in stirring the nanoparticles in a heated and

pressurized vessel with CO_2. It was also shown that at least one of the dry powder processing methods performed nearly as well as the solvent-based method in terms of producing a homogeneous mixture of nanoparticles.

1.4.2 Surface Modification of Nanofillers

Improved dispersion can be achieved through physical or chemical interactions between the filler and the modifier. When nanoparticles are modified by one of these methods, either the character of the surface is changed from hydrophilic to hydrophobic (and vice-versa), or specific groups are chemically bonded on their surface (change in functionality). Fillers are typically hydrophilic and do not disperse easily within most polymeric materials, which are usually hydrophobic. Such modification not only contributes to reinforcement, but also increases the interactions of the particles to impact rheological properties, prevents sedimentation, aids dispersion, or prevents agglomeration. In addition, improved dispersion of the nanoparticles can also be achieved with solvents.

1.4.2.1 Physical Methods

Surface modification by physical methods is achieved using a low molecular weight surfactant resulting in secondary (van der Waals, electrostatic, and/or hydrogen bonding) forces between the nanoparticles and the modifier. A surfactant (surface active agent) is a molecule that, when added to a liquid at low concentration, changes the properties of that liquid at a surface or interface [25]. The principle of surfactant treatment is the preferential adsorption, or tendency for a surfactant molecule to collect at the interface, due to polar groups on the surfactant molecules interacting favourably with the high energy surface of the filler. A surfactant is characterized by its tendency to adsorb at surfaces and interfaces. The

surfactant concentration at the boundary depends on the surfactant structure and also on the nature of the two phases defining the interface. There is no effective surfactant for all uses; the choice depends on the application [26].

Surfactant adsorption is determined by two main factors: the interactions of the surfactant with the surface and the hydrophobicity of the surfactant. In addition, hydrophilic nanofillers stored under ordinary conditions (reagents room, laboratory, etc.) have their surface partly blocked by adsorbed species, and this condition lowers their effectiveness. To activate the surface of the nanofiller, thermal treatment may be required.

All surfactants consist of at least two parts, one which is soluble in a specific fluid, known as the lyophilic part (or hydrophilic part, in aqueous systems), and one which is insoluble, known as the lyophobic (or hydrophobic) part. Thus when a surfactant adsorbs from an aqueous solution on a hydrophobic surface, its hydrophobic group usually orients to the surface while its polar group is exposed to water. Since the surface becomes more hydrophilic, the interfacial tension between the surface and water is reduced.

By 1993, around 2900 different types of surfactants were in use in the industry [27]. Rahul *et al*. [28] developed a microemulsion-based surface modification method for the introduction of different functional groups to the surface of silica nanoparticles to keep the particles well dispersed. Tetraethyl orthosilicate (TEOS), Triton^{TM} X-100, and various organosilane reagents were added for that purpose. By using this surface modification scheme, nanoparticle aggregation was minimized.

1.4.2.2 Chemical Methods

A variety of coupling agents including silanes, titanates, and zirconates have been used to improve the adhesion between inorganic fillers and organic matrices. For example, silanes can be used to reduce the hydrophilic properties of silica. However, uniform surface coverage by coupling agents is hard to attain with nanoparticles by simple physical and mechanical means.

Stearic acid has thus been used with nano $CaCO_3$, with the result of virtually no agglomerates of nanoparticles remaining with proper dosage of the dispersing agent [29]. Some results for the surface modification of SiO_2 nanoparticles with oleic acid obtained by Zongwei *et al.* [30] also confirmed that nanoparticle agglomeration decreased because of increased spacing (decreased attraction) between the nanoparticle cores due to the layer of surface modifier.

Another non-reactive modifier used by Seon *et al.* [31] to make the filler surface hydrophobic is stearic acid. The presence of adsorbed stearic acid on the surface of the silica nanoparticles reduced the interactions between the silica nanoparticles within agglomerates, which could be broken down more easily.

1.4.3 Thermal Treatment of Nanoparticles (Calcination)

Nanofillers stored under ordinary conditions found in reagent rooms or laboratories have their surface partially blocked by adsorbed species, mainly in the form of moisture. For silica, this condition translates into a lower effectiveness in dispersion. Calcination is one way to activate the silica surface, and an additional benefit of this process is the disintegration of the silica aggregates and pellets formed during storage [32].

CHAPTER 1. INTRODUCTION

Many of the properties of silica such as adsorption, adhesion, chemical, and catalytic properties depend on the chemistry and geometry of their surface. Silanol (-OH) groups on the silica surface are the main centers for the adsorption of water molecules [33, 34]. The concentration of silanol groups on the silica surface, expressed as the number of -OH groups per square nanometer, is often called the silanol number. The numerical value, obtained by Zhuravlev, is α_{OH}=4.6 -OH groups per square nanometer (3.65 for fumed silica) [33].

Dehydration of the silica surface, i.e. the removal of physisorbed (adsorbed) water occurs at temperatures below 473 K. The concentration of silanol groups on the surface also decreases monotonically with increasing temperature when silica is heated under vacuum according to Zhuravlev [33].

According to Wypych [35], most of the adsorbed water is removed at approximately 423 K. Internal silanol groups (structurally bound water inside the silica skeleton and very fine pores of diameter lower than 1 nm) begin to condense at about 873 to 1073 K, and in some cases at lower temperatures. At higher temperatures, from 1273 to 1373 K, only isolated silanol groups remain on the silica surface.

At a sufficient surface concentration, the -OH groups make the silica surface hydrophilic. On the other hand, the predominance of siloxane bridges on the silica surface makes the surface hydrophobic. Figure 1.3 relates the concentration of surface hydroxyl groups α_{OH} to the temperature of thermal treatment in vacuum up to 1373 K [33].

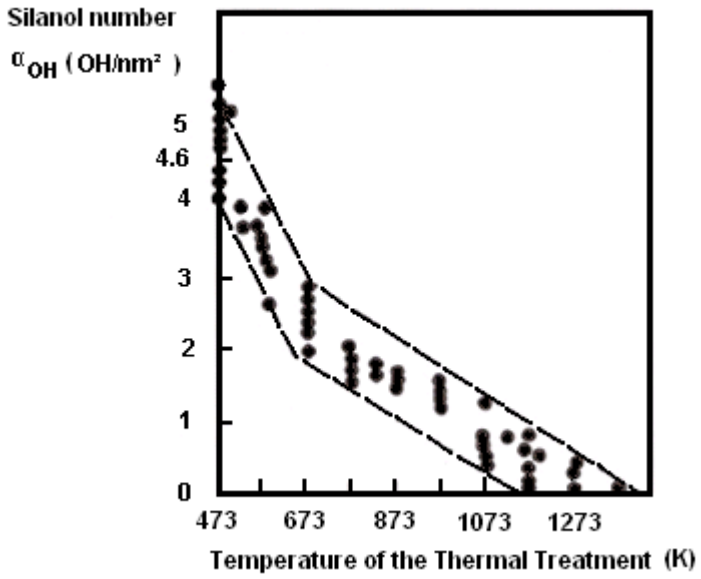

Figure 1.3 Silanol number as a function of the thermal treatment temperature of SiO_2 [33].

1.5 Aim of the Present Work, and Thesis Organization

Researchers have completed a range of studies, and they compared the performance of nano and micro particle filled composites, but some of the published results are controversial [11-22]. In the majority of cases, the nanofillers improved the properties of the dielectrics, but sometimes the microcomposites performed better than the nanocomposites. The variation was related primarily to a non-uniform distribution of filler in the composite. Thus, there is a great need to investigate alternative ways of obtaining a better dispersion of nanofillers. With the use of nanocomposites, the electrical properties of the materials can be improved as long as the nanoparticles are well dispersed.

Most of the electrical engineering research on SiR materials, and other insulating materials, does not mention surface treatment of the nanofillers prior to mixing. Only in technical

publications on chemical aspects are suggestions often made for obtaining a better dispersion of the nanoparticles, such as the use of surfactants or the elimination of aggregates of the nanofillers.

Consequently, the focus of this thesis is primarily on the surface treatment of nanofillers to improve their dispersion. The most common nanofillers found in the literature were selected to be analyzed; from these nanofillers, the ones that performed best were selected to reinforce composites. On the other hand, the mixtures of micro and nanofillers in the same matrix are a good option to improve the properties of the new nanodielectrics, and are considered in this research. For a number of reasons, nanofillers have never been included in commercial outdoor insulation.

The thermal stability of the nanocomposites is an important issue for outdoor insulation housing applications. Consequently, this investigation considers the evaluation of thermal aspects such as thermal conductivity, thermogravimetric analysis, thermal models for composites, and temperature profiles in nanocomposites under laser heating, which simulates the hot spot from dry band arcing.

Along with the aforementioned points, this thesis is focused on improving the dry band arcing erosion resistance of nanofilled silicone dielectrics, with the objective of increasing the service life of polymer insulators in polluted outdoor service environments.

In addition to the study of nanofilled silicone composites for outdoor high voltage insulation, the mechanisms in nanofilled dielectrics can provide a better understanding of degradation, so that the design of insulating materials can be improved.

CHAPTER 1. INTRODUCTION

The main objectives of this thesis in the field of nanofillers for outdoor insulation are listed below:

- A better understanding of the dry band arcing mechanism in nanofilled silicone composites.
- An evaluation of the eroded mass and thermal characteristics of nanofilled silicone materials.
- The development of a new surface treatment method to obtain high erosion resistance composites for outdoor insulation.

In view of the above perspective, this thesis is organized into the following chapters. In Chapter 2, the selection of the materials used in this work is presented, including the technique for preparing the nanofilled silicone dielectric composites. The surface treatment of the filler to improve the dispersion is also discussed. The methodology and how the investigation can help in understanding the degradation and failure mechanisms in nanofilled silicone dielectrics are also outlined. Finally, the experimental setups for evaluation and the modelling of the thermal properties of the composites are presented.

Chapter 3 provides the results of the different evaluations of the nanocomposites prepared to seek improvements in their electrical and mechanical properties, as well as their resistance to arcing erosion. The investigation focuses mainly on nano fumed silica and the surfactant Triton^{TM} X-100 (hereafter referred to as Triton) in a SiR matrix. The improvement in dispersion of the filler into the silicone rubber matrix is verified by scanning electron microscopy (SEM). After that, nano fumed silica and micro silica are selected to reinforce a SiR matrix with the surfactant Triton in the final composites. These composites are evaluated

using the inclined plane, laser ablation, and salt fog tests. A correlation analysis is done to examine the relationship between the eroded mass among the three test methods. A contact angle test and mechanical tests such as tensile strength, elongation at break, and hardness are done in order to analyze the effect of the surfactant in the composites. Thermal measurements, thermal modelling, SEM, Energy Dispersive X-ray analysis (EDAX), and X-ray diffraction (XRD) analysis techniques are used to determine the protective mechanism of the nanofillers in the SiR matrix.

A discussion of the results is presented in Chapter 4. The advantages of using a nonionic surfactant rather than an ionic surfactant are described. Reinforcing in the micro-filled formulation with nanofiller and surfactant is analyzed with respect to the number of silanol groups, which was determined experimentally. On the other hand, the effect of the surfactant on the contact angle and on the mechanical properties is compared for the different composites tested. The improvement in the thermal stability of the nanocomposites is analyzed according to the amount of surfactant added into the composite. The results of the salt fog, inclined plane, and laser ablation tests are examined. A comparison of the thermal conductivity obtained from the ASTM method, theoretical models, and from the proposed model is analyzed as well as the experimental and modelled temperature profiles. Finally, the protective mechanism for the nanocomposites in a silicone rubber matrix during laser ablation or dry band arcing is discussed.

In Chapter 5, a summary of the conclusions and suggestions for further studies are provided.

Chapter 2

Materials, Experimental Setup, and Modelling

Over the last decade, significant improvements have been obtained in the electrical and mechanical properties of nanodielectric materials. However, some adverse and contradictory results have also been noted, and some of these effects have been attributed to filler agglomeration. To improve an electrical or mechanical property, the dispersion of nanofiller in the matrix material is of the utmost importance. Therefore various mixing techniques have been examined in an attempt to obtain a uniform dispersion of nanofiller. An alternative method to obtain a uniform dispersion is to treat the surface of the nanofillers. The use of surfactants and nanofiller pre-treatment through calcination are methods to minimize the agglomeration of nanofillers that are explained in this chapter.

The composite preparation as well as the eroded mass assessment, mechanical tests, thermal characterization, and thermal modelling are described in the next sections. The tests used to assess the relative improvement of various nanofillers in SiR are the inclined plane, laser ablation, and salt fog tests. Also, various analytical tests such as FTIR, SEM, EDAX, and XRD are utilized to determine the protective mechanism of nanofillers in SiR composites.

2.1 Types of Nanofilled Silicone Dielectric Composites

In order to investigate nanofilled dielectric materials, several nanofillers are selected based on the information found in the literature. Among these, nano fumed silica is favoured because of its low cost, also because micro silica is use as one of the main fillers in outdoor

insulation, and compatibility could exist between them. Fumed silica is an amorphous material that is produced in a flame process of silicon tetrachloride reacting with oxygen and hydrogen.

A low content of nano fumed silica results in a comparable performance, in dry band erosion tests, to conventionally filled composites [15, 16]. Materials with combinations of micro- and nano-sized fillers have also yielded good results, with increased time to breakdown with ac (alternating current) voltage in epoxy resin [36]. According to Fréchette *et al.* [37], the real advantage of nanodielectrics comes with the admixing of both micro and nanofillers (micro-nanofillers). However, a better understanding of the preparation of micro-nanofillers is necessary to gain the advantages of both types of fillers. From an industrial viewpoint, the micro-nanofilled materials must be cost competitive; however, a slightly higher cost for improved performance can be acceptable. Therefore, combinations of microfillers and nanofillers are also investigated in this research.

Several nanofillers are selected for the investigation, namely both fumed and natural silica (SiO_2), alumina (Al_2O_3), barium titanate ($BaTiO_3$), titanium dioxide (TiO_2), and zinc oxide (ZnO); all of them obtained from the supplier Sigma Aldrich with a purity ≥ 99%. The fillers most commonly used with SiR are alumina trihydrate (ATH), alumina, and silica. However, ATH is not yet available in nanosize. In this research, the base silicone material selected is RTV 615^{TM}, manufactured by the General Electric Company. This RTV is selected because it does not contain fillers, and has the same outstanding properties as the regular heat curing silicone rubbers used in SiR insulators. The curing process is simplified with this RTV silicone, as no special or expensive additives, tools, or machinery are required. Furthermore,

exact control of the curing temperature is not required for reproducibility of the crosslinking or vulcanization of the rubber.

2.1.1 Selection of the Conditions for Mixing

Mixing is a critical step in the preparation of polymeric nanocomposites, and a mixer with a high shear force is necessary to tear apart and wet the particles, in order to achieve the uniform dispersion of the nanofillers within the silicone rubber matrix. Several high shear mixers are available commercially, and the one used in this research is the model HSM-100LSK, manufactured by Ross.

For most industrial applications, Degussa [38] suggest tip speeds of 8-10 m/sec (peripheral velocity) to obtain an adequate dispersion. For the Ross mixer with a blade diameter of 16 mm, the rpm is calculated as:

$$rpm = \frac{peripheral \quad velocity \ (m/\sec) \cdot 60 \cdot 1000}{d(mm) \cdot \pi} \qquad \textbf{2-1}$$

The wet-in time is defined as the time for all the nanoparticles to be wetted by the liquid medium, which is achieved by low shear mixing at 6,000 rpm. Once the nanoparticles are wetted, the mixing speed can be increased up to 12,000 rpm to begin dispersion.

Another critical aspect is the blade to vessel ratio. This ratio is selected between 1:2 to 1:3 to observe a clear vortex during mixing. Optimum mixing time and temperature are system specific and must be established empirically for each formulation.

2.1.2 Surface Treatment of Nanofillers

The surface properties of nanofillers can be modified by treating them with various surfactants and reactive polymers. In this thesis, surfactants are investigated, as the adsorption of surfactants on fillers is fast and effective.

Based on the fact that nonionic ethoxylated surfactants and poly(ethylene oxide) have been found to adsorb on silica [39], Triton, stearic acid, and oleic acid are investigated in an attempt to improve nanofiller dispersion. The amount of surfactant required for uniform dispersion is estimated according to Seon's results [31]. A high surfactant concentration can compromise the adsorption of the matrix polymer chains on the filler particles, so it is necessary to establish a balance between matrix adsorption and the dispersion of the particles. Mechanical properties such as the tensile strength, elongation at break, and hardness may suffer from excess surfactant. In addition, excess surfactant can lead to surface wetting properties different from composites containing none. Better wetting due to the migration of excess surfactant to the surface of the silicone may favour arcing in a wet environment, so the amount is determined experimentally and tested in order to minimize detrimental effects on the properties of the nanocomposites.

In addition, solvents including hexane, methanol, ethanol, and toluene are also investigated to facilitate nanoparticle dispersion. Sonication is used with these solvents to improve nanofiller dispersion.

2.1.3 Calcination of the Nanofiller

Pre-treatment, or calcination to activate nanofillers, is accomplished in a Lindberg furnace at the temperatures of 573 K, 873 K, or 1173 K for one hour. Tests are done to determine the optimal temperature for the investigated nanofillers [32, 39].

2.2 Performance Studies of the Nanocomposites

2.2.1 Eroded Mass Assessment

In the evaluation of the eroded mass of the nanocomposites under the influence of dry band arcing, several methods can be applied. One technique is the inclined plane test (IPT) based on ASTM D 2303 [40]. In this method, the electrical discharges cause localized thermal and chemical decomposition, erosion, and eventually the formation of a conductive path across the tested material.

Since heat from dry band arcing is the main degradation factor in filled composite materials, the degradation is considered to be thermal in nature. The laser method developed by Meyer *et al.* [41] to simulate the effects of dry band arcing is used to evaluate the erosion resistance of the composites. The laser test has clearly yielded results equivalent to dry band arcing in the inclined plane test.

A long-term performance evaluation, called the salt fog test, is often used to evaluate material formulations for outdoor applications. This test is essential but has not yet been investigated. The salt fog test is used to evaluate the aging effects caused by electrical discharges on the surface of the nanofilled dielectrics. So, the tests used to assess the relative effectiveness of the various nanofillers in SiR are the inclined plane, laser ablation, and salt fog tests.

2.2.2 Thermal Characterization

Discussions regarding the thermal conductivity of nanofilled dielectrics are riddled with contradictions. Some authors have found no correlation between the thermal conductivity and

the amount of filler [15], whereas Rätzke *et al.* [11] have found a good correlation between these two parameters leading to improved resistance to erosion. In another study, Meyer *et al.* [42] found a good correlation between thermal conductivity and microfiller content: the higher the filler concentration in the SiR composites, the higher the thermal conductivity, and the greater the resistance to dry band arcing erosion. Although there are theoretical, semi-theoretical, and empirical models, none consider the particle size and particle size distribution, which results in inaccurate thermal conductivity estimates [43]. Thus, it is important to investigate the role of the nanofillers on the thermal conductivity as a function of particle size and concentration.

In this thesis, the thermal conductivity is measured by a standard ASTM method and is estimated by different theoretical and experimental methods for comparison. It is also modelled in COMSOL Multiphysics^{TM} and solved by a finite element method (FEM).

2.3 Materials and Sample Preparation

Based on the literature on nanofillers mentioned in Section 1.3.1, different nanofillers are selected to investigate the influence of the nature of the fillers on the properties of dielectric materials. The main characteristics of these nanofillers, obtained from Sigma Aldrich, are summarized in Table 2.1.

For comparison, composites with different amounts of microfillers are also examined. The microfiller used is Min-U-Sil 5, produced by U.S. Silica; the particle diameter reported for this material is less than 5 μm (97% of the particle size distribution below 5 μm).

Several composites are prepared with different compositions of microfiller, nanofiller, micro-nanofiller combinations, and a nonionic surfactant, Triton ($C_{14}H_{21}O(C_2H_4O)_nH$ where

n = 9-10). This surfactant has a hydrophilic poly(ethylene oxide) group and a hydrocarbon lipophilic or hydrophobic group as shown in Figure 2.1.

Table 2.1 Characteristics of the nanofillers.

Filler	**Average particle size (nm)**	**Specific surface area (m^2/g, BET)**	**Density (kg/m^3) @298 K**	**Melting point (K)**
Fumed Silica[a]	7	390±40	2200	1983
Aerosil R812 (fumed silica treated with HMDS)[b]	7	260±30	N/A	N/A
Aeroxide LE 1[b]	N/A	160±30	2000	768
Natural Silica	10	590-690	2200-2600	>1873
Alumina	2-4	350-720	4000	2313
Barium Titanate	30-50	N/A	6080	1523
Titanium Dioxide (Anatase)	5	200-220	3900	2098
Zinc Oxide	50-70	15-25	5610	2248
Micro Silica	5000	5	2650	1883

N/A: Not available

[a] Pyrogenic silica or thermal silica, by combustion of $SiCl_4$

[b] HMDS: Hexamethyldisilazane yields trimethylsilyl groups on the surface

BET stands for the scientists Brunauer, Emmett, and Teller, who optimized the theory for measuring surface area.

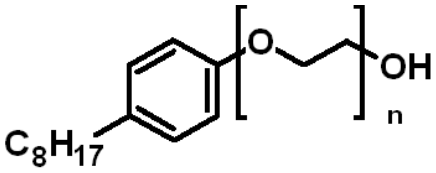

Figure 2.1 Structure of Triton.

The viscosity of the silicone-filler mixtures increases with the amounts of nano- and microfillers added. A high shear force mixer enables better dispersion within the mixture which, in turn, enhances the electrical and mechanical properties of the composites.

The first step is to calculate the amount of RTV silicone (parts A and B), micro particles, and nanoparticles required to make the formulation or mixture. This is denoted by the weight percentage of each component. The ratio used for the silicone matrix is 10 parts resin (part A) to 1 part curing agent (part B).

The higher concentration mixtures are obtained by gradually increasing the amount of filler. This requires an increased stirring rate at each step, increasing the overall mixing time. The desired amount of nanofiller is added in small portions and mixed with the matrix (part A) until lumps in the mixture are no longer visible. In this procedure, the rotation of the micro mixer and the continuous friction of the material under shear cause the mixture to heat, but the temperature is controlled by cooling the polymer compound so as not to exceed 313 K. This temperature is selected to achieve consistent results.

After part A is mixed with the filler, the sample is cooled to ambient temperature, part B is added and mixing is continued for 3 minutes. Further, the mixture is degassed in a vacuum oven at 100 kPa vacuum (~ 29 in Hg). If the mixture is extremely viscous, it is preferable to degas it directly in the mould. The composites are cured at room temperature for 24 h and

post-cured in an oven at 360 K for 4 h. For composites mixed with a solvent, the filler is added to 25 ml of solvent and sonicated for 1 hour prior to mixing with the silicone resin.

For composites with surfactant, the additive is mixed with part A for 3 minutes prior to adding the nanofiller. For composites containing micro-nanofiller, first the microfiller is mixed, then the surfactant, and finally the nanofiller. Since there is no pre-treatment of the filler with the surfactant prior to mixing with the matrix, this corresponds to an *insitu* method.

According to Seon *et al.* [31], the amount of stearic acid (which has the same function as the Triton surfactant) for the surface modification of fumed silica can be calculated from:

$$X = \frac{A}{\omega} B \qquad \textbf{2-2}$$

where X is the mass of surfactant needed to obtain complete coverage of the nanofiller particles (g), B is the mass of nanofiller (g), A is the specific surface area of the filler (m^2/g), and ω is the wetting surface of the surfactant (m^2/g).

According to the equation above, for nano fumed silica with a surface area A = 390±40 m^2/g and with ω = 542 m^2/g of wetting surface for the surfactant, the amount of Triton required per gram of nanofiller to saturate the surface is 0.6 g.

The nano fumed silica is put into a porcelain crucible and calcinated in a Lindberg furnace at a temperature of 573 K, 873 K, or 1173 K for one hour. After the filler is cooled, it is stored in a desiccator until further use. Nano fumed silica without any pre-treatment is also used in the preparation of some composites.

2.4 Test Setups and Procedures

2.4.1 Inclined Plane Test (IPT)

This technique is based on the ASTM D 2303 standard [40]. Six samples are tested; each sample is 50 mm wide x 130 mm long x 5 mm thick.

For each formulation, the upper side and the mould side are tested. The composites are energized at 3 kV, and then the voltage is increased by 0.25 kV every hour. The final step occurs at 3.75 kV, after 3 hours; the duration for the complete test is 4 hours. The flow rate of the NH_4Cl solution is 0.30 ml per minute and the concentration 1 g/dm^3 in deionized water.

After the test, the composites are inspected and cleaned. The eroded mass of the material is determined from the difference in weight. The mean and the standard deviation of the eroded mass are calculated for each formulation.

2.4.2 Laser Ablation Tests

The method for performing this test consists in applying the same energy to each sample; in this case, a Coherent infrared model FAP laser with an operating wavelength of 802 nm is used. The heat produces molecular vibrations causing the polymer to break down [41].

Heat from dry band arcing is the main degradation factor in SiR used in outdoor insulation; consequently, the degradation is thermal in nature, and the laser test can be used to simulate the effects of dry band arcing. To simulate the conditions encountered during an IPT test, the maximum temperature during the electrical discharges and failure of one sample is recorded. The sample is energized starting at 3 kV, and the voltage is increased by 0.25 kV during each 5 minute period. Using a thermal camera, the maximum temperature is recorded. The

maximum temperatures are 383 K, 479 K, 984 K, and 985 K for step voltages of 3 kV, 3.25 kV, 3.5 kV, and 3.75 kV, respectively. When electrical discharges appear in the sample, the temperature rises to 479 K as shown in Figure 2.2(a). During failure of the sample, the temperature reaches the maximum value in the test (985 K) as shown in Figure 2.2(b). This information is required to set up the laser (time, power, pulse mode, etc.).

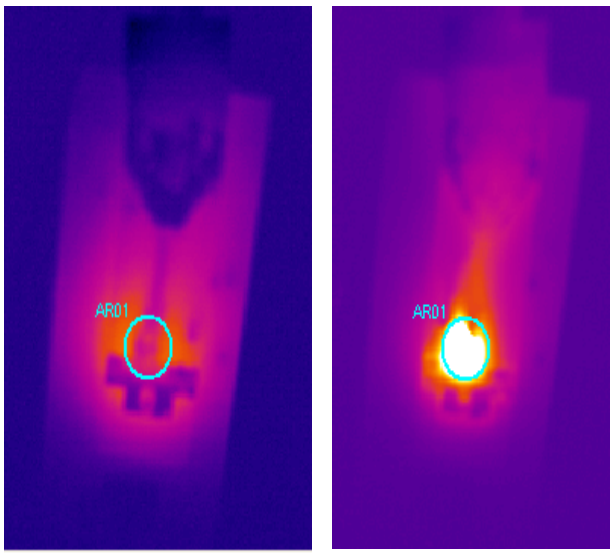

(a) (b)

Figure 2.2 Temperature in the inclined plane test.

Several tests are conducted to adjust the diode laser, which is operated in the continuous wave (CW) mode with a current of 17.5 A (power equivalent to 8.8 W) for 7 minutes, corresponding to a calculated total energy of 3700 Joules. The sample is located 50 mm from the laser source in all the tests.

The maximum temperature achieved for several composites during the laser test (983 to 995 K) is very close to that obtained in the IPT test at 3.75 kV (985 K). Figure 2.3 represents a plot of the temperature reached for the sample with 2.5% nano fumed silica plus surfactant.

In the laser test, the composites require a darker colour to ensure uniform absorption of the laser radiation; this is achieved by including 2.5% wt of iron oxide in the mixture for all the composites [41]. Since Fe_2O_3 is stable at high temperatures, above the decomposition temperature of the SiR matrix, it may be considered otherwise inert [44].

To verify the reproducibility of the laser method, different formulations are selected and two composites of each type are prepared, each from a different mixing batch. The maximum variation observed among composites with the same formulation is about 6% which is far better than with the IPT method.

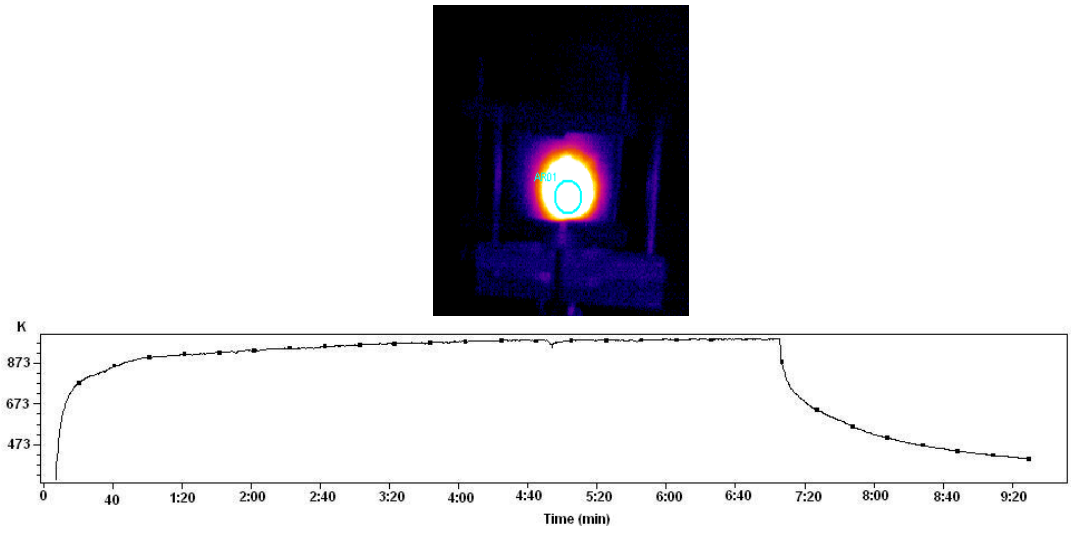

Figure 2.3 Temperature profile for 2.5% nano fumed silica plus surfactant in the laser ablation test.

2.4.3 Salt Fog Test

A stainless steel salt fog chamber with a volume of 1 m^3, with the dimensions 1 m x 1 m x 1 m is used. Four nozzles are located on each side of the chamber [45]. Salt water is prepared by mixing 2.5 kg of NaCl per cubic meter of water. This concentration is used for all the

tests, and the conductivity is maintained at 0.42 S/m during each test. The air pressure in the nozzles is 140 kPa, and the flow rate is 0.1 litre per minute. The composites are of the solid rod type, with dimensions of 19.5 mm diameter x 150 mm length. The voltage applied is 3.5 kV over a leakage distance of 110 mm, corresponding to a stress of 31.8 V/mm. For each formulation four rods are tested for a maximum of 300 hours according to the procedure described in IEC 61109 [46]. During the salt fog tests, the test voltage and leakage current on the rods are recorded by a data acquisition system.

2.4.4 Contact Angle Measurements

One possible negative effect of excess surfactant can be a decrease in the contact angle on the surface of the composite; however, enhanced wettability of the nanofiller by the silicone rubber matrix is also achieved [47]. According to Young's equation, three forces act on the droplet: $\sigma_{LV}\cos\theta=\sigma_{SV}-\sigma_{SL}$ where σ_{LV} is the liquid–vapor interfacial surface tension, σ_{SV} is the solid–vapor interfacial surface tension, σ_{SL} the solid–liquid interfacial surface tension, and θ is the contact angle. If the volume of the droplet and the surface tension remain constant, the contact angle does not change either.

In order to evaluate this behaviour in nanocomposites, the static contact angle is obtained from digital images recorded with a digital camera and stored on a computer. The analysis of each image is done with the Visio™ software to measure the contact angle. A precision pipette is used, and the volume of each droplet is 10 µl. For each sample 10 droplets are put on the surface and the contact angle is measured. New flat composites are cleaned with deionized water and rested for 48 hours before measuring the contact angle.

2.4.5 Mechanical Evaluation

2.4.5.1 Tensile Strength

Stress–strain measurements are done at room temperature in the uniaxial extension mode and along the direction of increasing elongation. The tensile tester, a Minimat 2000, is used following the procedure described in the ASTM D1708 standard. For each formulation, 5 to 10 composites are tested. The testing speed is 100 mm/min (speed D) [48]. The stress, σ, is calculated as:

$$\sigma = \frac{f}{A_0} \qquad \textbf{2-3}$$

where f and A_0 are the measured force and the initial cross-sectional area, respectively.

2.4.5.2 Hardness Measurement

The hardness of the composites is measured according to the ASTM D2240 standard [49] using a durometer Model 408 ASTM type A for applications in soft rubbers, elastomers, and flexible polyacrylics. Following the standard, five measurements are recorded for each sample and the mean and the standard deviation are reported. The objective of these tests is to evaluate the behaviour after adding surfactant to the composites.

2.4.6 Temperature Measurements using Infrared Camera

The surface thermal measurements are conducted with an infrared camera, FLIR SC500, and with thermo vision acquisition software. The detector emissivity is between 7.5 and 13 μm, and the temperature image is displayed in a 320x240 pixel array. The thermal sensitivity of the detector is 273.07 K at a temperature of 303 K, with an accuracy of 273 ±2 K up to 1773

K. The acquisition software ThermaCAM^{TM} allows different types of post-processing of the temperature distribution in the infrared image. The emissivity calibration is adjusted to 0.98 for the composites. The emissivity is determined by comparing two temperatures, namely the camera temperature of composites heated to 360 K in an oven and the temperature of the thermocouple in the oven.

2.4.7 Thermal Gravimetric Analysis (TGA)

TGA is a technique in which the weight change of a material is monitored as a function of increasing temperature, and is therefore a measure of its thermal stability. As the temperature increases, a weight loss occurs due to the release of moisture or gases from the decomposition of the material. In the end, only a non-volatile residue remains.

The thermal gravimetric analysis work is done using a TA Instruments SDT 2960. The measurements are done in an air atmosphere, and the temperature is ramped at a rate of 20 K/min, from 473 K up to 1073 K. The weight loss as a function of temperature is recorded with a sensitivity of 0.1 mg and 1% accuracy. An extrapolation technique is used to determine the degradation temperatures at 75% and 50% of residual mass, and the final temperature corresponding to a constant residual sample weight.

2.4.8 Fourier Transform Infrared Analysis (FTIR)

The FTIR system used is a Bruker Tensor 27 spectrometer. The polymer specimens are analyzed at 1 cm^{-1} resolution, and 16 scans are averaged in the absorbance mode. The spectrum analysis is done with the software for the instrument.

FTIR spectroscopy is used to determine the concentration of silanol groups in nano fumed silica and in micro silica using a technique developed by Kokai *et al.* [50]. In this method organosilanol compound solutions in CCl_4 are used to calibrate the instrument by integrating the peaks in the absorbance mode from 4300 – 4700 cm^{-1}. The concentration of silanol groups in the fillers is determined by comparing the calibration curve to the peak area for the samples dispersed in the same solvent.

2.4.9 Scanning Electron Microscopy (SEM)

To ascertain the degree of dispersion of the nanofillers in the insulating materials, a LEO 1530 FE-SEM electron microscope system is used to analyze the morphology of the composites. The function of this electron microscope is similar to its optical counterpart except that a focused beam of electrons is employed instead of light to "image" the specimen and to gain information on its structure and composition.

2.4.10 Energy Dispersive X-ray Analysis (EDAX)

EDAX is done using the LEO 1530 FE-SEM electron microscope equipped with an EDAX Pegasus 1200 integrated EDX system. The accelerating voltage was 15 to 20 kV in all cases. The samples are placed on carbon conductive tape and coated with a gold film of 20 nm thickness using a high vacuum sputter. EDX analysis collects the X-rays generated by the electron beam of the SEM, and provides information on the elemental composition of the material.

2.4.11 X-ray Diffraction (XRD)

XRD is used to obtain the chemical composition and crystallographic structure of the residue and char from the tested nanocomposites. The X-ray diffraction pattern is obtained with a Rigaku AFC-8 diffractometer, with a wavelength of 0.1542 nm, operated at 50 kV, 40 mA, and a beam diameter of 0.8 mm.

2.5 Measurement of Thermal Conductivity of Nanocomposites

2.5.1 Based on ASTM D5470

Thermal conductivity (TC) measurements are performed based on the ASTM D5470 standard [51]. Bondline thickness measurements are performed during the test using a Mitutoyo laser scan micrometer, LSM 503H. Tests are performed under atmospheric conditions at a mean joint temperature of 373 K. Temperature readings from resistance detectors in the heat flux meters are used to calculate two quantities, namely, the total heat flow rate through the joint, Q, and the temperature drop across the joint, ΔT. From these two quantities, the joint resistance is calculated:

$$R_j = \frac{\Delta T}{Q} \qquad \textbf{2-4}$$

Thermal conductivity is calculated from the overall joint resistance using the relationship:

$$k = \frac{t_{BLT}}{R_j A} \qquad \textbf{2-5}$$

where A=625 mm^2 and t_{BLT} is the measured bondline thickness from the laser micrometer.

2.5.2 Based on Temperature Profile

The surface thermal measurements are conducted with an infrared camera, FLIR SC500, the main characteristics of which are mentioned in Section 2.4.6.

For these experiments the laser is set at 0.24 W, and the surface of the sample is irradiated for 3 minutes, after which the laser is switched off. The temperature heating and cooling profiles are measured using the infrared camera for a total of 5 minutes – 3 minutes of heating and 2 minutes of cooling. The composites are located 50 mm from the laser source in all tests. The temperature profile for each formulation is recorded and analyzed to determine the thermal conductivity.

The cooling or decay profile is fitted to calculate the thermal conductivity following the technique developed by Meyer *et al.* [42]. The principle is based on the known thermal conductivity of the unfilled sample and on the assumption that the heat transfer is mainly by conduction, so that heat transfer due to radiation and convection is negligible. The fitting is done according to the equation:

$$T = T_R + T_0 e^{-\alpha t} \qquad \textbf{2-6}$$

where T_R is the ambient temperature, T_o is the initial temperature, and $\alpha = C\,k$ where C is a proportionality constant, and k is the thermal conductivity.

2.6 Calculation of Thermal Conductivity of Nanocomposites

2.6.1 Based on Theoretical Models

The initial model selected is the rule of the mixtures. In this model, the thermal conductivities and volume fractions of the filler and the matrix are used to calculate the thermal conductivity of the composite. However, this model does not consider particle size [52].

In order to consider the packing fraction and shape of the filler particles, a semi-theoretical model developed by Lewis and Nielsen [53] is used as the second model.

2.6.2 Using a Simplified Steady State Model of Dispersed Composites

A sphere in a cube is considered for this steady state model. A filler particle is introduced in the center of a cube according to the approach suggested by Karayacoubian *et al*. [54] and Araki *et al.* [55]. Perfect thermal contact between the filler and the matrix is assumed.

The volume of one micro silica particle, with a diameter of 5 μm, assuming that it is a sphere, is 65.45 μm^3. In a formulation with 20% weight of micro silica (8.8% by volume), the calculated unit cell has 9.06 μm on each side as shown in Figure 2.4. Similarly, for a composition of 2.5% weight nano fumed silica with a diameter of 7 nm (1.85% volume), each side of the cell is calculated to be 0.64 μm.

It is assumed that the fillers and the SiR matrix are isotropic and that their thermal conductivities are constant. The boundary conditions for the four faces of the cell parallel to the axis “z” are adiabatic. The other two faces are isothermal, and the heat goes from the upper face to the bottom.

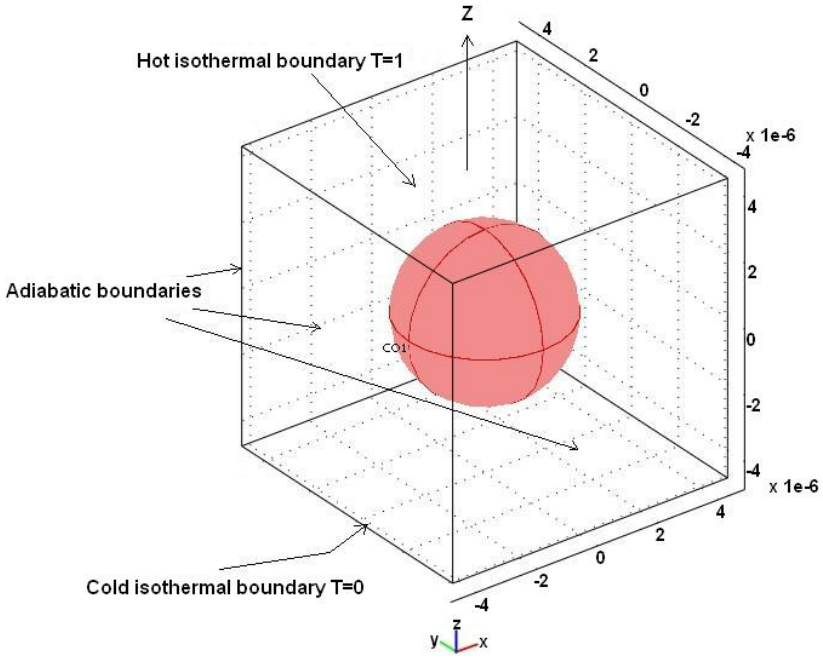

Figure 2.4 A simplified three dimensional model for dispersed composites.

The heat conduction through the cubic cell is given by Fourier's law as:

$$Q=k_e A\frac{\Delta T}{L}=\frac{\Delta T}{R_j} \qquad \textbf{2-7}$$

The thermal conductivity of the cell is K_e, A is the cross-sectional area, L is the distance between the isothermal boundaries, ΔT is the temperature drop across the cell, and R_j is the total resistance of the cell.

The boundary conditions on the four adiabatic boundaries are:

$$\left(\frac{\partial T_m}{\partial x}\right)\Big|_{x=\pm L/2}=0 \qquad \textbf{2-8}$$

$$\left(\frac{\partial T_m}{\partial y}\right)\Big|_{y=\pm L/2} = 0 \qquad \textbf{2-9}$$

and on the two isothermal boundaries:

$$T_m\left(x, y, \frac{L}{2}\right) = 1 \qquad \textbf{2-10}$$

$$T_m\left(x, y, -\frac{L}{2}\right) = 0 \qquad \textbf{2-11}$$

The total heat flow into or out of the cell is obtained by Fourier's law across either of the isothermal boundaries [54]:

$$Q = \int_{-L/2}^{L/2}\int_{-L/2}^{L/2}\left[k_m\left(\frac{\partial T_m}{\partial z}\right)\right]_{z=L/2} dxdy \qquad \textbf{2-12}$$

For the above problem a simple analytical solution is unavailable, and a numerical method is required to determine the temperature. The finite element method in COMSOL is used to solve the problem [56].

2.7 Temperature Profile in the Composites Using a Simplified Transient Model

The temperature profile of the different formulations under laser ablation test conditions is simulated assuming a 3D transient model using the heat transfer module in COMSOL. The equation solved in the software using the FEM technique is [56]:

$$\rho C_p \frac{\partial T}{\partial t} + \Delta \cdot \left(-k \Delta T\right) = Q \qquad \textbf{2-13}$$

where ρ is the density, C_p is the heat capacity, k is the thermal conductivity, and Q is the heat source. The heat generation is defined as a function of the laser power, and an inward heat flux of 19,100 W/m^2 is calculated and used in the analysis [57]. For this model, the geometry considered is a cylinder 36 mm in diameter with seven layers of filler intercalated between eight layers of silicone rubber matrix according to the volume fraction of each component in the formulation. It is not possible to simulate any more layers due to restrictions in the memory of the computer and the selected size of the mesh.

Chapter 3

Results

Using the procedures described in Section 2.3, the experimental setups in Section 2.4, and the methodology for modelling contained in Section 2.5, the composites are evaluated to understand the arcing erosion resistance processes in nanofilled silicone dielectrics. Some tracking and erosion tests resulted in a broad variation in the eroded mass when the inclined plane test is used.

As is mentioned in the literature, proper dispersion of the particles plays a very important role in obtaining consistent properties, and in this thesis the dispersion is improved using surface treatment methods. Aiming for improved dispersion and using the laser ablation tests, different fillers and surfactants are used. The best filler that enhanced the erosion resistance of the composite is found to be nano fumed silica in combination with Triton. After that finding, this combination is used to reinforce a microfilled composite. The influence of the surfactant on the mechanical properties as well as the thermal stability of the composites, and the interactions between the filler and the SiR matrix are analyzed by several techniques. In addition, thermal modelling helps to analyze the effect of the filler on the thermal conductivity of the nanocomposites.

3.1 Tests to Identify the Best Filler and Amount of Surfactant

The composition of the composites is designated by the nomenclature shown in Table 3.1; this nomenclature will be used in the subsequent sections.

Table 3.1 Nomenclature used for the composites.

Nomenclature	Formulation (% weight)
2.5%nfs	2.5% nano fumed silica
2.5%nns	2.5% nano natural silica
20%m	20% micro silica
20%m+2.5%nfs	20% micro silica + 2.5% nano fumed silica
20%m+2.5%Aerox dust	20% micro silica + 2.5% aeroxide dust
2.5%nfs+Hexane	2.5%nano fumed silica+hexane solvent
20%m+2.5%nfs (573 K)	20% micro silica + 2.5% nano fumed silica calcinated at 573 K
10%m+20pph T	10% micro silica + 20 parts per hundred of Triton
40%m+2.5%nfs(1273 K)+5 pph T	40% micro silica + 2.5% nano fumed silica calcinated at 1273 K + 5 parts per hundred of Triton

3.1.1 Inclined Plane Tests

The first composites are prepared by directly mixing the nanofiller without any surfactant or pre-treatment. The procedure used is the one laid out in Section 2.3, the composites are tested in the IPT, and the results are displayed in Figure 3.1. The mean eroded mass is represented by the dot, and the bars mark the 25th and 75th percentiles for six composites per formulation.

There is no consistent pattern for the results obtained in most cases. Most samples with nanofiller are compounded and tested seven times with very different results. This suggests

two things. First, direct mixing of the nanoparticles does not result in a very good dispersion, even if all the composites are prepared in the same way (procedure and methodology). Second, the IPT method exhibits a high variability, an inherency of this method. As a result, more tests are run with surfactants and after calcination of the nanoparticles.

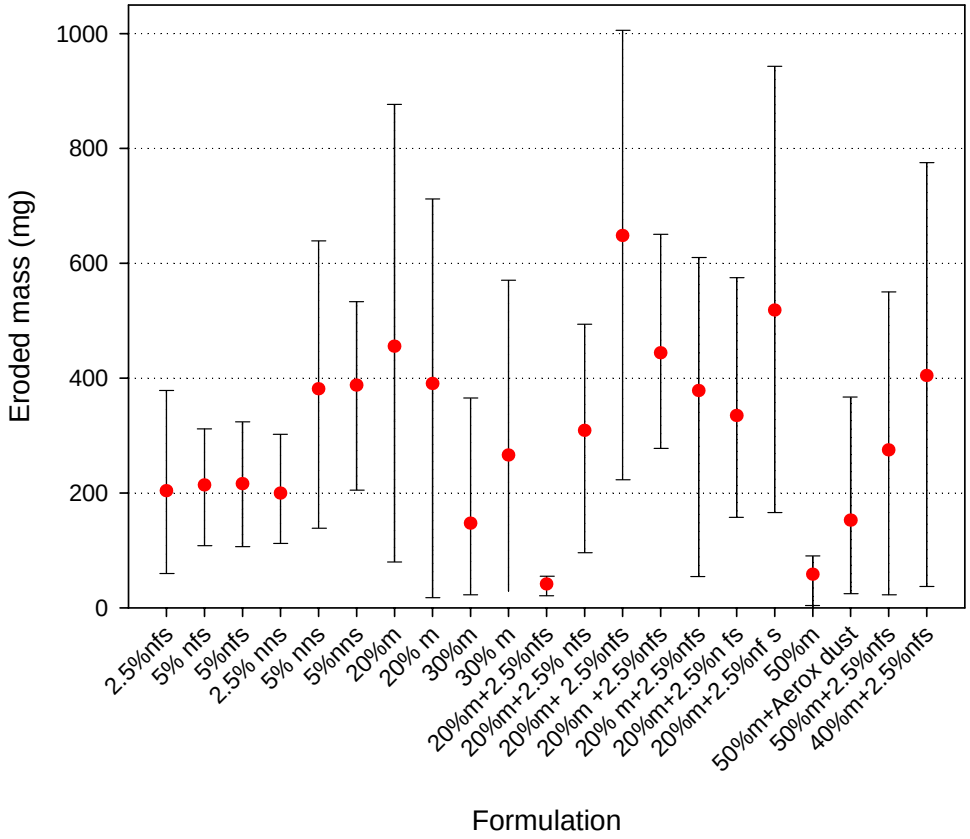

Figure 3.1 Average eroded mass of six composites per formulation in the inclined plane test. The average eroded mass is represented by the dot; the 25th and 75th percentiles are represented by the horizontal lines of the bars.

3.1.2 Scanning Electron Microscopy (SEM) Observations

The particle size distribution of the nanofillers is analyzed by scanning electron microscopy (SEM). The dispersion of the nanofiller, as mentioned before, is very important in obtaining consistent properties in the nanofilled material.

For SiR as a matrix and nano calcinated fumed silica filler, several composites containing 5% nano calcinated fumed silica by weight, with and without added surfactant, are prepared to observe the dispersion of the nanoparticles, as shown in Figure 3.2. The electron micrographs on the right are with 33 pph of surfactant and those on the left do not contain surfactant. It is obvious that the presence of surfactant improves the dispersion of the nanoparticles.

Even after calcination at 1273 K some hydroxyl groups still remain on the surface of nanosilica. According to Zhuravlev *et al.* [33] the number of active sites is $\alpha_{OH} < 1$ –OH group per square nanometre but these silanol groups can interact with the surfactant and facilitate the dispersion.

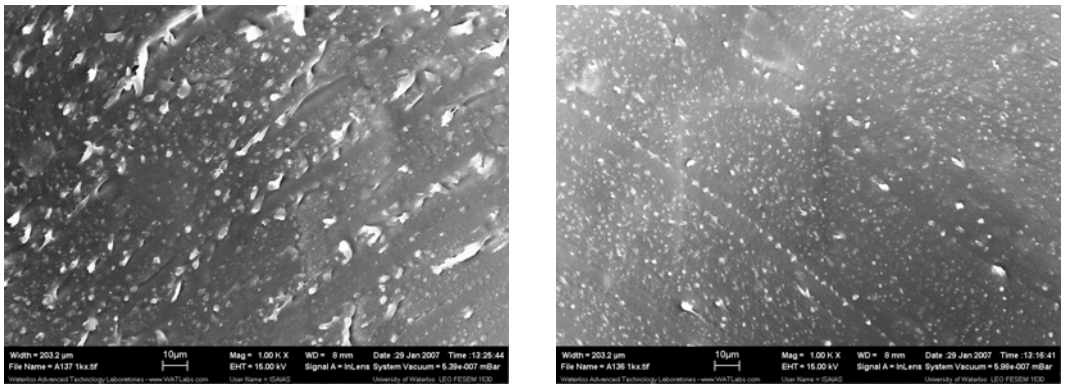

Magnification 1000 x

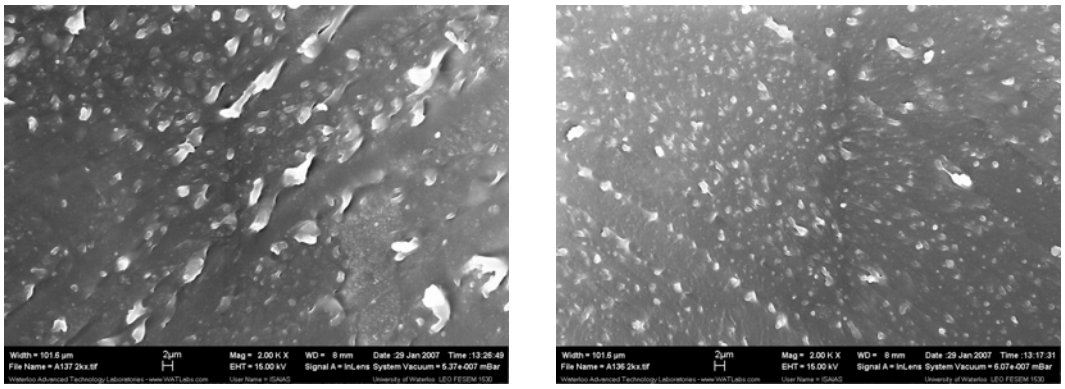

Magnification 2000 x

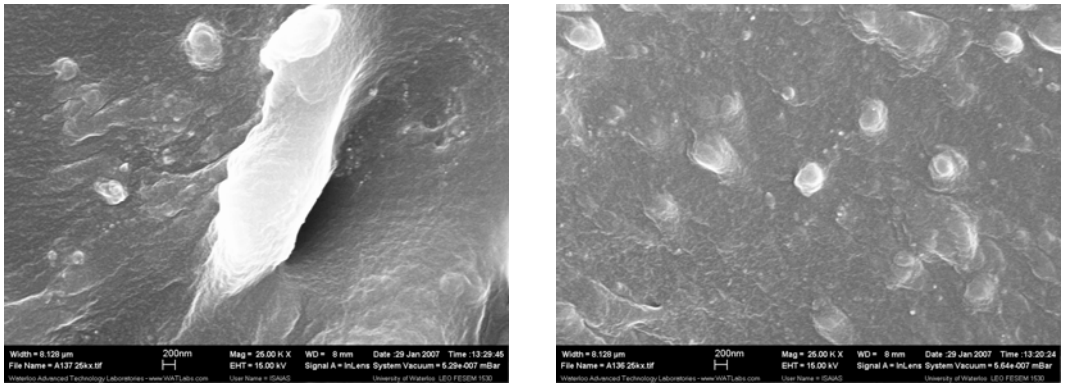

Magnification 25000 x

Figure 3.2 Effect of Triton in composites containing 5% by weight of nano calcinated fumed silica + 95% SiR (left column without surfactant; right column with surfactant).

Composites with nanoalumina (2.5% wt) are also prepared with and without surfactant for SEM analysis. These results are shown in the micrographs of Figure 3.3 (left column without surfactant and right column with surfactant). The composite without surfactant clearly forms large agglomerates, which is in agreement with the findings of Rätzke *et al.* [11]. The micrographs with surfactant show that the surfactant aids in achieving good dispersion of the nanofiller, although some agglomeration persists. It is clear that the formation of large agglomerates of nanoalumina and nano calcinated fumed silica is favoured in the SiR matrix without surfactant.

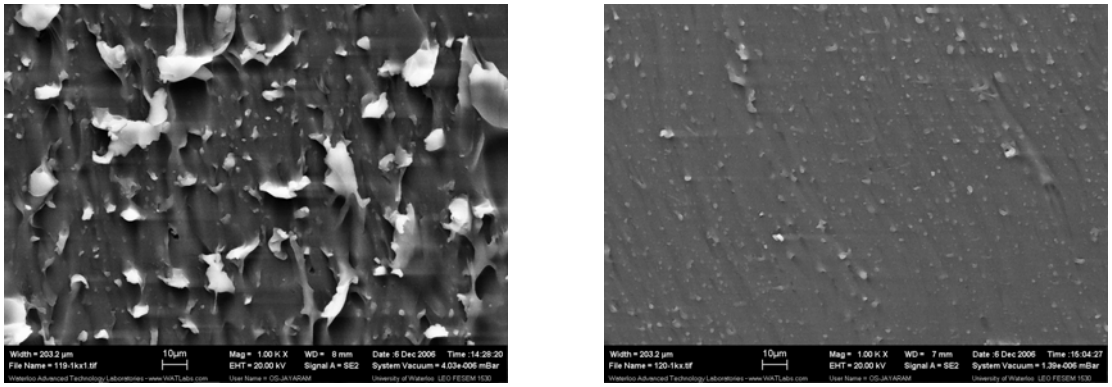

Magnification 1000 x

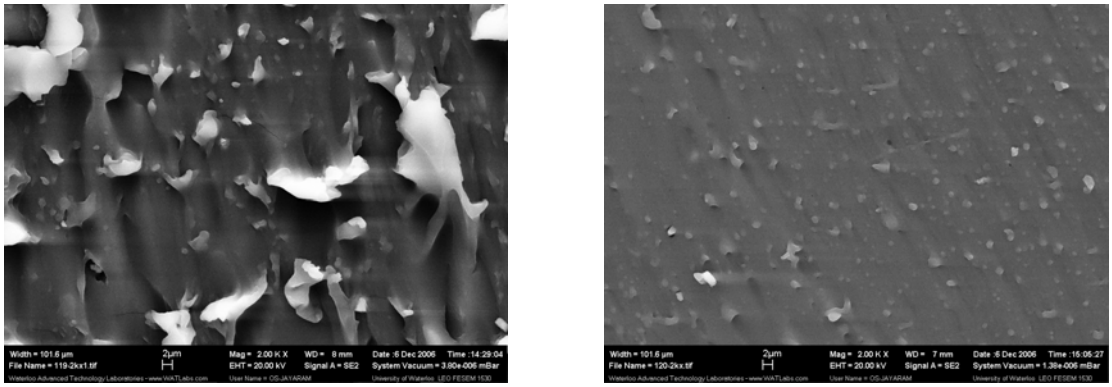

Magnification 2000 x

Figure 3.3 Effect of Triton in composites containing 2.5% by weight nano Al_2O_3 + 97.5% SiR (left column without surfactant; right column with surfactant).

Other SEM tests with TiO_2, ZnO, and $BaTiO_3$ nanofillers in SiR matrix are conducted to verify the particle dispersion with surfactant. However, for these nanofillers, the surfactant does not appear to improve the dispersion (Figure 3.4, Figure 3.5, and Figure 3.6).

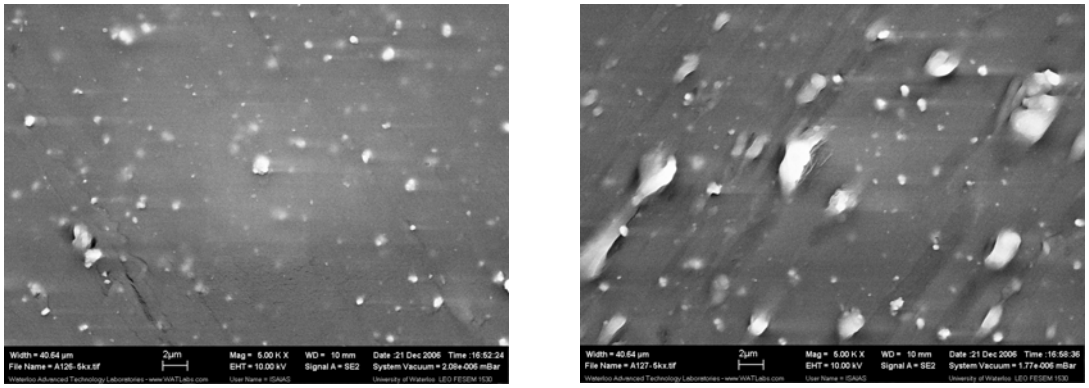

Magnification 5000 x

Figure 3.4 Effect of Triton in composites containing 2.5% by weight TiO_2 + 97.5% SiR (left micrograph without surfactant; right micrograph with surfactant).

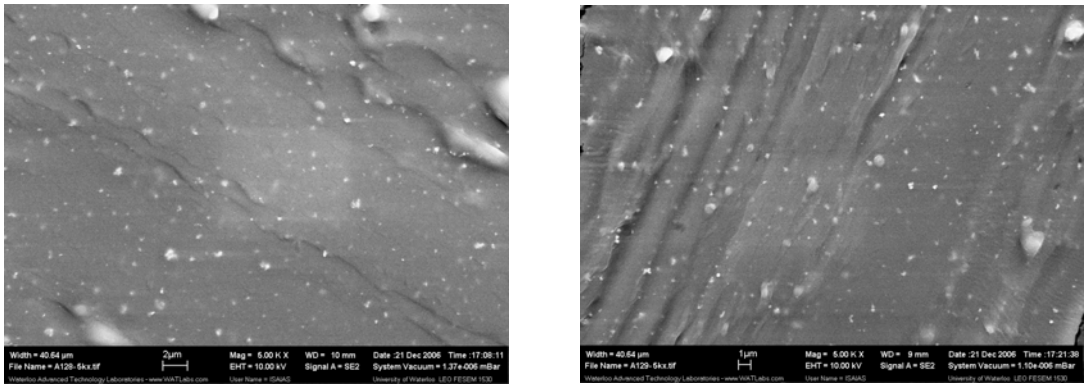

Magnification 5000 x

Figure 3.5 Effect of Triton in composites containing 2.5% by weight ZnO + 97.5% SiR (left micrograph without surfactant; right micrograph with surfactant).

These results suggest that only certain surfactants are able to adsorb efficiently on the surface of specific nanofillers. In this case, Triton appears to interact favourably with

nanosilica, presumably through its hydrophilic poly(ethylene oxide) segment and with the SiR matrix through its hydrophobic component. However, it cannot interact efficiently with the other nanofillers.

Due to the large number of compositions investigated, the influence of the surfactant concentration on the dispersion level is not evaluated by SEM analysis for all the samples. However, more detailed examples of SEM micrographs for different surfactant concentrations (0, 14, 21, 27, 33, 51, and 79 pph of Triton) are shown in Appendix A for the 2.5% nanoalumina composite. In these micrographs the effect of the surfactant is evident; the agglomeration of the nano alumina is reduced as the concentration of surfactant increases.

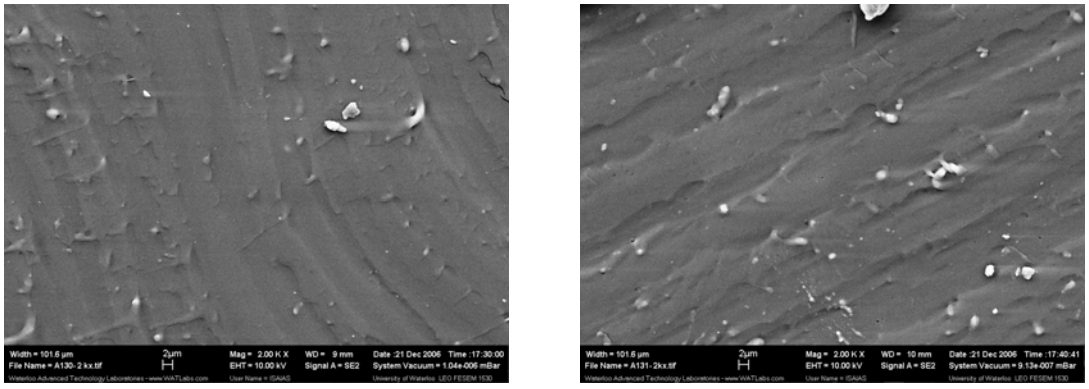

Figure 3.6 Effect of Triton in composites containing 2.5% by weight $BaTiO_3$ + 97.5% SiR (left micrograph without surfactant; right micrograph with surfactant).

3.1.3 Laser Test Results

The eroded mass of the composites is determined from the weight measured before and after testing using a Sartorius balance AC 211S-00MS with a readability of 0.1 mg. For each sample, three tests are carried out. In the following plots the average eroded mass is

represented by the dot; the 25th and 75th percentiles are represented by the horizontal lines of the bars.

3.1.3.1 Composites with Nanofillers, Solvents, and Surfactants

The average eroded mass values for all the composites prepared with nano fumed silica plus solvent are lower than for the composites without solvent, as seen in Figure 3.7. The solvents providing a better performance are methanol and ethanol, possibly because they are more volatile.

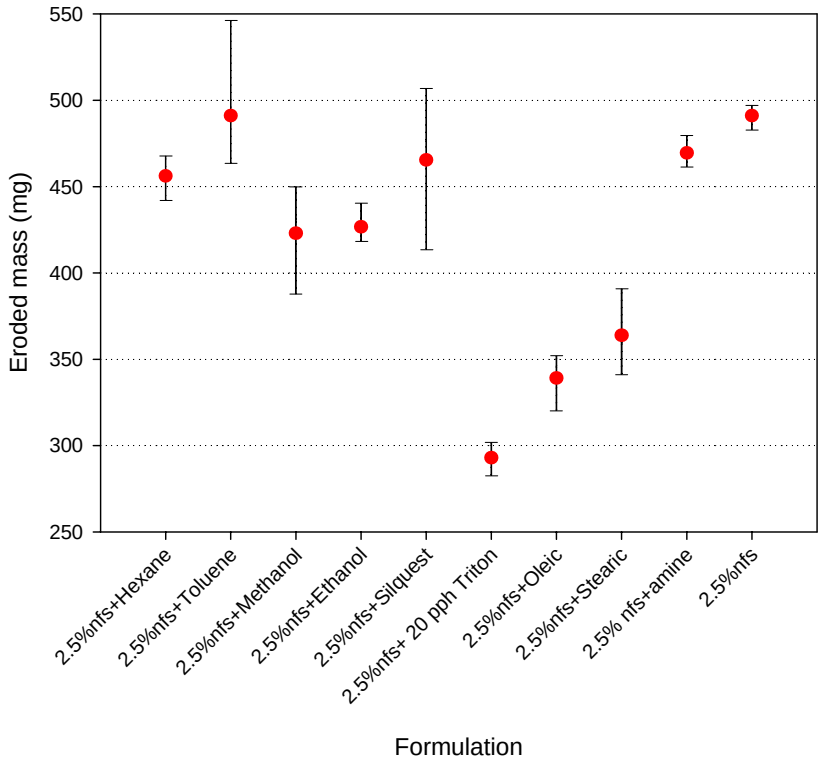

Figure 3.7 Eroded mass of composites with nano fumed silica mixed with solvents or surfactants. The average eroded mass is represented by the dot; the 25th and 75th percentiles are represented by the horizontal lines of the bars.

However, the lowest eroded mass value is obtained for the composites with only 2.5% wt of nanofiller and Triton, albeit the results are close to the composites with oleic and stearic acid. Thus, the surfactant consistently modifies the surface of the nanofiller and enhances erosion resistance. On the basis of these results, Triton is selected as the main surfactant for the composites.

3.1.3.2 Composites with Different Amounts of Surfactant and Filler

Three composites at each composition consisting of either 2.5 or 5 wt % of nanofiller and various Triton additions (expressed in pph of nanofiller by weight) are tested. In Figure 3.8 through Figure 3.13, the average eroded mass of three composites at different Triton concentration is provided by each point. First order linear regression analysis of the data is done up to 33 pph of surfactant due to with lower concentration of Triton is obtained a good improvement in eroded mass, also because a higher concentration of surfactant can affect the mechanical properties of the composite as is shown in Section 3.2.1.

a) Composites with Nano Fumed Silica

Figures 3.8 and 3.9 show the results for 2.5 wt % and 5 wt % nano fumed silica, respectively. About a 50% decrease in eroded mass is observed when approximately 20 pph of surfactant is added to the composites containing either 2.5% or 5% nanofiller. The first order linear regression coefficient R is 7 for the 2.5 wt %, and 6.5 for the 5 wt % concentrations. These slopes demonstrate a significant improvement in erosion resistance with the addition of surfactant; however, no significant difference in eroded mass is obtained at the higher concentration of nano fumed silica.

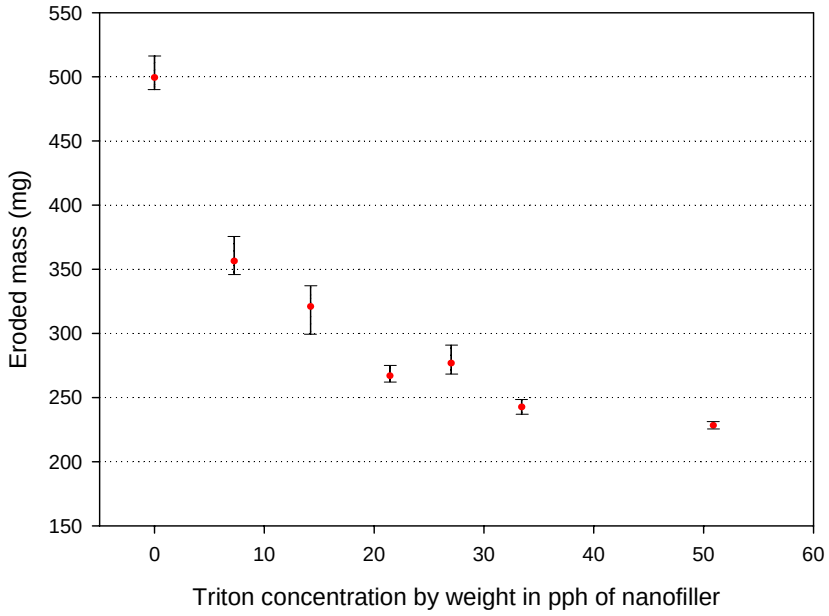

Figure 3.8 Eroded mass of composites with 2.5 wt % nano fumed silica for various Triton concentrations (in pph of nanofiller). The average of three composites is shown for each formulation.

If it is assumed that Triton is adsorbed on the filler particles proportionally to their BET surface area as suggested by Seon *et al.* [31], then the following can be calculated. For a specific surface area of 350 – 430 m^2/g for nano fumed silica and a wetting surface of 542 m^2/g for Triton, the maximum amount of surfactant that can be adsorbed per gram of nanofiller would be between 0.65 – 0.8 g or 65 – 80 pph by weight. If it is further assumed that a homogeneous mixture is obtained and that this gives rise to uniform particle dispersion, then a linear relationship between the eroded mass and the amount of Triton added would be expected up to this maximum. Beyond that limit, the presence of excess Triton may affect the curing chemistry of the silicone.

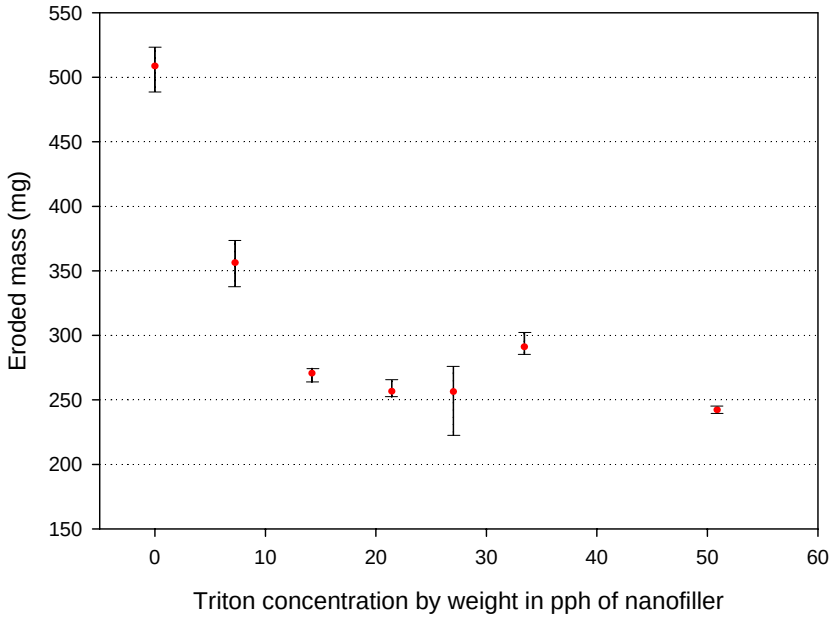

Figure 3.9 Eroded mass of composites with 5 wt % nano fumed silica for various Triton concentrations (in pph of nanofiller). The average of three composites is shown for each formulation.

b) Composites with Nano Natural Silica

In this case the first order linear regression coefficients are 5.1 and 5.9 for the 2.5 and 5 wt %, respectively, as shown in Figure 3.10 and Figure 3.11. Following the argument put forward for the nano fumed silica, if Triton is taken up by filler particles proportionally to their BET surface area, a maximum of 110 – 130 pph of Triton by weight of nanofiller can be added. Consequently, linearity in the eroded mass plot should be evident up to this limit. Once again, it appears that there is no further reduction in the eroded mass at higher concentrations of nano natural silica. Furthermore, the effectiveness of nano natural silica in reducing the mass loss is lower than for nano fumed silica.

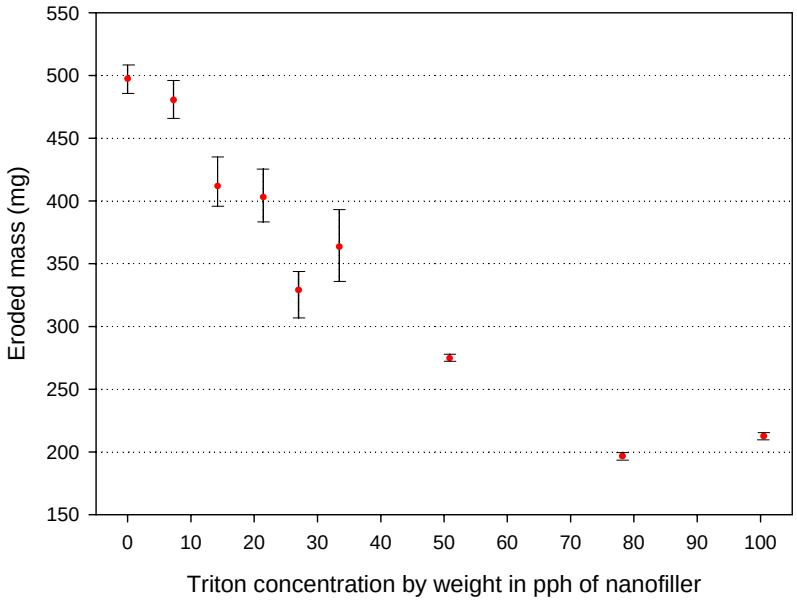

Figure 3.10 Eroded mass of composites with 2.5 wt % nano natural silica for various Triton concentrations (in pph of nanofiller). The average of three composites is shown for each formulation.

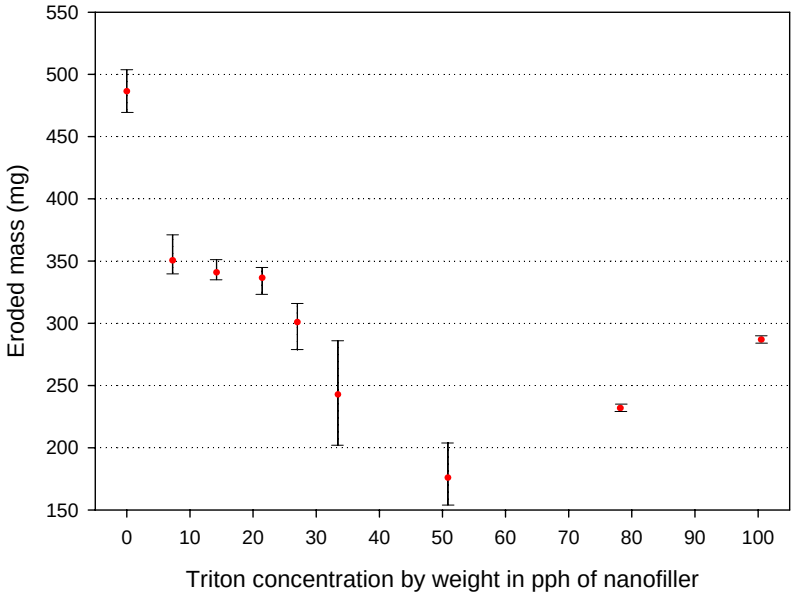

Figure 3.11 Eroded mass of composites with 5 wt % nano natural silica for various Triton concentrations (in pph of nanofiller). The average of three composites is shown for each formulation.

c) Composites with Nanoalumina

In these compositions, the coefficients of the regression are 3.5 and 2.8 for the 2.5 and 5 wt % nanoalumina filler contents, respectively, as shown in Figures 3.12 and 3.13. These coefficients are the lowest obtained for the three type of nano fillers analyzed. From the BET surface area, the optimum addition of Triton is more than 65 pph but less than 135 pph by weight for nano alumina.

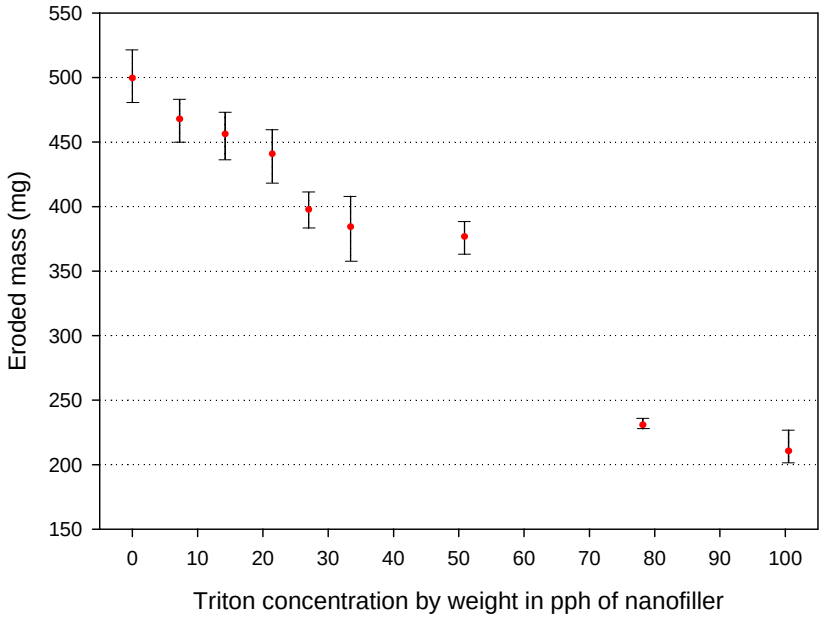

Figure 3.12 Eroded mass of composites with 2.5 wt % nano alumina for various Triton concentrations (in pph of nanofiller). The average of three composites is shown for each formulation.

In comparison to nano natural silica and nanoalumina, at the same amount of surfactant, nano fumed silica showed the lowest reduction in the ablated mass under infrared laser heating, followed by natural silica. The highest eroded mass is obtained with alumina. In these tests it is noticed that a white deposit develops in the composites at higher surfactant

concentrations, which is a deposit of silica, and this mechanism has been reported previously [59].

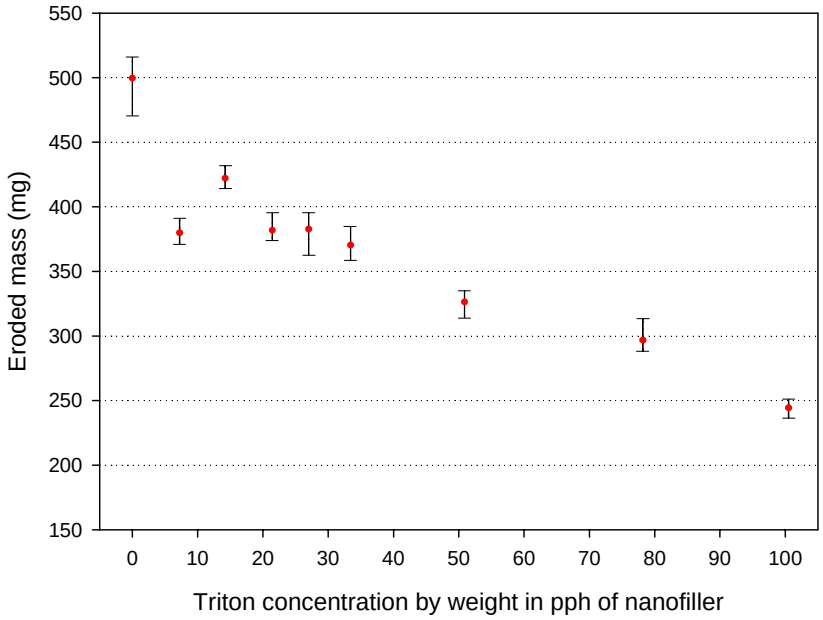

Figure 3.13 Eroded mass of composites with 5 wt % nano alumina for various Triton concentrations (in pph of nanofiller). The average of three composites is shown for each formulation.

In particular, the decomposition of SiR in contact with air produces white silica particles [60]. The white deposit is therefore not only due to filler residues, but also to the decomposition of the PDMS matrix in air. The white deposit appears at a lower concentration of surfactant in the nano fumed silica filled composites than in nano natural silica filled composites, and finally at a higher concentration in nano alumina filled composites. Composites with nano fumed silica with 78 pph and 100 pph or surfactant are not evaluated with the laser technique, because the laser beam is reflected by the white layer. The composites with a white deposit are never considered in the eroded mass calculations. It is

also noticed that the thickness of the deposit seems to increase for increasing Triton concentrations (100 pph). Therefore, it appears that this silica deposit forms a heat-resistant shield preventing further heat ablation of the underlying SiR matrix.

3.1.4 Composites with Micron- and Nano-Sized Fumed Silica

From a commercial viewpoint, the combination of micro and nanofillers is lower in cost than formulations incorporating only nanofillers. Also, an advantage of composites is that it is possible to mix micron- and nano-sized fillers [58, 19, 20]. For outdoor insulation applications this appears to be a promising area of study, and for this reason several composites are investigated.

It was shown in the previous section for nano fumed silica (Figure 3.8 and Figure 3.9), that improved erosion resistance could be achieved for silicone at relatively low surfactant concentrations, which are 7, 14, 21, and 28 pph with respect to the nanofiller.

Three composites at each composition consisting of 20% micro silica filler, different amounts of nano fumed silica, and several Triton concentrations are subjected to the laser ablation test. Both fillers are used without any thermal treatment. The results obtained are summarized in Figure 3.14. The standard deviation obtained for the different tests using the laser method is considered low as compared to other evaluation techniques such as the inclined plane test or the salt fog test. Five percent of nano fumed silica is the upper loading limit examined, since at this level mixing becomes quite difficult to achieve. However, it is evident that the eroded mass decreases with the addition of nano fumed silica. Furthermore, the addition of 28 pph of Triton is more beneficial than 14 pph in reducing the mass loss.

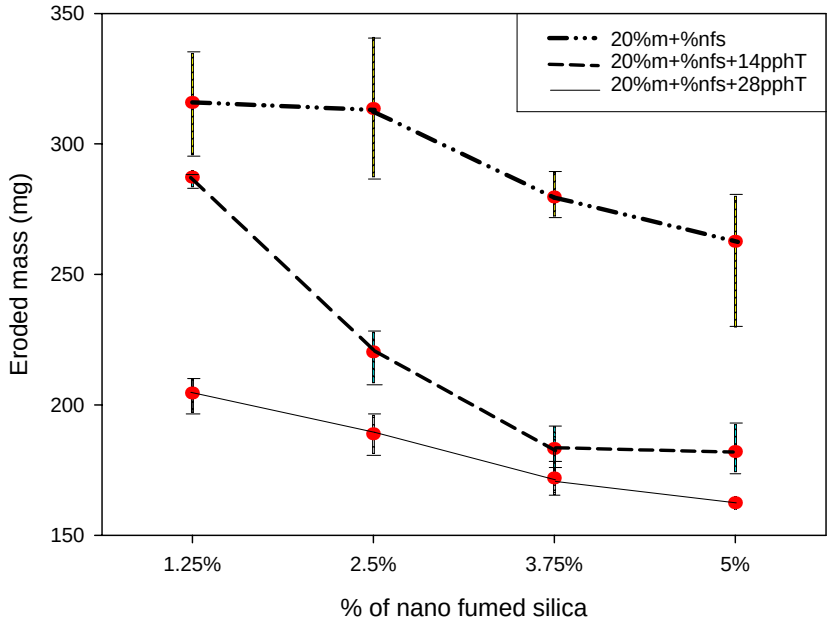

Figure 3.14 Average eroded mass of composites with 20% micro silica for various nano fumed silica loadings and Triton concentrations (expressed in pph of nanofiller by weight). The average eroded mass is represented by the dot; the 25th and 75th percentiles are represented by the horizontal lines of the bars.

To examine the eroded mass in the laser ablation test using fillers treated by calcination, a known technique for stripping the hydroxyl groups from the filler surface, composites are prepared after heating for one hour at various temperatures (573 K, 873 K, and 1173 K). Calcination also breaks up aggregates and pellets of the nanofiller, and it eliminates adsorbed water. These results are shown in Figures 3.15 and 3.16 for several fillers and as a function of the Triton concentration. It appears that calcination does not have as much influence on the eroded mass as the addition of Triton, since all the curves tend to converge with the addition of 28 pph surfactant.

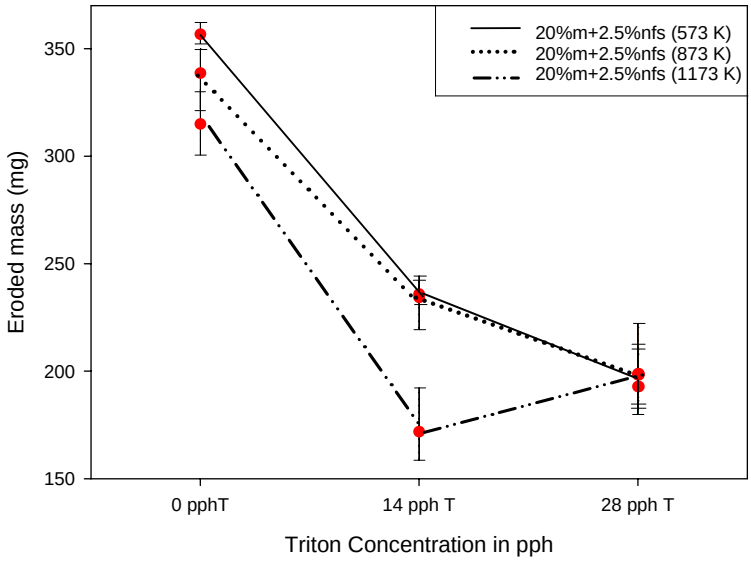

Figure 3.15 Eroded mass of composites with 20% micro silica and 2.5% nano fumed silica calcinated at different temperatures and for various Triton additions (expressed pph of nanofiller by weight). The average eroded mass is represented by the dot; the 25th and 75th percentiles are represented by the horizontal lines of the bars.

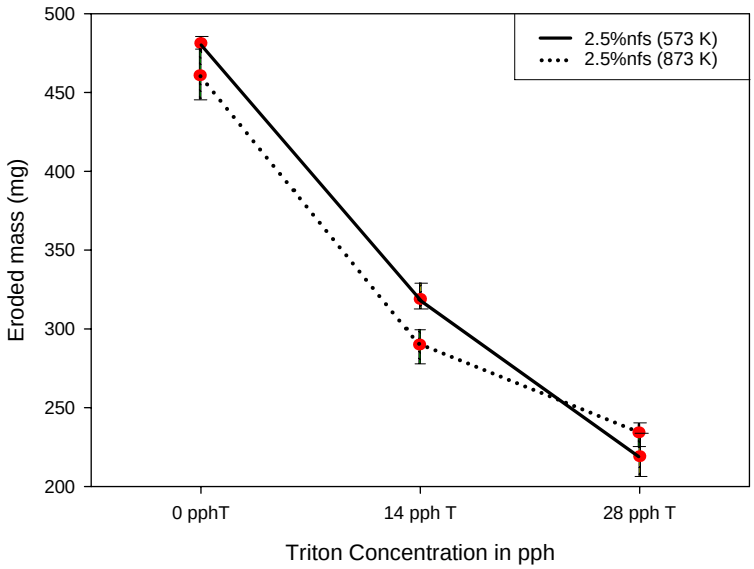

Figure 3.16 Eroded mass of composites with 2.5% nano fumed silica calcinated at different temperatures and for various Triton additions (expressed in pph of nanofiller by weight). The average eroded mass is represented by the dot; the 25th and 75th percentiles are represented by the horizontal lines of the bars.

In these tests it is noticed that for the composites with 2.5% nfs treated at 1173 K, a white deposit develops during the test. This is most likely a silica layer; such a protective mechanism decreasing sample erosion has been reported previously [59]. The decomposition of SiR in air is also known to produce white silica particles [60, 61]. The white layer is therefore attributed to filler residues and to the decomposition of the SiR matrix in air. For this reason, composites with 2.5% nfs thermally treated at 1173 K are not evaluated by the laser technique. The reflection of the laser beam by the white layer likely biases the erosion level determined by laser ablation under these conditions. The silica layer also forms a heat-resistant shield that can hinder further ablation of the underlying SiR matrix.

3.1.5 Composites with 40% of Micro Filler and Nano-Sized Fumed Silica

Composites containing 40 wt % of microfiller and 2.5 wt % of nano fumed silica, both non-calcinated and calcinated at 1273 K, are investigated. The results for mass loss by the laser heating technique are shown in Figure 3.17.

The sample with 40% micro silica+2.5%nano calcinated fumed silica+20 pph Triton possesses a 60% lower eroded mass than the sample with only 40% micro silica. With the incorporation of surfactant and the use of calcinated nanosilica, the behaviour of the 40% micro silica+2.5% nano calcinated fumed silica composition is improved (40%m+2.5%nfs(1273 K)). Different amounts of surfactant are added, and the optimal amount for this composition with higher amount of microfiller is 20 pph, yielding a lower eroded mass of 89 mg. The decrease in eroded mass observed upon adding surfactant to a mixture of micro- and nano calcinated fumed silica reaches 15% with 20 pph of surfactant. In the case of the mixture of micro- and nano fumed silica it is higher, reaching 24% with 39

pph of surfactant. From these results it is very clear that the surfactant helps to obtain more resistant nanocomposites, still with the combination of micro-nanofillers as a consequence of improved dispersion.

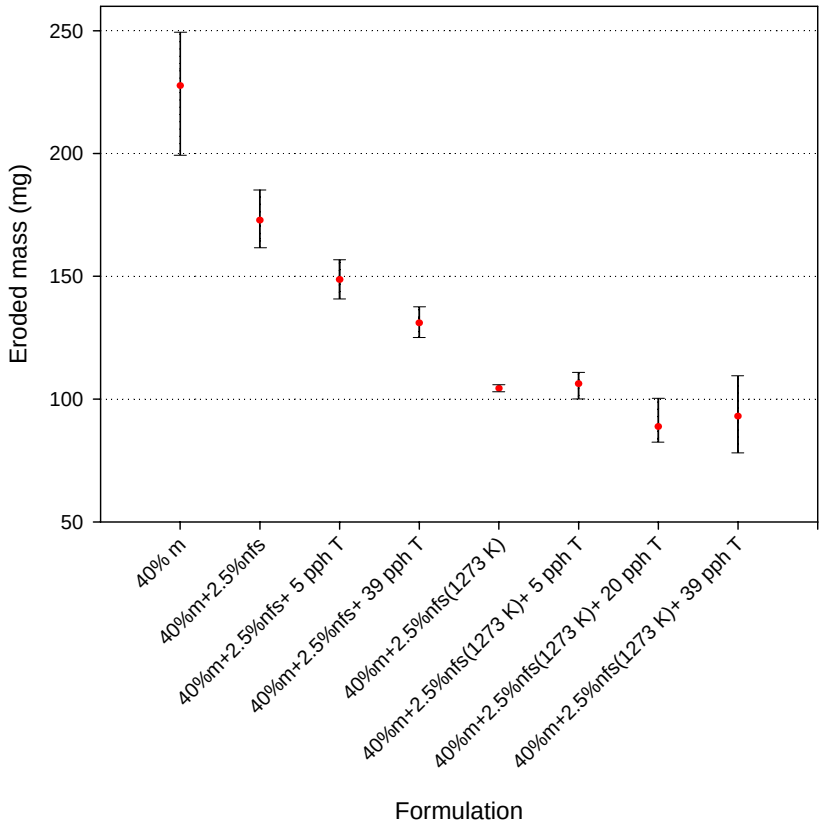

Figure 3.17 Eroded mass for composites with micro- and nanofillers with surfactant. The average eroded mass is represented by the dot; the 25th and 75th percentiles are represented by the horizontal lines of the bars.

The main advantage in the use of surfactant is that it lowers the surface energy of the nanofiller. This lowering of the surface energy of the particles reduces agglomeration and makes it easier to separate the particles during mixing, thereby allowing improved dispersion of the nanofillers. Calcination, up to a certain temperature, also helps because it destroys the

aggregates and pellets of nanoparticles, and eliminates adsorbed water; however, at higher temperatures calcination can cause almost the complete loss of silanol groups [33].

In order to analyse nanofiller distribution in the micro filled composites, imaging of the micro+nano-filled composites is investigated. The composites of 40% micro+2.5% Al_2O_3+ silicone rubber without and with surfactant, 40% micro+4% nano fumed silica+Epoxy resin, and 20% micro+2.5% nfs are examined by SEM, and it is concluded that any changes occurring in the nanofiller aggregation level are masked by the microfiller particles under these conditions. This is due to the small amount of nanofiller in the mixture and to the large size of the microfiller particles, as shown in Figure 3.18.

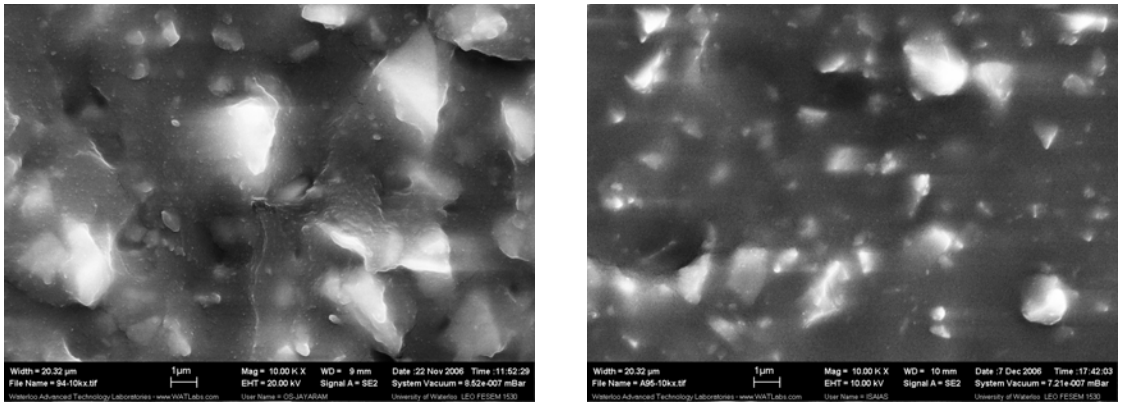

Figure 3.18 SEM of samples with 40% micro+4% nano fumed silica+epoxy resin (left side without surfactant, right side with surfactant).

3.1.6 Composites with only Microfillers

Composites with only microfillers are prepared and tested. The eroded mass results are illustrated in Figure 3.19. It is evident that the eroded mass varies linearly for the 0%, 10%, 20%, 30%, 40%, and 50% compositions. In all cases, for the formulations including 20 pph of Triton, the eroded mass is lower than that of the same formulations without surfactant.

Based on that linear variation, the eroded mass value for sample 60% micro (not shown in the figure) is inferred to be closer as for sample with 60% micro silica+Triton.

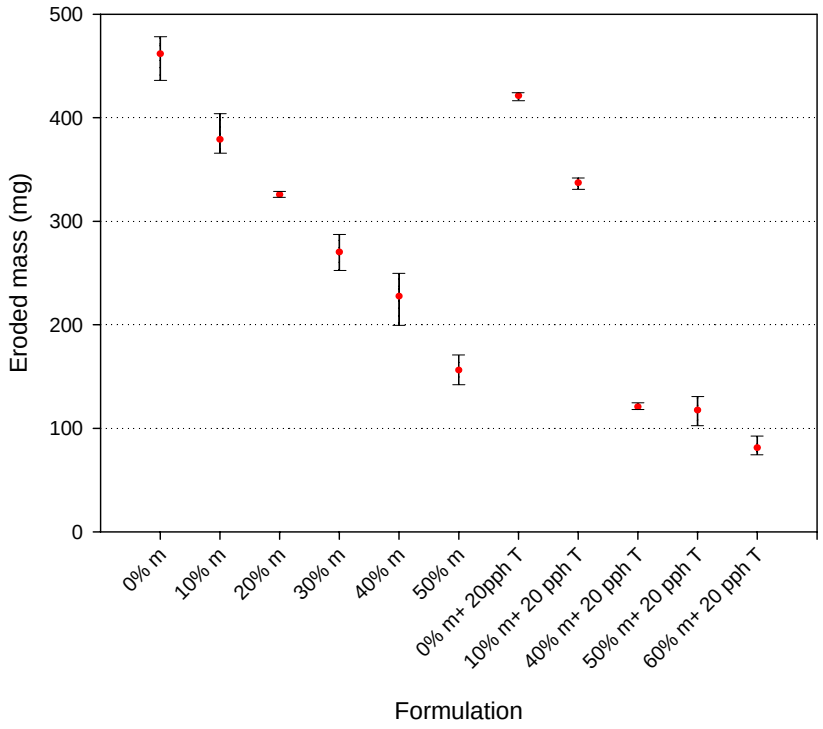

Figure 3.19 Eroded mass of composites with micro silica filler and Triton. The average eroded mass is represented by the dot; the 25th and 75th percentiles are represented by the horizontal lines of the bars.

3.2 Tests with Adjusted Amounts of Surfactant and Fillers

After the main nanofiller and the method to improve dispersion are selected based on the performance of nanocomposites evaluated in the laser ablation test, micro-nano composites, and a composite with only nanofiller are prepared and characterised by different techniques. The results for each test are described in the following sections.

3.2.1 Mechanical Evaluation

It is important to note that a large amount of surfactant may compromise the adsorption of the silicone rubber chains on the filler particles; therefore, it is necessary to establish a balance between particle dispersability and chain adsorption. On the other hand, tensile strength, elongation at break, and hardness are bulk properties of the silicone that are affected by the filler type and loading. The interactions (bonding) present with the polymer matrix also affect these properties. Since the addition of surfactant to disperse the filler can have adverse effects on bonding, the mechanical properties may be negatively impacted by excess surfactant.

To examine the influence of the surfactant on the properties of the composites, concentrations of 14, 28, and 100 pph are selected. Since a decrease in eroded mass is observed in Section 3.1.3 for surfactant concentrations of up to approximately 50 pph, the mechanical properties of a formulation incorporating 100 pph of surfactant are also examined.

In Figure 3.20, the ultimate tensile strength is compared for composites with nanofiller and micro+nanofillers at several concentrations of surfactant. The actual tensile strength values obtained are summarized in Table 3.2, as well as the hardness and elongation at break. While the average tensile strength is higher for the micro+nanofilled composites as compared to the nanofilled composites, it is evident that the addition of 14 pph surfactant has little effect on the tensile strength. At 28 pph surfactant an insignificant (approximately 4%) reduction in the average tensile strength is found with respect to the composites without surfactant. While 14 – 28 pph of surfactant sufficed to ensure proper dispersion of the nanofillers, these concentrations had little influence on the tensile strength.

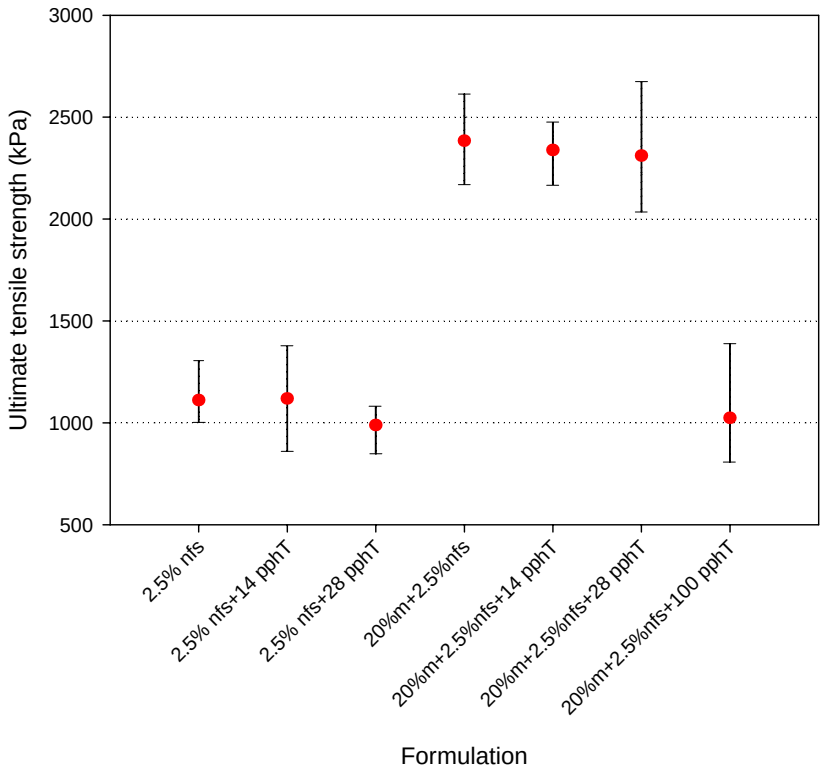

Figure 3.20 Ultimate tensile strength of nanofilled and micro+nanofilled composites. The average eroded mass is represented by the dot; the 25th and 75th percentiles are represented by the horizontal lines of the bars.

However, with 100 pph of surfactant, the tensile strength dropped by almost 60% as compared to the sample without surfactant. A 25% drop in hardness is also observed for the same sample. Hence it can be stated that for 14 – 28 pph of surfactant, below the saturation limit of 65 – 80 pph for the nanofiller surface, the tensile and the hardness are not significantly affected. However, at 100 pph of surfactant the mechanical properties are negatively impacted.

Table 3.2 Summary of mechanical evaluation.

Sample	Ultimate tensile strength (MPa)	Coefficient of variation, CV (%)	Elongation (%)	Hardness (Type A)
2.5% nfs	1.11	15	238	52
2.5% nfs+14 pphT	1.12	25	235	50
2.5% nfs+28 pphT	0.99	14	219	50
20%m+2.5%nfs	2.38	9	214	62
20%m+2.5%nfs+14 pphT	2.34	8	209	61
20%m+2.5%nfs+28 pphT	2.31	14.9	227	58
20%m+2.5%nfs+100 pphT	1.02	33.8	207	47

3.2.2 Spectroscopic Analysis of the Components

ATR (Attenuated Total Reflectance)-FTIR spectroscopy is used initially for surface analysis of the nanocomposites (spectra not shown). However, because the infrared beam penetrates only a few micrometers below the surface, under these conditions, the spectra do not display additional peaks of the type observed in the transmission mode. Consequently, the ATR spectra do not reflect the bulk composition of the composites, and transmission FTIR spectra are used in subsequent analysis work.

The transmission FTIR spectra obtained for the individual components of the nanocomposite, consisting of Triton, uncured RTV, micro silica, and nano fumed silica are compared in Figure 3.21. These are obtained as reference spectra.

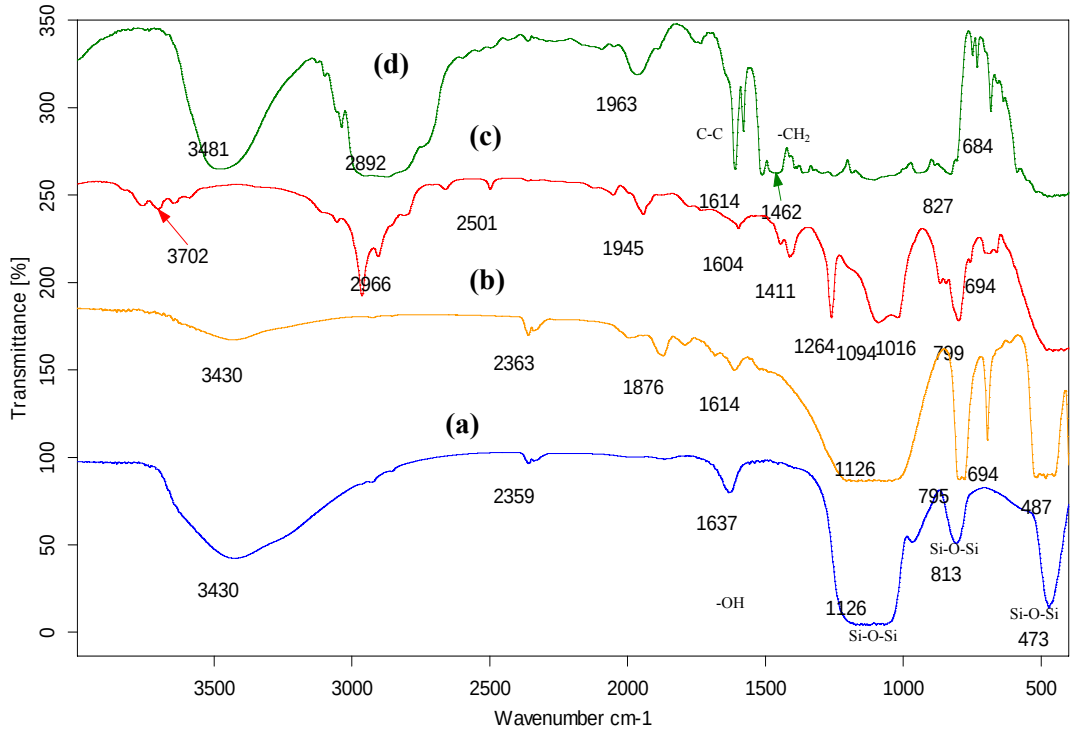

Figure 3.21 Transmission infrared spectra of the main components in the nanocomposite (a) nano fumed silica, (b) micro silica, (c) uncured RTV 615, and (d) Triton. Spectra (b)-(d) are shifted for clarity.

The nano fumed silica used in this research is a nonporous silica with a low bulk density and for which adsorbed water can be removed under vacuum at 293 K; nonetheless, drying of the filler is carried out at 423 K to remove trace impurities [62]. FTIR spectroscopy can be used to characterize the silica phase in the region from 3200 – 3800 cm^{-1}, corresponding to the νOH stretching mode of silanol groups [63]. Absorption bands can be identified in the silica spectra corresponding to free –OH (3746 cm^{-1}), geminal –OH (3742 cm^{-1}), and oxygen-perturbed –OH (3520 cm^{-1}) [64]. Unfortunately, the infrared absorption bands for the different types of silanol groups overlap with the signal for H_2O molecules adsorbed on silica

(3400-3500 cm^{-1}) [65]. Another infrared vibration for molecular water appears at 1625 cm^{-1}. Furthermore, the 3481 cm^{-1} absorption corresponds to the -OH vibration mode of Triton. Finally, in the spectrum of the nano fumed silica, the band at 1126 cm^{-1} corresponds to siloxane bonds (Si–O–Si).

Due to overlapping of the silanol groups with the signal for H_2O molecules adsorbed on silica, the technique described in Section 2.4.8 is preferred to determine the concentration of silanol groups in the fillers. In this method, the first step is the preparation of solutions of triphenylsilanol in carbon tetrachloride to obtain a calibration curve in the 4200-4800 cm^{-1} range, characteristic for the silanol group, as shown in Figure 3.22. The area under each of the peaks is calculated and fitted on to a linear plot as shown in Figure 3.23, verifying the proportionality of the area-concentration relationship according to the Beer-Lambert law [66].

The same types of solutions are prepared for each kind of filler for the analysis of their silanol group concentration. The FTIR spectra obtained for the nano fumed silica and the micro silica samples in the near IR region are provided in Figure 3.24 to Figure 3.27.

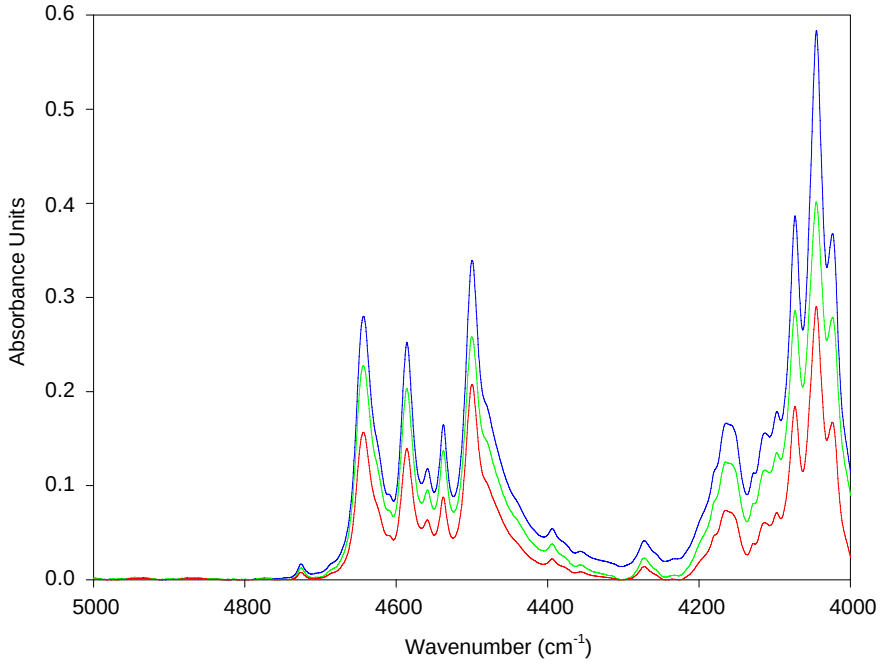

Figure 3.22 FTIR of triphenylsilanol and CCl_4 solutions.

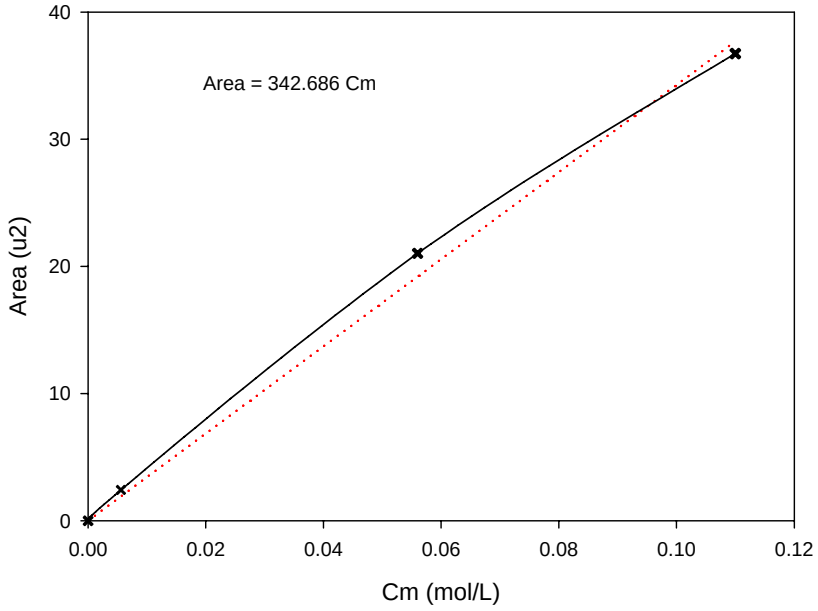

Figure 3.23 Calibration curve for triphenylsilanol solutions in CCl_4.

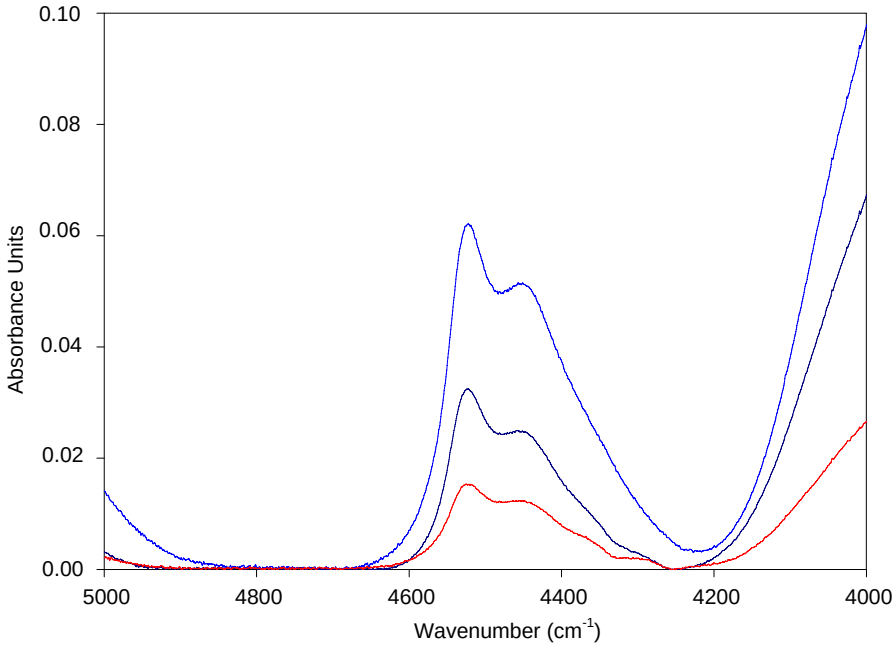

Figure 3.24 FTIR of nano fumed silica and CCl_4 solutions.

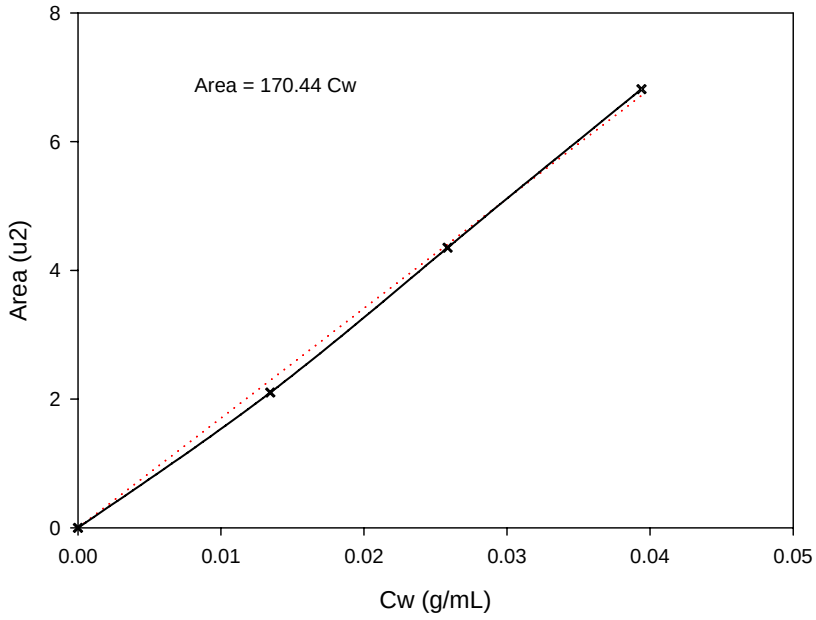

Figure 3.25 Absorption curve for nano fumed silica dispersions in CCl_4.

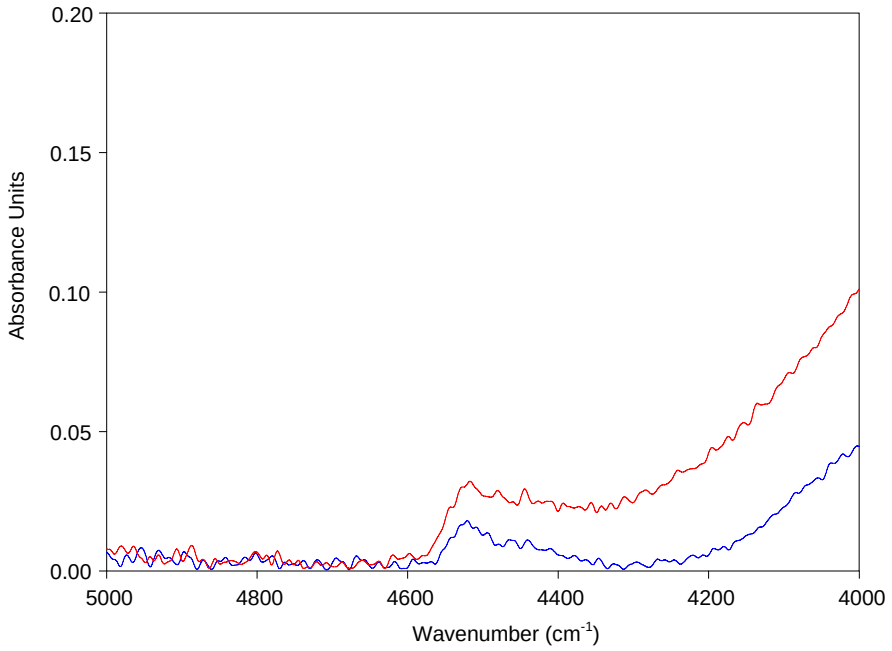

Figure 3.26 FTIR of micro silica and CCl_4 solutions.

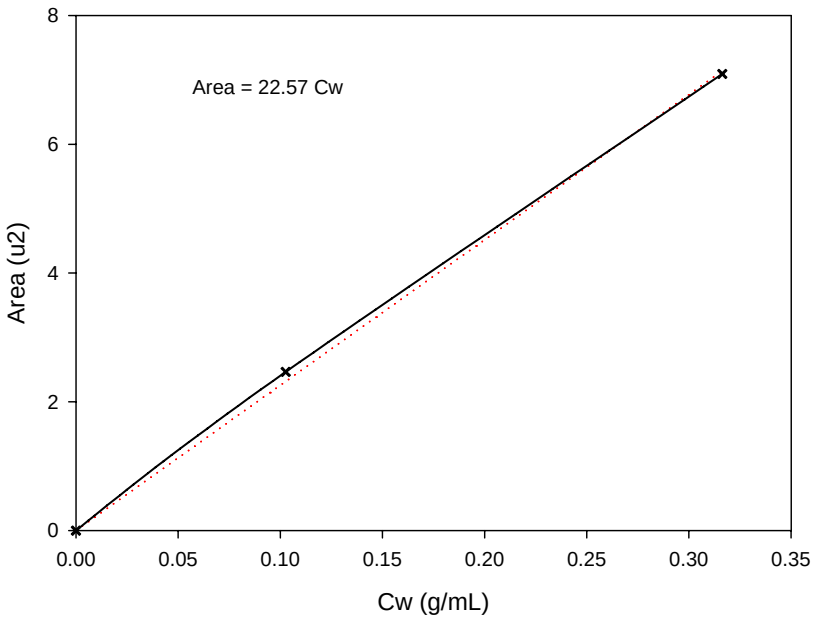

Figure 3.27 Absorption curve for micro silica dispersion in CCl_4.

The concentration of silanol groups in nano fumed silica is calculated as:

$$C = \frac{C_m}{C_w} = \frac{S/342.686}{S/170.44} = 0.4974\,mmol/g \qquad \textbf{3-1}$$

And the concentration of silanol groups in micro silica:

$$C = \frac{C_m}{C_w} = \frac{S/342.686}{S/22.57} = 0.06586\,mmol/g \qquad \textbf{3-2}$$

The ratio of silanol group concentrations for nano fumed silica/micro silica is therefore equal to 0.4974/0.06586 = 7.55.

To confirm the obtained ratio of 7.55 another organosilanol, namely *tert*-butyldimethylsilanol, is used to obtain a calibration curve in CCl_4; the results obtained are shown in Figure 3.28 and Figure 3.29.

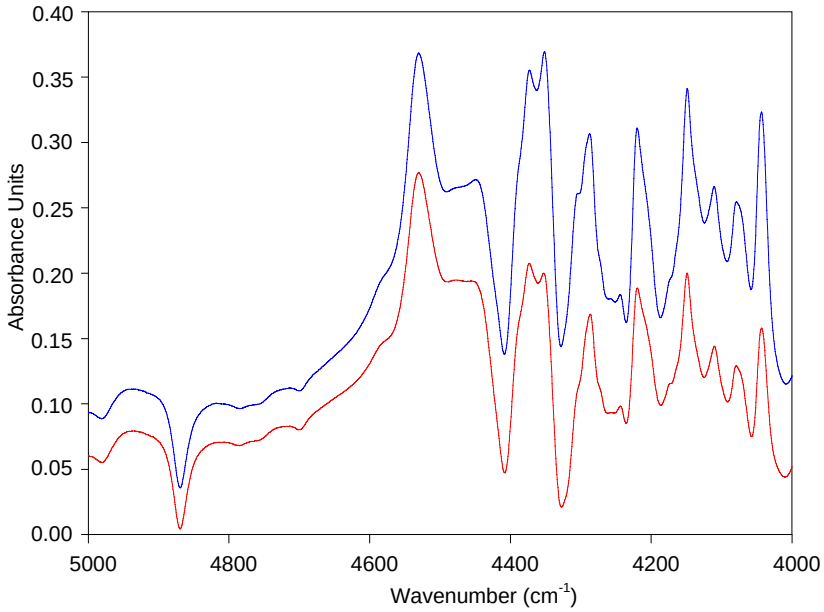

Figure 3.28 FTIR spectra of *tert*-butyldimethylsilanol solutions in CCl_4.

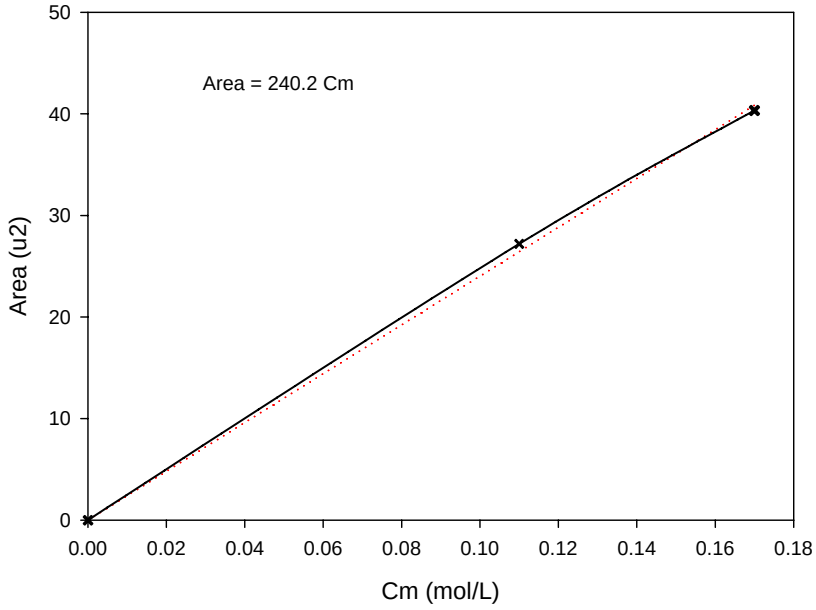

Figure 3.29 Calibration curve for *tert*-butyldimethylsilanol solutions in CCl_4.

The corresponding calculations using the *tert*-butyldimethylsilanol calibration are as follows:

Concentration of silanol groups in nano fumed silica:

$$C = \frac{C_m}{C_w} = \frac{S/240.2}{S/170.44} = 0.7095\,mmol/g \qquad \textbf{3-3}$$

Concentration of silanol groups in micro silica:

$$C = \frac{C_m}{C_w} = \frac{S/240.2}{S/22.57} = 0.09396\,mmol/g \qquad \textbf{3-4}$$

Ratio of silanol groups in nano fumed silica /micro silica = 0.7095/0.09396 = 7.55

So, the ratio of silanol groups in nano fumed silica/micro silica is 7.55 using both the triphenylsilanol and the *tert*-butyldimethylsilanol calibration curves.

The FTIR spectra obtained at the highest concentrations of nano fumed silica and micro silica used in the analysis are compared in Figure 3.30. The ratio of concentrations of silanol groups determined by FTIR spectra for nano and micro silica samples not subjected to calcination is 7.55. This means that per gram of filler, the concentration of silanol groups in nano fumed silica is about 7.55 times higher than in micro silica.

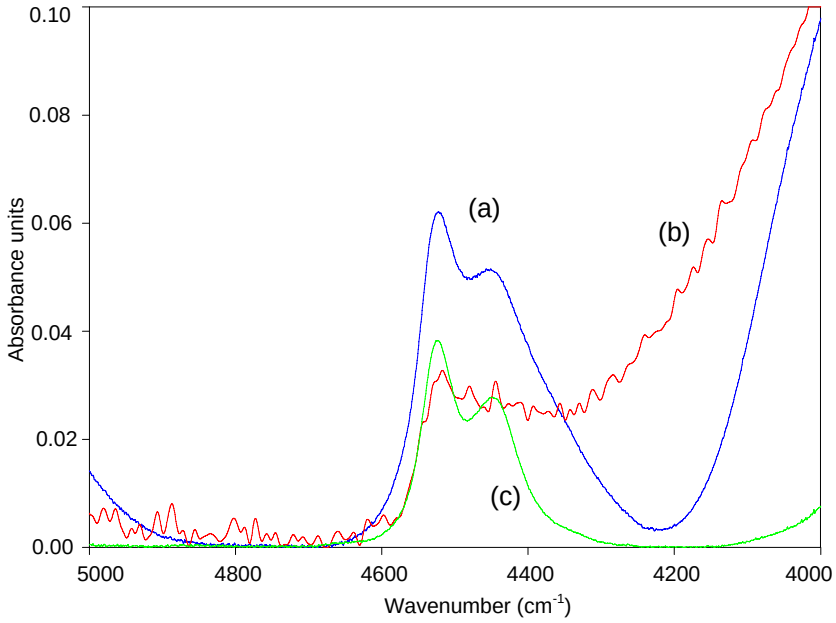

Figure 3.30 FTIR spectrum in CCl_4 for dispersions of (a) nano fumed silica (0.0394 g/mL), (b) micro silica (0.316 g/mL), and (c) nano fumed silica calcinated at 1173 K (0.0394 g/mL).

The large number of silanol groups on nano fumed silica originates from the manufacturing process used to obtain these materials. These silanol groups can form hydrogen bonds between the silica particles and the oxygen atoms of the polymer backbone in the SiR matrix

[67]. Because nano fumed silica has a larger number of silanol groups than micro silica, it interacts more efficiently with the polymer matrix. Although this physical interaction is not as strong as chemical (covalent) bonding, their large number makes the interactions significant. This explains the higher residual weight and the higher degradation temperature observed in TGA for samples filled with 2.5% nfs as compared to 2.5% micro silica (Figure 3.32 and Table 3.3).

Zhuravlev determined that the calcination of nano fumed silica reduces the number of silanol groups present on the surface of the filler [33]. For nano fumed silica calcinated at 1173 K, the absorption band for the silanol groups is indeed significantly weaker than for the non-treated nano fumed silica, as seen in Figure 3.30 when comparing curves "c" and "a", respectively, obtained at the same filler concentration. This explains the lower residual weight and the lower degradation temperature observed in the TGA tests (Figure 3.34), when comparing composites 20%m+2.5%nfs (1173 K)+14 pph T and 20%m+2.5%nfs (873 K)+14 pph T.

Hydroxyl groups are also found to play an important role in nanocomposites by Nelson *et al* [68] who noticed that the –OH group in nanocomposites has a significant influence on the cross-link density of an epoxy resin matrix filled with nano TiO_2.

3.2.3 Thermal Gravimetric Analysis

The thermal decomposition of silicone rubber can be induced by different chemical processes depending on the environmental conditions, and it can be related to the hydrolysis of siloxane bonds, the exchange of siloxane bonds, the oxidation of hydrocarbon groups making up cross-links, the oxidation of hydrocarbon side groups, depolymerization, the condensation of

silanol groups, and the formation of silica. These processes can lead to a decrease in the effective cross-link density, but TGA detects only weight losses due to the formation of cyclic compounds (depolymerization) and other gases resulting from the oxidation of hydrocarbon groups [69].

TGA measurements are first carried out for a sample formulation without surfactant, in order to establish baseline data. The residual weight observed for pure SiR without fillers and without surfactant is about 27%, which corresponds to silica formed by decomposition of the silicone matrix as shown in Figure 3.31. A sample containing surfactant displays a degradation temperature lowered by approximately 20 K and a residual weight of only 20%. This can be explained in part by the slightly lower amount of silicone rubber in the composites, but mainly by the influence of the surfactant on the curing reaction of the SiR.

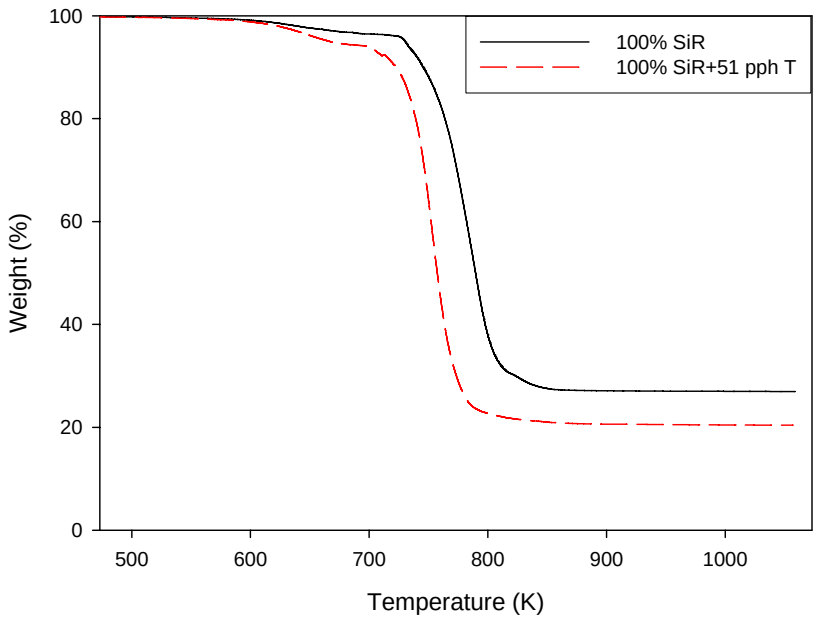

Figure 3.31 Thermal degradation of SiR with and without surfactant (pph concentration expressed with respect to a 2.5% wt filler content).

Composites filled with nano fumed silica, nano natural silica, and nanoalumina are also tested for comparison. It appears that nano fumed silica imparts greater thermal stability to the SiR matrix than the other fillers, as demonstrated by the lower slope and higher residual weight in the TGA curve shown in Figure 3.32. Nevertheless, the onset of thermal degradation is similar for all composites. This result is consistent with the eroded mass behaviour observed previously during the laser ablation tests; consequently, nano fumed silica is considered to be the best reinforcing filler.

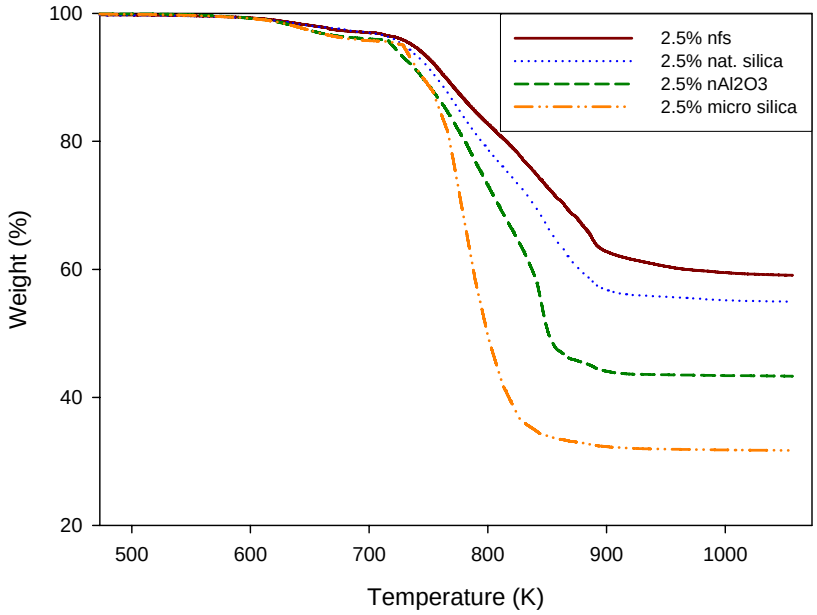

Figure 3.32 Thermal degradation of composites with different fillers.

The higher residual weight observed for the sample containing 2.5% nfs than for the one with 2.5% micro silica (and all the other fillers), as demonstrated in Figure 3.32, is attributed to the large number of silanol groups in that material. The composite with 2.5% nfs is prepared with different amounts of surfactant and shown (Figure 3.33). The addition of larger amounts of surfactant in the composite, for example 100 pph, results in a lower

residual weight; excess surfactant can thus have adverse effects on the mechanical and electrical properties of the composite.

The TGA results for composites combining micro silica and nano fumed silica fillers with 14 pph of surfactant are compared in Figure 3.34. Fumed silica calcinated at 573 K and 873 K gave identical results (curves exactly overlapping in Figure 3.34) and a residual weight of 55%, but the residual weight decreased to 49% for silica calcinated at 1173 K, as shown in Table 3.3. For the same composite (20%m+2.5%nfs (1173 K)+14 pph T), a lower value is also observed for the temperature at 75% of residual mass (824 K).

The differences in thermal stability observed as a function of the calcination temperature could be related to the physical interactions of the SiR chains with the silanol (Si–OH) groups on the silica surface, since the number of silanol groups left on the surface of silica is expected to decrease for higher calcination temperatures [33]. The interactions between the SiR matrix and the filler should be weaker under these conditions.

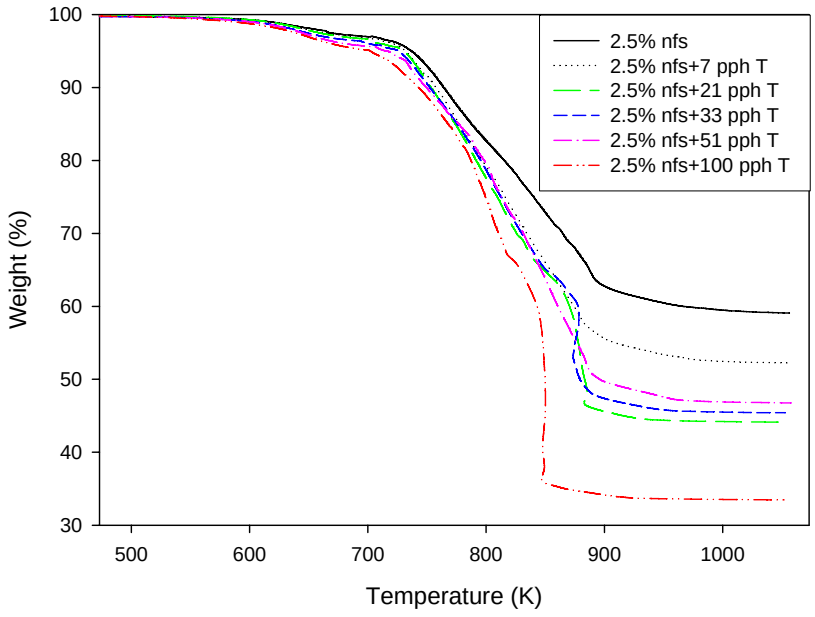

Figure 3.33 Thermal degradation of nanocomposites with different amounts of surfactant.

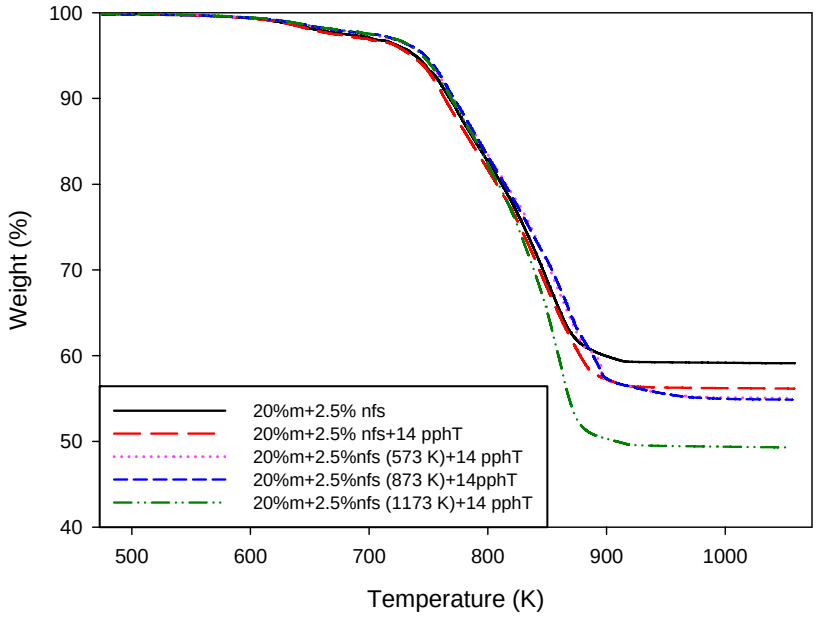

Figure 3.34 Thermal degradation of the SiR in combination with micro- nanofiller and surfactant.

In all cases the incorporation of fillers nonetheless increased the decomposition temperature of the matrix polymer, as shown in Table 3.3.

A mechanism previously suggested for the enhanced thermal stability of silica-filled SiR is the retardation of the depolymerization reaction by silanol groups on the filler [70]. The formulations with 14 pph of surfactant yielded improved heat stability for the nanocomposites, possibly because of enhanced filler dispersion.

Although an increase in the amount of surfactant used leads to a decrease in residual weight, as the surfactant affects the curing reaction of the silicone rubber matrix, higher degradation temperatures are obtained in most cases where surfactant is used. Another benefit of surfactant addition is the improved dispersion of the filler.

Table 3.3 Summary of thermal degradation temperatures.

Sample	Residual weight (%)	Important Temperature Points (K)		
		75%	50%	Final
100% SiR	27	769	790	805
100% SiR +51 pphT	20	744	757	781
2.5% nfs	59	838	---	905
2.5% natural silica	55	815	---	890
2.5%nAl_2O_3	43	793	863	880
2.5%micro silica	32	774	802	825
20%micro silica	54	815	---	857
20%m+2.5%nfs	59	829	---	872
20%m+2.5%nfs+14 pphT	56	826	---	883
20%m+2.5%nfs (573 K)+14 pphT	55	836	---	894
20%m+2.5%nfs (873 K)+14 pphT	55	834	---	900
20%m+2.5%nfs (1173 K)+14 pphT	49	824	---	874

The inclusion of nanofiller led to higher residual weights in all cases. This can be explained by the weight of the filler itself, but can also be linked to the interactions between the filler and the matrix. The same argument could be used when comparing residual weights for combinations of micro and nano silica fillers, since the surface density of silanol groups is higher in the nano fumed silica.

3.2.4 Inclined Plane Tests

The results for this test are shown in Figure 3.35. In practically all cases the addition of 14 pph of surfactant helped in obtaining a lower eroded mass. The composite with the lowest eroded mass is the formulation 20%m+2.5%nfs+14 pph; in Figure 4 it is barely discernible, due to the minimum eroded mass obtained.

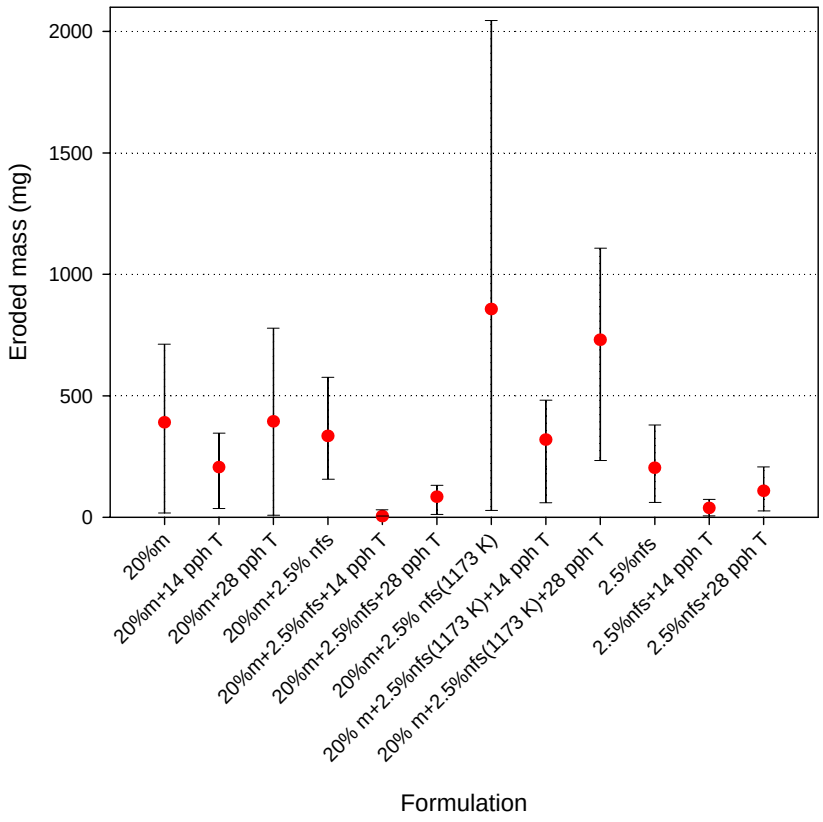

Figure 3.35 Average eroded mass after inclined plane test of six composites per formulation with micro silica, nano fumed silica loadings and Triton concentrations (expressed in pph of nanofiller by weight). The average eroded mass is represented by the dot; the 25th and 75th percentiles are represented by the horizontal lines of the bars.

In this test the nanofilled formulations with surfactant (2.5%nfs+14 pphT and 2.5%nfs+28 pphT) had a low eroded mass. The composites with higher eroded mass are the formulations

with calcinated filler, which could be due to the breaking of the siloxane bond caused by contact with water [62]. The eroded mass for the 20% micro filler composite is higher than that of the nanofilled formulation (2.5% nfs).

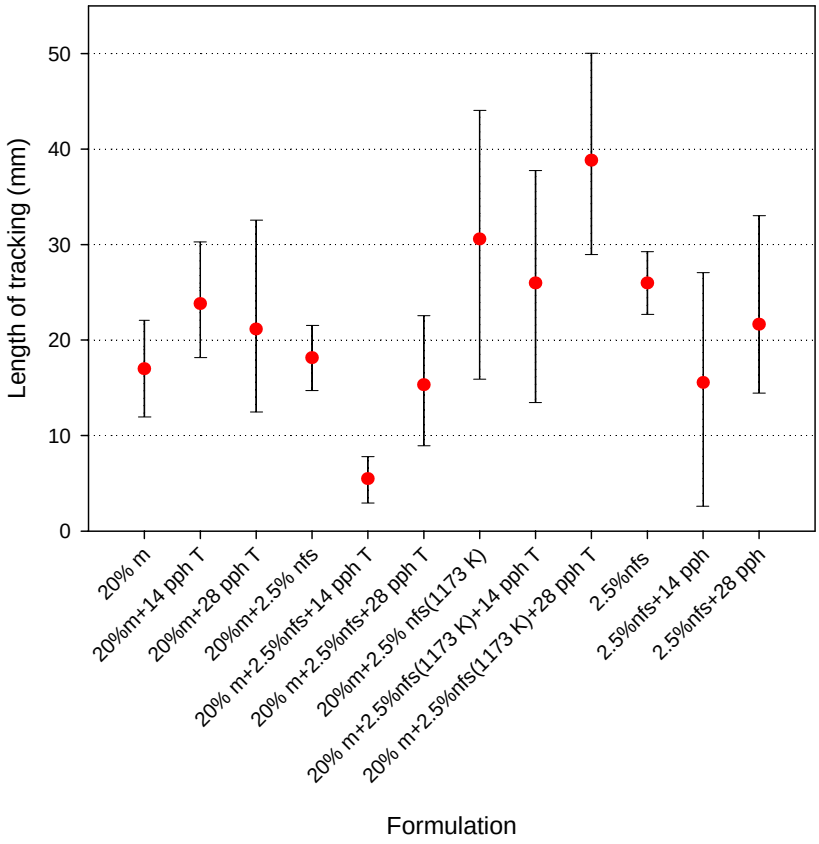

Figure 3.36 Length of tracking in inclined plane test of six composites per formulation with micro silica, nano fumed silica loadings and Triton concentrations (expressed in pph of nanofiller by weight). The average eroded mass is represented by the dot; the 25th and 75th percentiles are represented by the horizontal lines of the bars.

Concerning the length of tracking, the shorter tracking paths are obtained for the composites 20%m+2.5%nfs+14 pph and 20%m+2.5%nfs+28 pph, as shown in Figure 3.36. The higher tracking lengths are for the composites with nano calcinated fumed silica

[20%m+2.5%nfs(1173 K)]; similarly, these composites yielded highest eroded mass. The average length of tracking of composites with 20%m was quite similar to the formulation with 2.5%nfs+14pph T. The 2.5%nfs composite had higher length of tracking than formulation with 20%m.

3.2.5 Laser Erosion Tests

For all the tested composites, the eroded mass is lower when surfactant is used to disperse the nanofiller, which is likely due to improved dispersion of the particles. The resultant eroded mass for all the composites is shown in Figure 3.37.

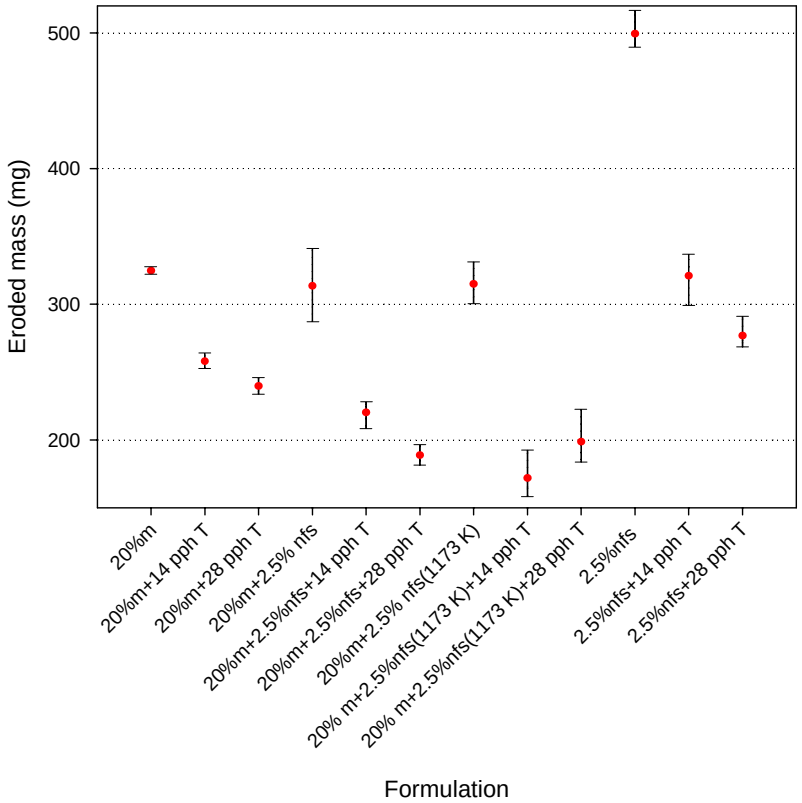

Figure 3.37 Average eroded mass after laser ablation test of three composites per formulation with micro silica, nano fumed silica loadings and Triton concentrations (expressed in pph of nanofiller by weight). The average eroded mass is represented by the dot; the 25th and 75th percentiles are represented by the horizontal lines of the bars.

The composites with the combination of micro and nanofiller (calcinated or non-calcinated) plus surfactant yielded lower eroded mass values. Among these, 20%m+2.5%nfs (1173 K)+14 pph T is the sample with the lowest eroded mass. Water is not involved in the laser ablation test, and consequently the siloxane bond remains stable.

3.2.6 Salt Fog Tests

The eroded mass in composites with 20% micro filler is 52% higher than the formulations with only 2.5% of nano fumed silica, as shown in Figure 3.38.

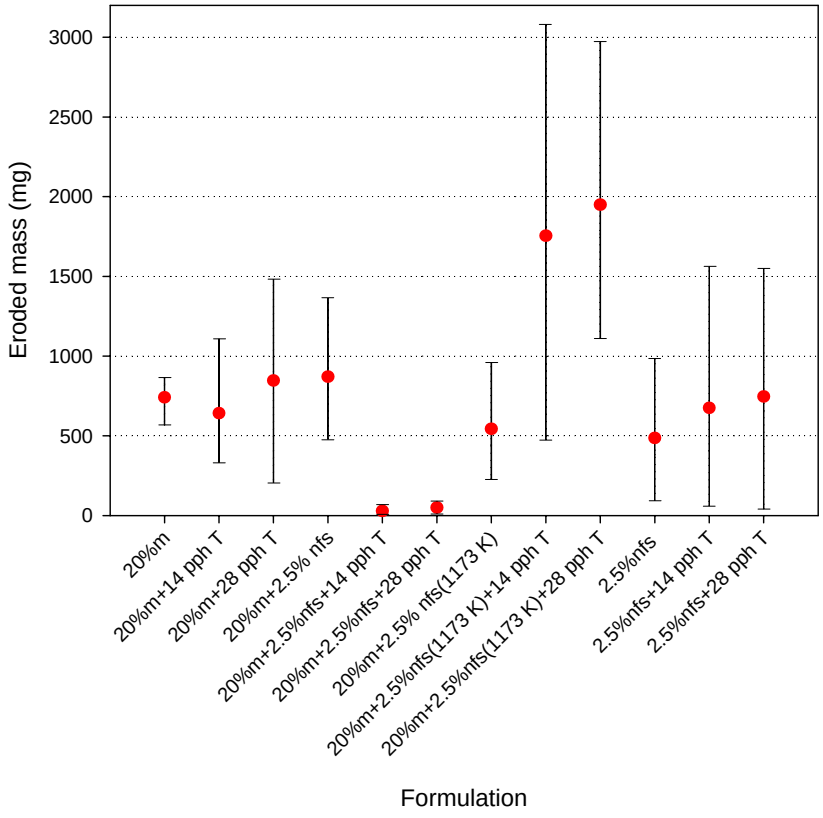

Figure 3.38 Eroded mass after salt fog test of four composites per formulation with micro silica, nano fumed silica loadings, and Triton concentrations (expressed in pph of nanofiller by weight). The average eroded mass is represented by the dot; the 25th and 75th percentiles are represented by the horizontal lines of the bars.

Eroded mass in composites with 20% micro filler is quite similar to the formulations with 2.5%nfs+14pph T and 2.5%nfs+28pph T. The formulations with lower eroded mass correspond to the samples containing micro and nanofillers plus surfactant (20%m+2.5%nfs+14 pph T and 20%m+2.5%nfs+28 pph T). On the other hand, the formulation with calcinated nanofiller resulted in the highest eroded mass among all formulations. It is hypothesized that this result comes from weaker bonding caused by the loss of silanol groups during calcination [33].

The nano fumed silica is calcinated at 1173 K; at this temperature there is little sintering, and the concentration of silanol groups is low. The surface of nano fumed silica can be considered to contain exclusively siloxane groups (Si – O – Si) under these conditions.

These siloxane bonds are hydrophobic from the point of view of physical adsorption of water, and this surface is unstable since these bonds can be broken gradually by contact with water molecules [62]. In the salt fog test these are always present on the surface of the composites.

The length of tracking is provided in Figure 3.39. The shorter tracking paths are obtained in the composites 20%m+2.5%nfs+14 pph T and 20%m+2.5%nfs+28 pph T; for these composites the eroded mass is also consistently lower when compared to the rest of the composites. In this case, the length of tracking of the 20% micro filler is larger than for the formulations with only 2.5% of nano fumed silica.

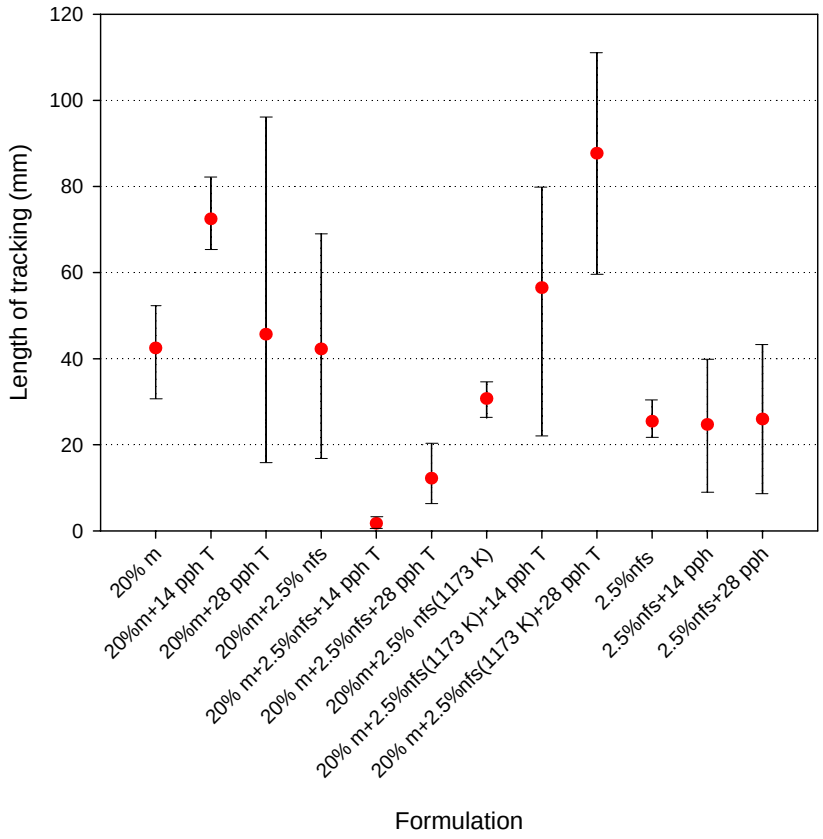

Figure 3.39 Length of tracking after salt fog test for four composites per formulation with micro silica, nano fumed silica loadings, and Triton concentrations (expressed in pph of nanofiller by weight). The average eroded mass is represented by the dot; the 25th and 75th percentiles are represented by the horizontal lines of the bars.

3.2.7 Contact Angle Measurements

The contact angle measurements obtained for flat composites are provided in Figure 3.40. With 14 pph of surfactant, the formulation 20%m+2.5%nfs is increased in 3° its average contact angle compared to the formulation without surfactant, while for 28 pph the average contact angle is diminished in 2° with respect to the sample with none; the addition of surfactant represents a variation in the contact angle of ±3% which is consider that will not affect the hydrophobic properties of the composites. For the formulation 2.5%nfs the

variation in the average contact angle is 3% with respect to the sample without surfactant. The composite with nano calcinated fumed silica shows an increase of 1% in the average contact angle.

It is speculated that excess surfactant not taken up by the filler migrates to the surface, thus affecting the contact angle. As suggested by Jeonggi *et al.* [47], the silicone rubber matrix releases the surfactant Triton upon contacting an aqueous solution, and this could be the reason for the decreased contact angle. On the other hand, the composite with nano calcinated fumed silica shows a slight increase in contact angle. Due to calcination of the filler, the adsorption properties may be different than for non-calcinated fillers.

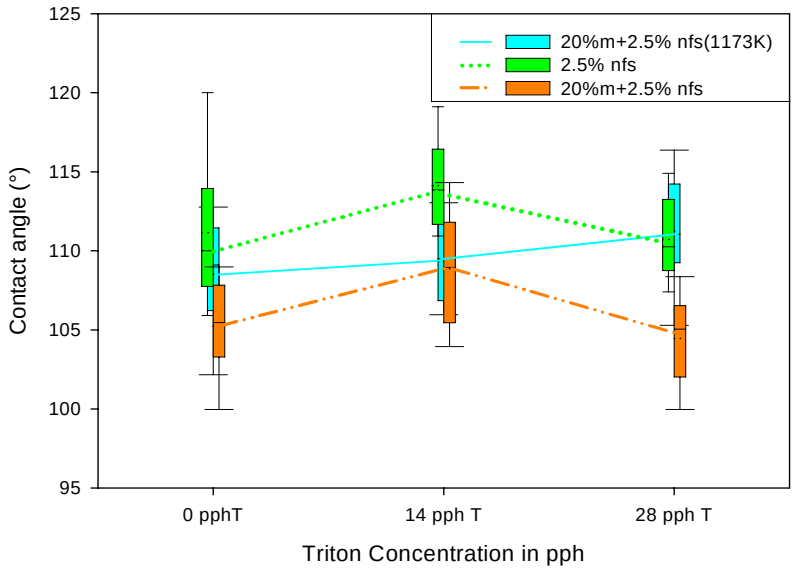

Figure 3.40 Contact angle in new flat composites for 3 different formulations. The average contact angle is represented by the horizontal line inside the box; the 25th, the median, and 75th percentiles are represented by the horizontal lines of the box. Error bars above and below the box indicate the 90th and 10th percentiles.

3.3 Measurement of Thermal Conductivity of Nanocomposites

3.3.1 Based on ASTM D5470

The results for the thermal conductivity (TC) of the composites are shown in Table 3.5. A lower thermal conductivity is obtained in the pure silicone rubber matrix. It is evident that the thermal conductivity increases as various amounts and types of filler are introduced into the matrix. In the same way, the addition of surfactant in the presence of nanofiller increases the thermal conductivity; a larger effect is particularly noticed in the sample with 28 pph of surfactant.

3.3.2 Based on Temperature Profile Measurements with Infrared Camera

As described in Section 2.5.2, the composites are irradiated for 3 minutes after which the laser is switched off. The temperature heating and cooling profiles are measured using the infrared camera for 3 minutes of heating and 2 minutes of cooling. Figure 3.41 shows the temperature profiles for each formulation. As expected, the unfilled silicone rubber sample reached the highest temperature during the test (482 K) whereas the maximum temperature for the nanofilled composite is slightly lower at 475 K. However, for the 20%m+2.5%nfs composite, the temperature is 445 K, 8% lower than for the unfilled sample. A similar temperature profile is obtained for all the formulations with 14 pph and 28 pph of surfactant.

The profile for the composite 20%m+2.5%nfs is shown in Figure 3.42. It is observed that in the cases where the surfactant is included, the maximum temperature reached by the composite during the laser ablation test is always lower than for the same composite without surfactant. This difference is attributed to better filler dispersion in the silicone rubber matrix.

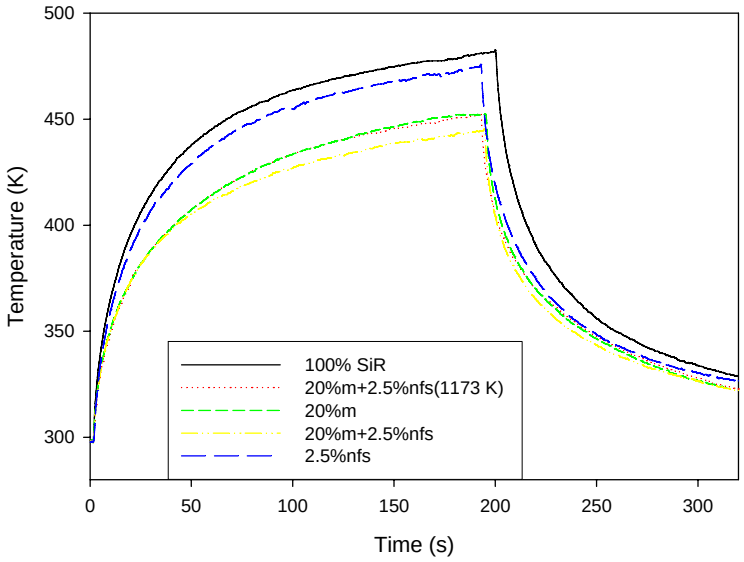

Figure 3.41 Temperature profile during laser test for composites without surfactant (nano fumed silica is calcinated at 1173 K in one formulation).

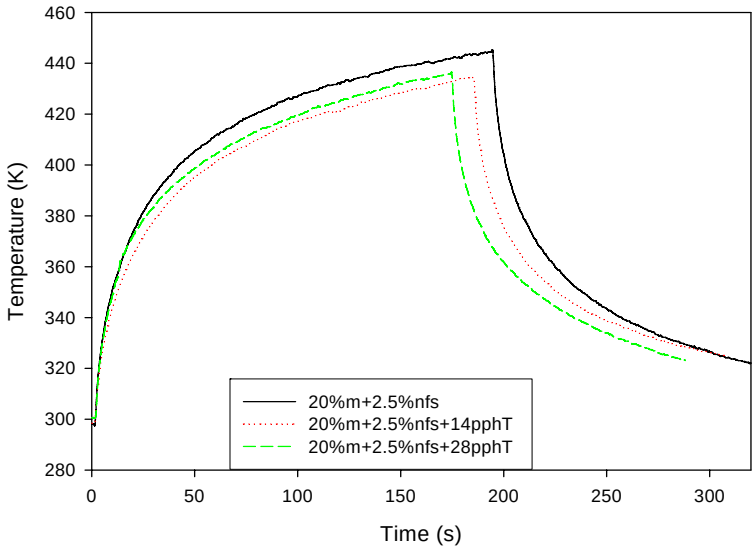

Figure 3.42 Temperature profile during laser test for composites 20%m+2.5%nfs without surfactant and with 14 pph or 28 pph of surfactant.

The surface temperature profiles on both sides of the laser beam are shown in Figure 3.43 for different composites. As expected, the maximum temperature is obtained in the unfilled sample and the lowest temperature is measured in the micro-nano filled composite.

Another measured temperature profile is shown in Figure 3.44 for the formulation 20%m+2.5%nfs with two concentrations of surfactant and without surfactant. The lowest temperature profile is obtained when surfactant is used, confirming the values of thermal conductivity calculated by the decay method.

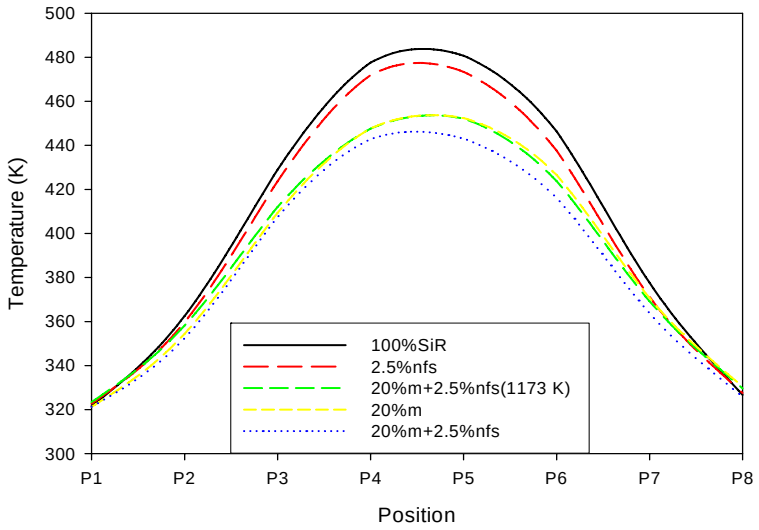

Figure 3.43 Maximum temperature along a line passing through the center of the composites and perpendicular to the laser beam (composites without surfactant).

Fitting of the temperature decay profile is done for each composite according to the procedure described in Section 2.5.2. The numerical values of TC are shown in Table 3.4, and the plots for more composites are provided in Appendix B. It is evident that the thermal conductivity of the composites increases with the amount of surfactant added. This behaviour is likely due to the improved distribution of filler achieved with surfactant. The composites

with the combination of micro and nanofiller (20%m+2.5%nfs) have the highest thermal conductivity of all the samples. This trend agrees with the results obtained according to the ASTM D5470 standard as shown in Table 3.5.

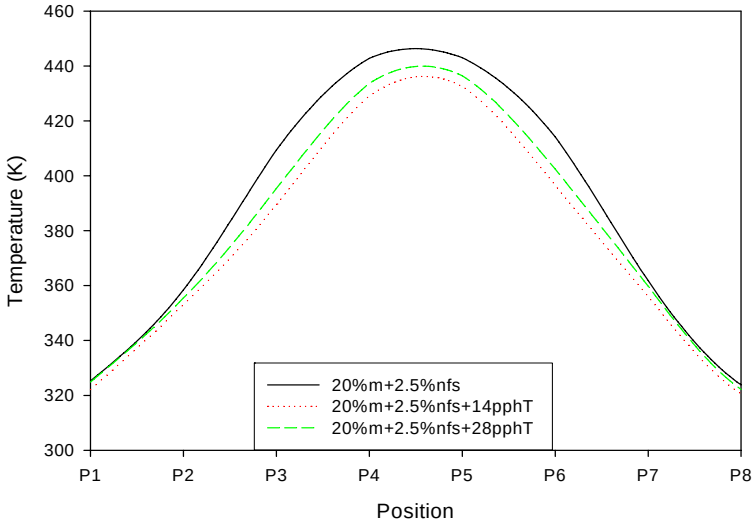

Figure 3.44 Maximum temperature along a line passing through the center of the composites and perpendicular to the laser beam (composites 20%m+2.5%nfs without and with surfactant).

Table 3.4 Thermal conductivity of composites with different amounts of surfactant by the decay profile technique.

Formulation	**Thermal conductivity (TC) (W/m K)**			**TC Average (W/m K)**
	Surfactant (pph)			
	0	**14**	**28**	
2.5% nfs	0.197	0.209	0.229	0.212
20% m	0.229	0.301	0.300	0.277
20%m+2.5%nfs	0.255	0.401	0.440	0.365
20%m+2.5%nfs(1173 K)	0.254	0.373	0.361	0.329

3.4 Calculation of Thermal Conductivity of Nanocomposites

3.4.1 Based on Theoretical Models

For comparison with the measured values, the results for the rule of mixtures, and for the Lewis and Nielsen models are included in Table 3.5.

For both models, the TC of the 2.5% nfs composite is very close to the value obtained using the ASTM D5470 standard with a maximum difference of 8%. However, for the 20%m formulation, the Lewis and Nielsen model yields a TC value 16.5% lower than that obtained with the standard. For the combination of nanofiller and microfiller (20%m+2.5%nfs), only the rule of mixtures can be used due to the variables in the model, and the calculation resulted in a TC value 2% higher as compared to the experimental value.

Table 3.5 Measured and calculated thermal conductivity of different formulations.

Formulation	Thermal conductivity (W/m K)			
	Measured	Calculated		
	ASTM D5470	Rule of mixtures	Lewis and Nielsen method	Proposed Model (steady state)
100% SiR	0.195	*	*	*
2.5% nfs	0.220	0.217	0.202	0.202
20% m	0.280	0.309	0.234	0.233
20%m+2.5%nfs	0.329	0.336	*	0.245[a] 0.247[b]
20%m+2.5%nfs+14 pph T	0.330	*	*	*
20%m+2.5%nfs+28 pph T	0.350	*	*	*

Notes: * No calculation possible.
(a) 3x3x3 cells, 1 micro particle and 8 nano particles in each cell.
(b) Circular arc with 1 micro particle and 29 nano spherical particles.

3.4.2 Using a Simplified Steady State Model of Dispersed Composites

As established in Section 2.6.2, the simulation of TC for 20% weight of micro silica is modelled with a cell of 9.06 μm on each side and one spherical micro silica particle of 65.45 μm^3, as shown in Figure 3.45 (a). Also, 3 x 3 x 3 cubic cells are stacked and analyzed as shown in Figure 3.45(b). Similarly, for a composition of 2.5% nano fumed silica, the same approach used in the micro filled composite is utilized, but in this case each side of the cell is calculated to be 0.64 μm.

The TC obtained for the nanofilled composite in the steady state model solved with COMSOL is in good agreement with the rule of mixtures, with the Lewis and Nielsen model, and with the measured values.

For the microfilled composite, the computed value with COMSOL is in good agreement with the Lewis and Nielsen model but not with the measured value and the rules of mixture model; the measured value was 16% higher than the modelled result. Whereas for the micro-nanofilled composite (20%m+2.5%nfs), it is not possible to model all the nanoparticles in the cubic cell. Therefore, two 3D cases studies are simulated, the first one with 1 micro silica particle in the centre of the cube and 8 fumed silica particles with a volume equivalent to the 2.5% weight of nanofiller aligned in the direction of each vertex as shown in Figure 3.46(a). After that, due to the limits on memory of the computer, a maximum of 3 x 3 x 3 cubic cells are stacked and analyzed as shown in Figure 3.46(b).

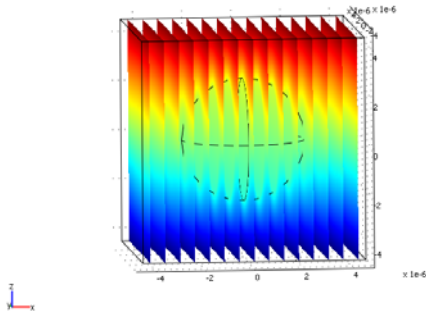

(a)

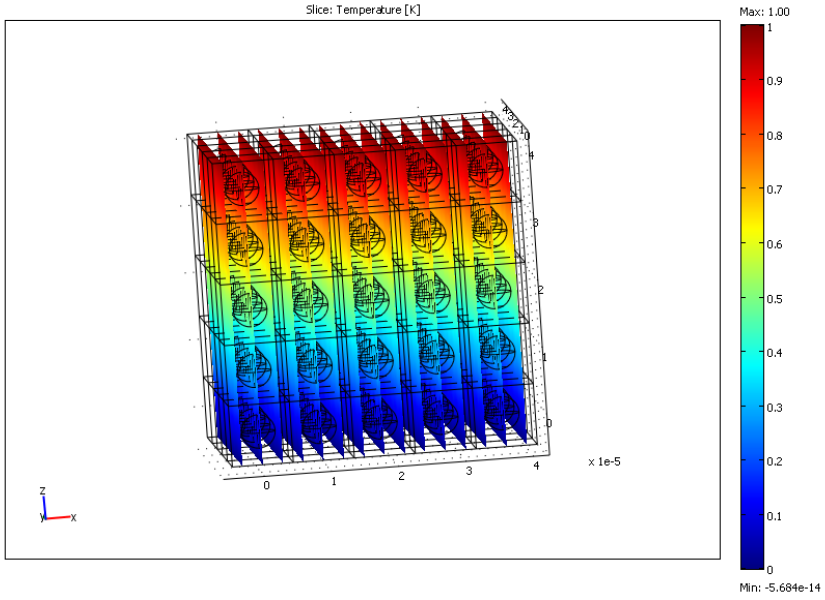

(b)

Figure 3.45 Temperature distribution of (a) One micro silica particle in a cell of 9.06 µm per side, (b) 125 micro silica particles inside of 125 cells (5 x 5 x 5 cells) of 9.06 µm per side.

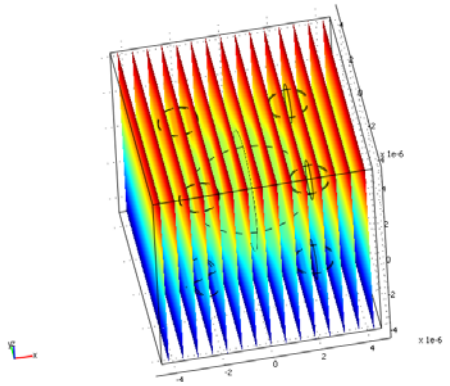

(a)

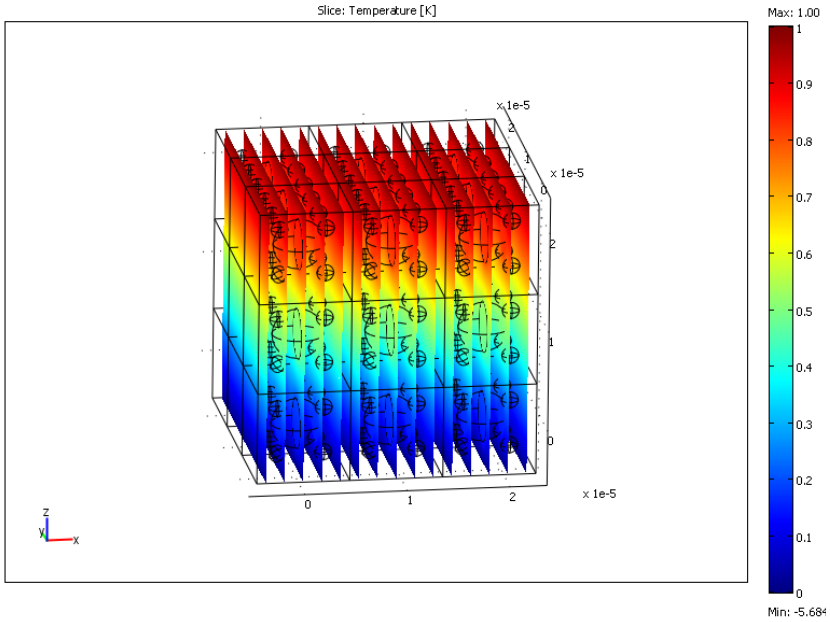

(b)

Figure 3.46 Temperature distribution in: (a) Basic cell with one micro silica particle and 8 nano silica particles into a cell of 9.06 μm per side and (b) Stack of 3x3x3 cells based on the basic cell mentioned in (a).

In the second case study, axial symmetry in the geometry is considered, and a cylindrical arc (3.6°) containing one slice of the micro silica particle in the center and 29 nano spherical

silica particles as shown in Figure 3.47(a). Also, it is used twenty-nine nano cylindrical silica particles as shown in Figure 3.47(b) distributed randomly in the arc for this simulation.

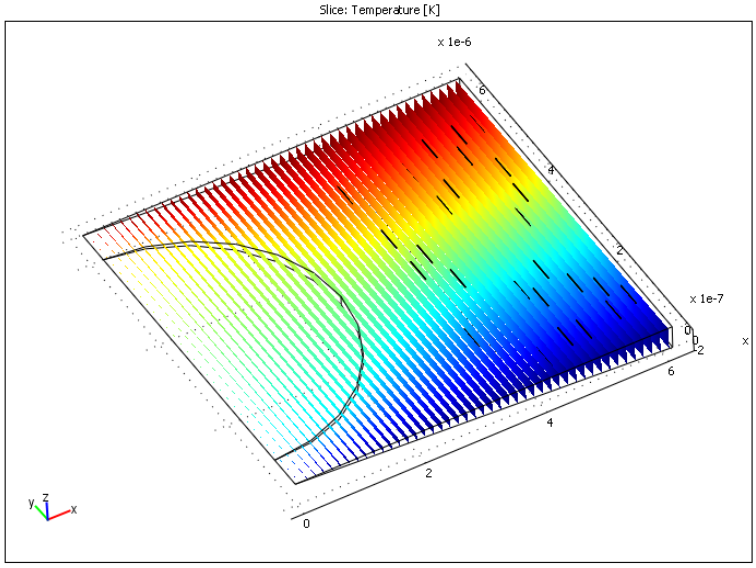

(a)

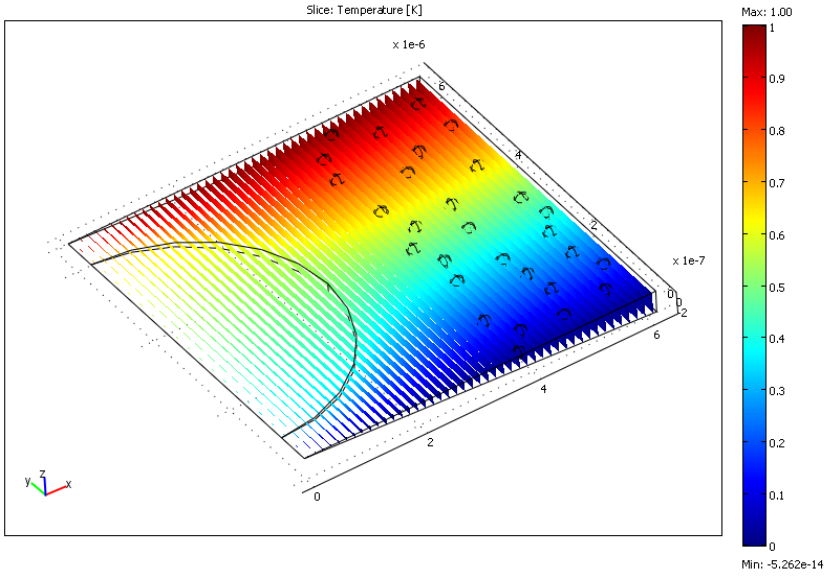

(b)

Figure 3.47 Temperature distribution in a cylindrical arc (3.6°) containing one slice of the micro silica particle and (a) 29 nano spherical silica particles or (b) 29 nano cylindrical silica particles.

In both case studies with the nano spherical or cylindrical fumed silica particles, the thermal conductivity obtained is approximately the same with a variation of less than 1%. However, the value obtained with COMSOL was 25% lower than the measured value.

It is important to note that in this modelling work the bonding between the matrix and filler could not be incorporated for the steady state model, even though it is an essential aspect of heat transfer. Without considering bonding, the interface between the filler and the matrix is basically a thin air space, thereby reducing the effective thermal conductivity of the particle [52].

3.5 Temperature Profile in the Composites Using a Simplified Transient Model

In this model, the heat transfer in a highly conductive layer is considered as a boundary condition to simulate a strong bonding interaction between the nanoparticles and the matrix. Without this consideration, the interface between the filler and the matrix is just a thin air space that reduces the effective thermal conductivity. Therefore, the resultant temperature profile is lower than that obtained in the experimental method without this boundary condition.

A 3D view of the temperature distribution in the upper part of the composite is shown in Figure 3.48 for the 20%m+2.5%nfs formulation. The maximum temperature is obtained in the center where the laser beam impinges the composite. The simulated temperature profile for a cross section of the cylindrical model is shown in Figure 3.49 for each of the analyzed formulations. It is evident that the heat penetration into the composite is reduced with the

introduction of filler and that the minimum temperature is obtained when the composite has microfiller and nanofiller.

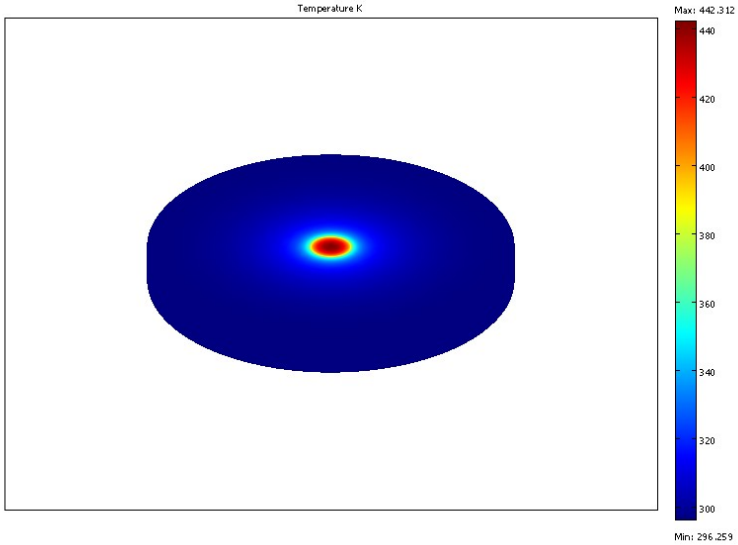

Figure 3.48 Temperature distribution for sample 20%m+2.5%nfs during modelled laser test.

The steepness and decay of the temperature profile is obtained from the temperature profile simulation as well. Figure 3.50 shows the heating and cooling profile of the different composites.

From the temperature profile simulation, the temperature across a line passing through the center of the composites is shown in Figure 3.51. The maximum developed temperature is obtained in the non-filled sample. The effect of the filler is demonstrated as the temperature is decreased in the filled formulations, as can be seen in Figure 3.51; the lower temperature is obtained in the micro-nanofilled composite.

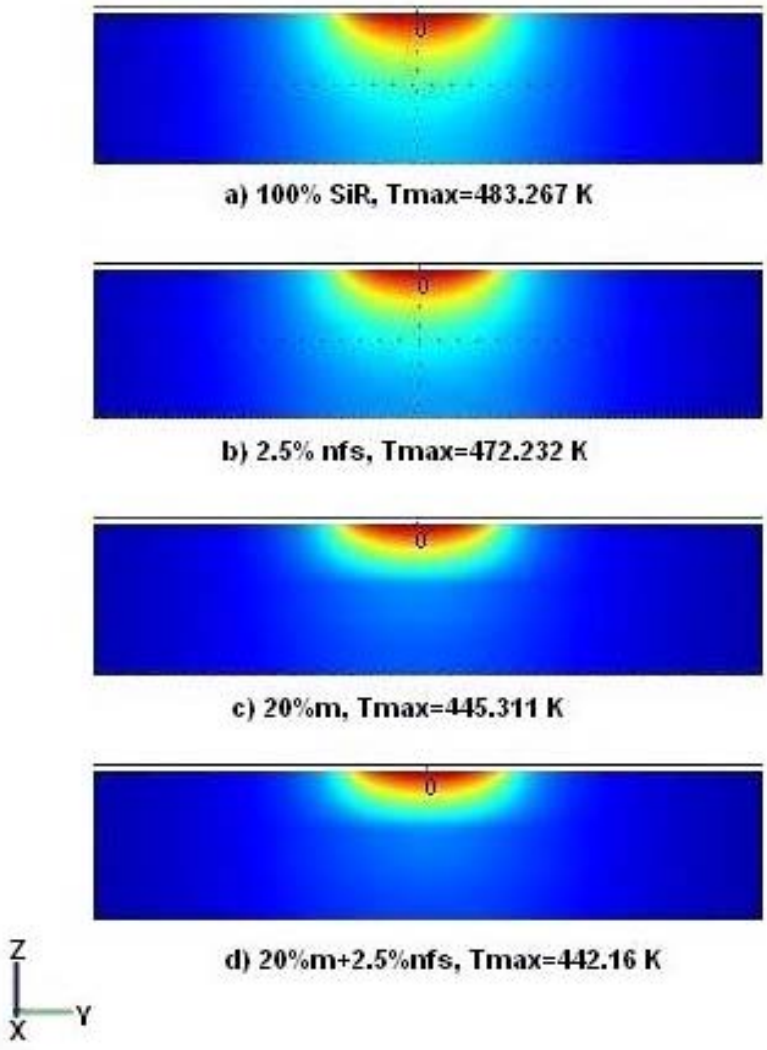

Figure 3.49 Simulated temperature profiles for different composites in a cross section of the center of a cylinder 36 mm in diameter during a laser test.

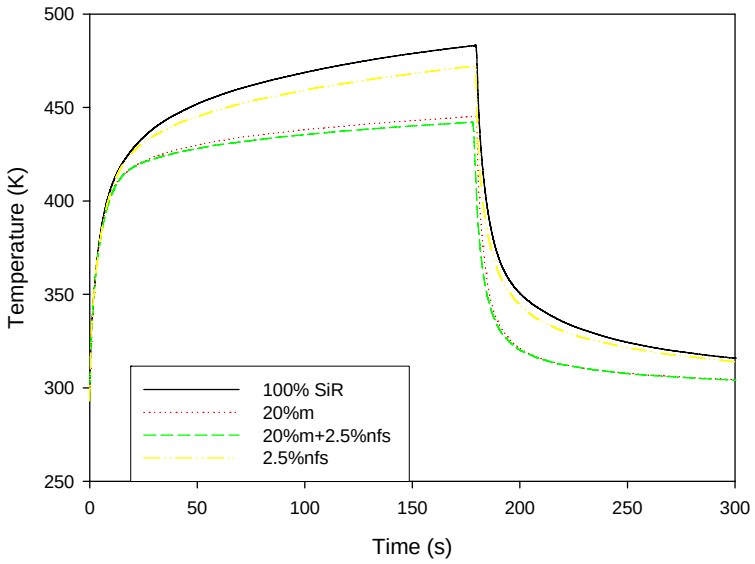

Figure 3.50 Simulated maximum temperature profile in the center of the cylinder during laser test (composites without surfactant).

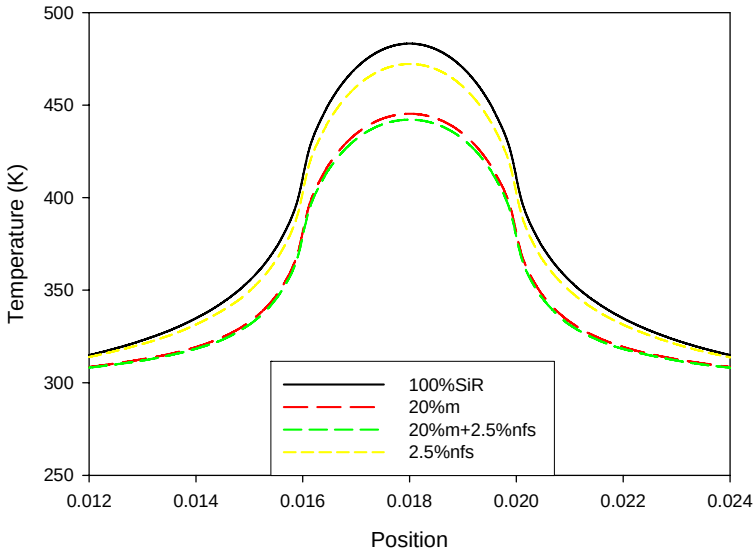

Figure 3.51 Simulated maximum temperatures along a line passing through the center of the cylinder (composites without surfactant).

Chapter 4

Discussion

Various tests are done with micro-nanofilled silicone composite formulations to shed light on the mechanism by which the combination of nano and micron size fillers improves the erosion resistance of the composites. It is shown in Section 3.1.2 that the surfactant is essential for this improvement; without it, no improvement is evident. It is shown that the large specific surface area of nanofillers favours strong physical and chemical interactions with the polymer matrix and that the silanol groups participate in these interactions [71]. The interactions are presumably hydrogen bonding between the silanol groups of the nanofiller surface and the siloxane linkages in the polymer matrix [62].

4.1 Improved Dispersion of Nanofiller with Surfactant

The results presented in Chapter 3 concerning the surface treatment of the nanofiller with different surfactants and solvents, conducted to obtain an improved dispersion of nanofillers, demonstrated that the surfactant Triton was beneficial. Surfactants are often viewed as having two parts, namely, hydrophilic and hydrophobic chain segments combined in the same molecule. Inorganic fillers are mainly hydrophilic in nature, and this characteristic facilitates their interaction with the hydrophilic portion of the surfactant. When the hydrophilic end of the surfactant is adsorbed on the filler particles, the hydrophobic group orients itself towards the silicone rubber matrix. Most researchers agree that SiR is physically adsorbed on the silica surface, although the exact mechanism remains an open question [72]. The surfactant thus lowers the surface energy of the filler and the interfacial

tension between the particles and the matrix, thereby facilitating the separation and improvement in the dispersion of the particles during high shear mixing.

It is shown that nonionic ethoxylated surfactants and poly(ethylene oxide), which have the same chemical composition as the polar component of the Triton surfactant, are efficiently adsorbed on the surface of silica particles [39]. Fumed silica has also been used to scavenge Triton from aqueous solutions for the same reason [32], so there is significant affinity between fumed silica and Triton. While other surfactants could be used for the purpose of dispersing the nanofiller, non-ionic surfactants such as Triton are certainly preferable because of the absence of ionic components. The presence of ionic components may contribute to conduction in the bulk, which is obviously an undesirable property for electrical insulation. The adsorption is considered to originate from hydrogen bonding rather than electrostatic interactions. Hydrogen bonding can occur between the oxygen atoms of the surfactant and the silanol groups of silica [62, 73]. However, some groups of nonionic surfactants can also exhibit minimal adsorption on silica. Since cationic surfactants are adsorbed due to electrostatic interactions, it is preferable to avoid them because of their ionic nature. On the other hand, anionic surfactants do not absorb on silica due to the similar charge on the solid and the adsorbate [62].

A high concentration of surfactant compromises the adsorption of the matrix material on the filler particles, as demonstrated in the mechanical tests. So, it is necessary to use an optimal amount to establish a balance between matrix adsorption and the dispersion of the particles.

It appears that composites containing considerable amounts of surfactant will have wetting properties different from those containing none. Better wetting due to migration of the

surfactant to the surface of the insulator may favour arcing in a wet environment. However, it should be pointed out that the best performance improvements have been obtained at relatively low surfactant concentrations, of around 20 pph with respect to the nanofiller. Problems associated with the potential migration of the surfactant to the surface of the composite are much less likely under these conditions, and this issue is confirmed in the salt fog tests shown in Figure 3.38.

4.2 Effect of Surfactant on Mechanical Properties

The large specific surface area of nanofillers favours strong physical and chemical interactions with the polymer matrix; consequently, the adhesive forces between the filler and the matrix are increased. The mechanical strength of the matrix is thus improved if the particles are well dispersed throughout the composite. At high filler concentrations, agglomeration can occur due to strong interactions between the nanoparticles. This can lead to a decrease in strength as filler content increases. It is shown that the addition of Triton greatly improved the dispersion of nanofillers in silicone rubber as well as the erosion resistance of the nanocomposites. The optimal amount of surfactant needed for enhanced resistance to erosion appears to be in the range of 14 – 28 pph for the nano fumed silica used in this thesis. With respect to mechanical properties, at surfactant concentrations above the saturation level for the filler surface (100 pph in the current case), a reduction in the average tensile strength by about 60% was found with respect to the composites without surfactant. A drop in Shore-B hardness by around 24% has been observed for composites containing 100 pph of surfactant as shown in Table 3.2. However, for composites with 28 pph and 14 pph of surfactant, the drop in hardness is only 6.5% and 1.6% respectively. From these results it is clear that the mechanical properties are not affected by a low concentration of surfactant. It is

recommended to use 14 pph of surfactant, which does not affect the hardness of silicone composites significantly.

This demonstrates that a proper amount of surfactant should be added in order to not impair the mechanical properties of the nanocomposites.

4.3 Influence of Silanol Groups in Micro and Nanofillers

The concentration of silanol groups per gram of filler is found to be about 7.5 times higher in nano fumed silica than in micro silica. For a 100 g sample of the 20%m+2.5%nfs formulation, using the silanol group concentrations reported in Section 3.2.2, the number of silanol groups present on each component is calculated as follows:

$No.\ of\ silanol\ groups = 20\,g \times 6.586 \times 10^{-5}\,mol/g \times 6.022 \times 10^{23}\,Si-OH/mol = 7.95 \times 10^{20}$ in micro silica, and

$No.\ of\ silanol\ groups = 2.5\,g \times 4.974 \times 10^{-4}\,mol/g \times 6.022 \times 10^{23}\,Si-OH/mol = 7.48 \times 10^{20}$ in nano fumed silica.

This means that 2.5 g of nanofiller in the 100-g sample contributes approximately the same number of silanol groups interacting with the matrix polymer as 20 g of microfiller. The interactions present between the surface of the nanofillers and the SiR matrix are presumably hydrogen bonding of the siloxane linkages in the polymer matrix with the silanol groups on the silica surface [62, 74]. The stability of the nanocomposites at higher temperatures is decreased when the fillers are thermally treated at 1173 K, since this also reduces the number of silanol groups present, as shown in Figure 3.30.

Triton, within the concentration range used in the current investigation, is shown to yield improved dispersion of filler particles within the SiR matrix. Consequently, the influence of thermal treatment on the mechanical and thermal properties can be explained only by weaker filler-matrix interactions upon dehydration of the silanol groups at high temperatures.

4.4 Thermal Stability of the Composites

The TGA evaluations showed in all cases that the incorporation of fillers increases the decomposition temperature of the matrix polymer. However, it appears that nano fumed silica imparts greater thermal stability to the SiR matrix than other fillers at the same concentration by weight of microfiller. The difference is attributed to the larger number of silanol groups in nano fumed silica.

The differences in thermal stability observed as a function of the calcination temperature of the filler could be due to the lower number of silanol groups left on the surface. The interactions between the SiR matrix and the filler should be weaker under these conditions.

The formulation with 14 pph of surfactant yields improved heat stability for the nanocomposites. The addition of surfactant also improves the thermal conductivity of the composites, but with the nanofiller alone no improvement is detected. According to Irwin *et al.*, the thermal conductivity of their polyamide films increased only if the nano particles were surface-treated [17]; however, for Leng *et al.* the use of an epoxy compound as a dispersing aid worsened the thermal properties of their composites [75]. This contradiction points out that each system has its own characteristics, and each system must be evaluated separately.

4.5 Performance of composites in Salt Fog Chamber, Inclined Plane, and Laser Ablation Tests

Figure 4.1 summarizes the average eroded mass in the salt fog, inclined plane, and laser tests. As can be seen in the figure, the lower eroded mass is obtained for the composition 20%m+2.5%nfs+14pph T in the salt fog and inclined plane tests. Due to the lower eroded mass for this composite in the laser tests, only 5.2 mg, another plot is provided in Figure 4.2 using a logarithmic scale for the eroded mass axis.

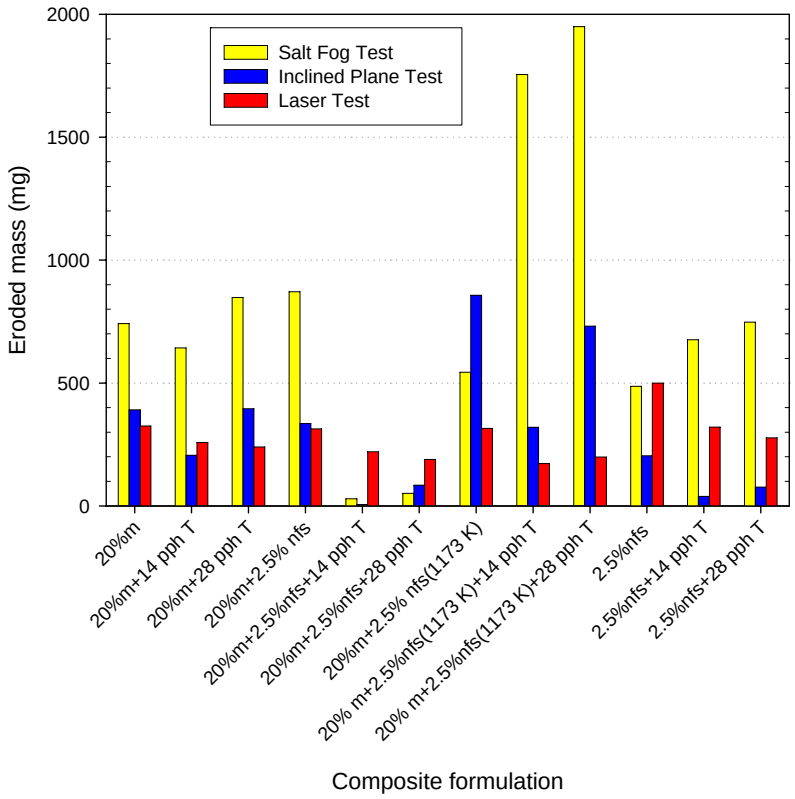

Figure 4.1 Average eroded mass on a linear scale for three kinds of tests and different formulations.

It is clearly seen that the formulation with calcinated filler has the highest eroded mass in the salt fog test and also in the inclined plane test.

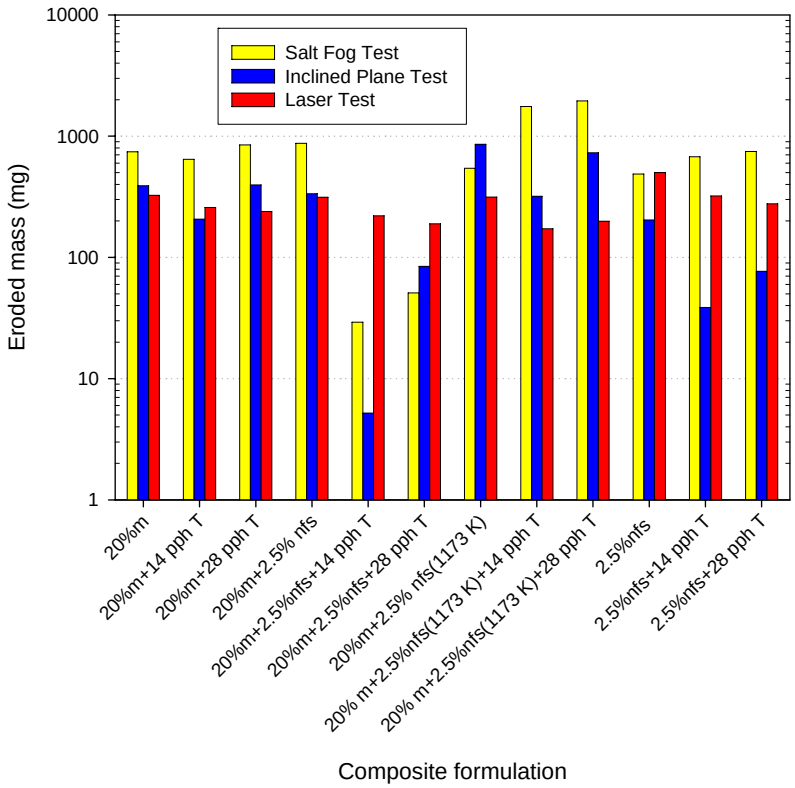

Figure 4.2 Average eroded mass on a logarithmic scale for three kinds of tests and different formulations.

The effect of the surfactant improves the composites in 18 out of 24 of the analyzed formulations. The addition of 14 pph is beneficial in 10 out of 12 different composites in the complete set of performed tests compared to those without any surfactant. This result is attributed to an improved dispersion of the filler in the composites. The addition of 28 pph of surfactant results in improvement in 8 out of 12 composites in the complete set of performed tests compared to those without any surfactant. The addition of 28 pph of surfactant causes

slightly higher eroded mass in 9 out of 12 cases compared to 14 pph for the salt fog and inclined plane tests. On the other hand, for the laser test the addition of 28 pph of surfactant results in lower eroded mass for 3 out of 4 formulations compared to the addition of 14 pph.

Correlation analysis is done to examine the relationship between the eroded mass among the three test methods. The analysis provides a dimensionless index ranging from -1.0 to 1.0, reflecting the extent of a linear relationship between the eroded mass obtained by each of the test methods. A positive correlation between the eroded mass data sets is determined if large values of eroded mass obtained in one test method tend to be associated with large values of eroded mass obtained in another test method. A negative correlation is obtained if small values of eroded mass in one test method tend to be associated with large values of eroded mass in the other test method. If the correlation is near zero, the values of both data sets of eroded mass tend to be unrelated. According to Cohen [76], a weak correlation is obtained if the absolute value of the coefficient is approximately 0.1; a medium correlation is 0.3, and a strong correlation is 0.5 or greater.

The results of the correlation analysis are shown in Table 4.1. As is evident from the table, for the formulation 20%m+2.5%nfs, the correlation is positive between all three test methods. In the case of the nanocomposite 2.5%nfs, the correlation coefficient is positive in the inclined plane - laser ablation tests but negative in the other tests. For sample 20%m+2.5%nfs (1173 K) the correlation is closer to 1 in two cases, and the remaining case is closer to 0.58. For the formulation 20%m, the correlation coefficients are -0.221 and 0.294 (weak to medium correlation), and 0.867 in the salt fog - inclined plane tests, showing a strong correlation here.

Only in 6 out of 12 cases the coefficients are closer to 1, showing a good correlation between all three test methods specifically for the 20%m+2.5%nfs composite. Moreover the salt fog, inclined plane, and laser ablation tests complement each other to evaluate the best composite which corresponds to the combination of micro-nanofiller and surfactant without thermal treatment of the fillers.

Table 4.1 Correlation factors among eroded mass obtained from salt fog, inclined plane, and laser ablation tests.

Formulation	**Correlation factor (-1≤0≤1) between**		
	Salt Fog - Inclined Plane	**Salt Fog - Laser Ablation**	**Inclined Plane - Laser Ablation**
20%m	0.867	-0.221	0.294
20%m+14 pph T			
20%m+28 pph T			
20%m+2.5% nfs	0.978	0.965	0.889
20%m+2.5%nfs+14 pph T			
20%m+2.5%nfs+28 pph T			
20%m+2.5% nfs(1173 K)	-0.582	-0.954	0.800
20%m+2.5%nfs(1173 K)+14 pph T			
20%m+2.5%nfs(1173 K)+28 pph T			
2.5%nfs	-0.883	-0.997	0.917
2.5%nfs+14 pph T			
2.5%nfs+28 pph T			

The reinforcing of the 20%micro-filled composition with 2.5% of nanofiller and 14 pph of surfactant results in the composite with the lowest eroded mass in the salt fog and inclined plane tests; this improved composite theoretically has twice the number of silanol groups.

In the case of the composite with nano calcinated fumed silica, a lower eroded mass is obtained in the laser ablation test when compared to the eroded mass obtained in the salt fog test. A similar performance is obtained if the eroded mass from the laser test is compared with the eroded mass from the inclined plane test. The performance of the nano calcinated fumed silica can be explained if it is assumed that siloxane bonds are unstable due to calcination at 1173 K, and that these bonds can be broken by contact with water molecules present in the inclined plane and salt fog tests. Furthermore, the removal of silanol groups from the nanosilica surface by calcination results in weaker interactions with the filler and the silicone polymer matrix.

In relation to the contact angle issue, in the work of Seo *et al.* [47], samples containing cross linked silicone rubber and different amounts of the surfactant Triton X-100 (up to 3% in weight of surfactant) led to diminishing dynamic contact angles down to 70°. Additional experiments showed that the surfactant was released from cross linked silicone rubber upon contact in an aqueous solution. However, in these samples no filler was included; consequently, the effects of the filler on the contact angle measurements and in the release of surfactant from the bulk were not considered.

In this work, 20% of micro silica and/or 2.5% of nano fumed silica are included in the composites, and due to the fact that the surfactant has been found to adsorb on silica [62], the addition of surfactant at low concentrations (maximum 0.7% in weight used in this thesis) does not significantly affect the contact angle, as demonstrated by the measurements of the

contact angle shown in Figure 3.40. Instead, the surfactant enhances the dispersion of the nanofiller in the matrix, as demonstrated with scanning electron microscopy measurements, and surfactant makes the composite more resistant to pyrolysis.

4.6 Interaction of Nano fumed Silica and Surfactant in a Polymer Matrix

The interaction mechanism proposed for improved dispersion of the nano fumed silica in the presence of surfactants is as follows: The nano fumed silica is hydrophilic; this characteristic facilitates the interactions with the hydrophilic poly(ethylene oxide) segment of the surfactant. When the surfactant is adsorbed, the hydrophobic group orients itself towards the silicone rubber matrix, exposing the hydrophilic group to nano fumed silica as shown in Figure 4.3. The surfactant lowers the surface or interfacial tension between the nanofiller and the silicone matrix. This lowering of the interfacial tension makes it easier to separate the particles during mixing, thereby allowing improved dispersion of the nanofillers.

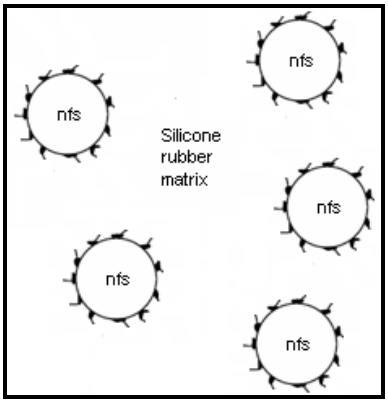

Figure 4.3 A simple adsorption model of non ionic surfactant on nano fumed silica in SiR matrix.

The adsorption of polymer chains on the surface of filler particles usually gives rise to the formation of loops [77]; the aggregates are then connected to one another by these loops [62]. Also, because of the large specific surface area of the nano fumed silica particles, their interactions in the SiR matrix restrict the mobility of the chains [78] and form a tightly bound polymer network [79]. Because of these effects, enhanced interactions are present between the filler and the SiR matrix when nanoparticles are used in addition to microfillers.

After calcination of the nanosilica at a high temperature (1173 K), the concentration of silanol groups is low, reducing the adsorption of the surfactant on the nanosilica surface; consequently, the effectiveness of the surfactant is decreased. It can be considered as nano fumed silica with only siloxane groups (Si – O – Si) on the surface, because the adsorbed water is removed at a much lower temperature. These siloxane bonds are hydrophobic from the point of view of water physisorption, and such a surface is unstable since these bonds can be broken gradually through contact with water molecules [62]. At temperatures lower than 473 K, calcination helps because it destroys the aggregates and pellets of nanoparticles.

4.7 Protective Mechanism of Nanofillers for Improved Resistance to Dry Band Arcing

During the laser ablation tests of nanofilled composites with a silicone rubber matrix, it was noticed that a white deposit develops in the impinged surface of the composites at higher surfactant concentrations. In order to explore this protective mechanism, nano fumed silica, nano natural silica, and nanoalumina are used as distinct fillers in a SiR matrix to produce the above mentioned surface deposit. The white deposit is shown in Figure 4.4(b). Each layer of

white dust from the 3 nanofilled composites is analyzed with the SEM and EDAX techniques.

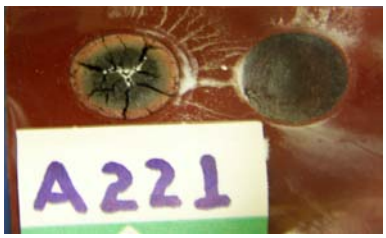

(a) (b)

Figure 4.4 Eroded composites (a) with normal charred surface and after the char is removed (b) with the formation of a white deposit.

The results for the analysis of the white layer are shown in Figure 4.5, Figure 4.6, and Figure 4.7. The compounds used to prepare the composites are silicone rubber (the components of which are Si, O, and CH_3), iron oxide (Fe_2O_3), and three kinds of fillers (fumed SiO_2, natural SiO_2, and Al_2O_3).

In EDAX analysis, the principal elements found in the surface layer of the composites with fumed and natural silica fillers are C, O, and Si. The high level of Si in both composites likely originates from the thermal decomposition of the SiR matrix or from the filler itself. The same elements are found in the composite with nanoalumina along with less than 1% of Al, a minor component in the mixture of the nanofiller. The Al distribution in the layer may also be non-homogeneous, e.g. depleted on the surface. It is important to mention that the white deposit analyzed is on the upper part of the char, so the bulk of char is never analyzed by EDAX. However, iron is not detected in the EDAX analysis; this may be due to the higher density of iron, which is not propelled to the surface in sufficient amount to be detectable by

the EDAX technique. For example, the amount of Al detected was 0.43% while the composite is prepared with 5% of this nanofiller by weight; therefore, the expectation is to obtain iron at a percentage lower than 0.43%, due to the iron oxide concentration of 2.5% by weight used in the composites.

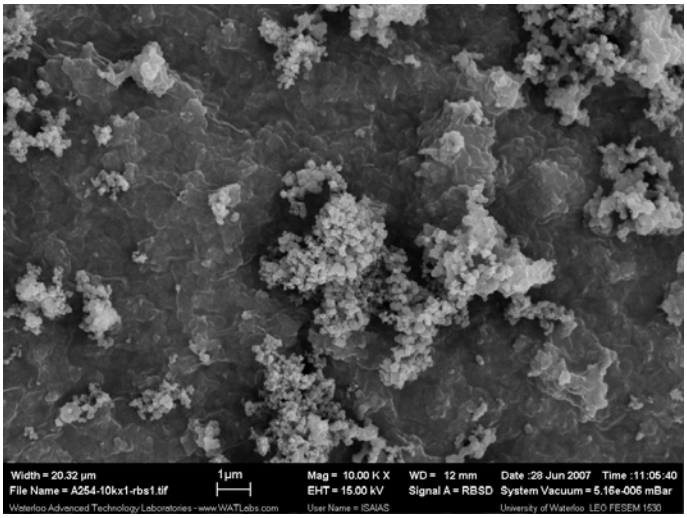

(a)

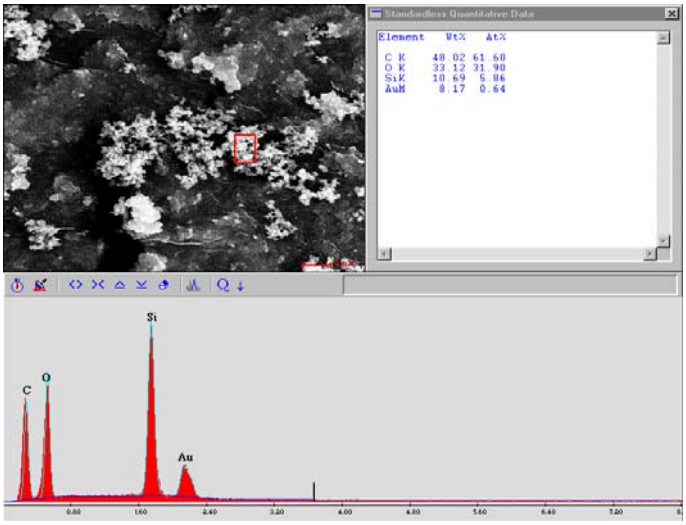

(b)

Figure 4.5 (a) SEM and (b) EDAX analysis of the white deposit obtained in a 2.5%nano fumed silica+51 pph Triton composite.

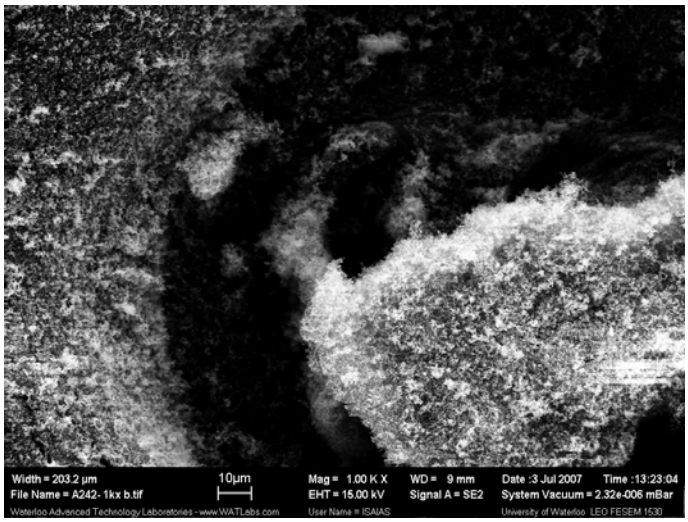

(a)

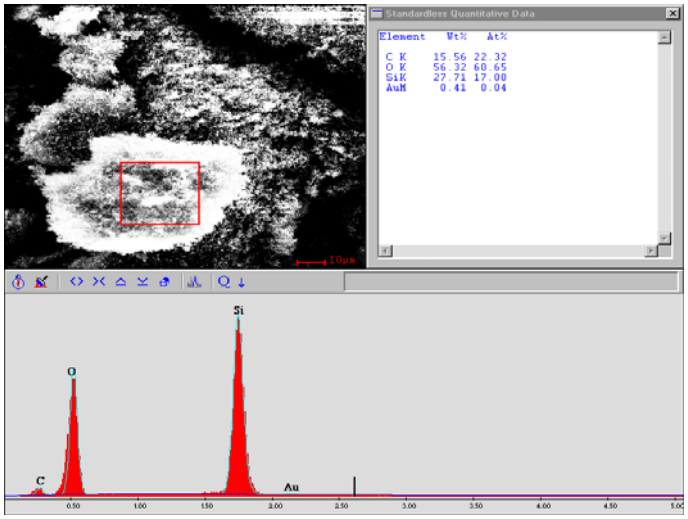

(b)

Figure 4.6 (a) SEM and (b) EDAX analysis for the white deposit obtained in a 5%nano natural silica+78 pph Triton composite.

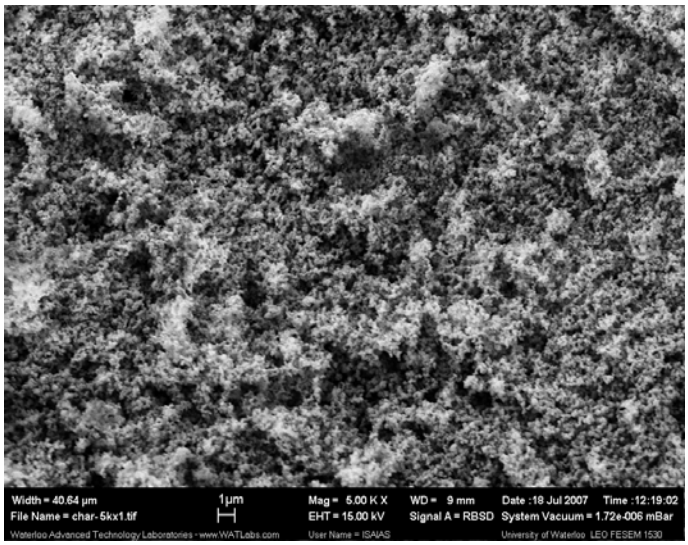

(a)

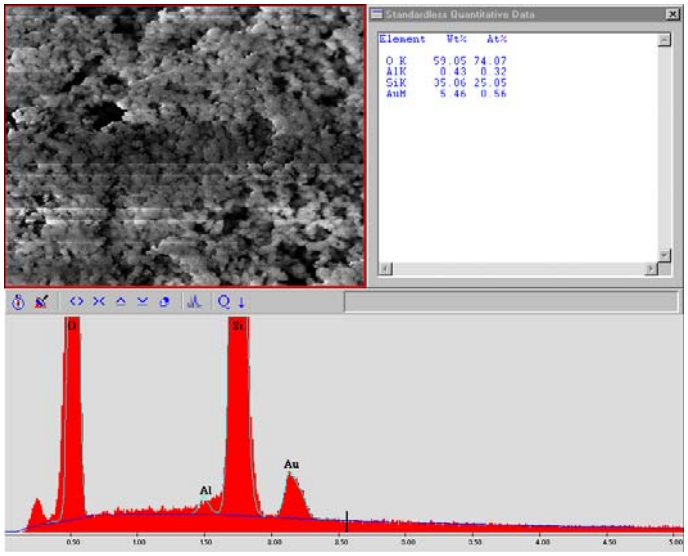

(b)

Figure 4.7 (a) SEM and (b) EDAX analysis for the white deposit obtained in a 5%nanoalumina+156 pph Triton composite.

Due to the low level of Al obtained in EDAX and the undetected Fe for the composite with nanoalumina, XRD analysis is also done. The results in Figure 4.8 show that the main elements and compounds in the white deposit are Al (from the filler), Fe_2O_3 (from the iron

oxide introduced in the composite for absorption of the laser beam), and $Fe+2Al_2O_4$ (possibly from a reaction of the filler and the iron oxide). On the other hand, the analysis of the char presented in Figure 4.9 shows that Al, Al_2O_3, and $Fe_{2.95}Si_{0.05}O_4$ (iron silicon oxide) are the main element and compounds present.

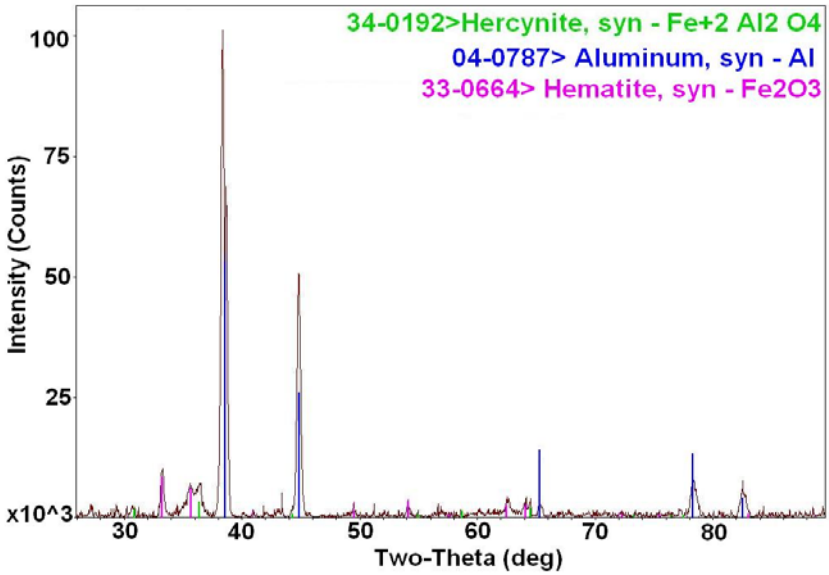

Figure 4.8 XRD test for the white deposit obtained in a 5%nanoalumina+156 pph Triton composite.

XRD analysis confirms that the protective mechanism for the three nanofillers analyzed (fumed silica, natural silica, and alumina) seems to be the same when they are combined with SiR and tested in the laser erosion test. The protective mechanism for the nanocomposites in a silicone rubber matrix during laser ablation or dry band arcing may be as follows. The heated area which undergoes thermal degradation results in the generation and movement of gases from the decomposition of surfactant and polymer, propelling nanofiller to the surface. Volatile species are forced to flow towards the unreacted solid and the already charred region

[80, 81]. When all the volatile materials are removed from the solid, a char layer is formed [82, 83]. The nanofillers tend to accumulate near the surface without sinking through the degraded polymer matrix during the heating process. The formation of a continuous deposit is therefore able to act as a thermal insulator, protecting the material underneath from further decomposition [84, 85, 86].

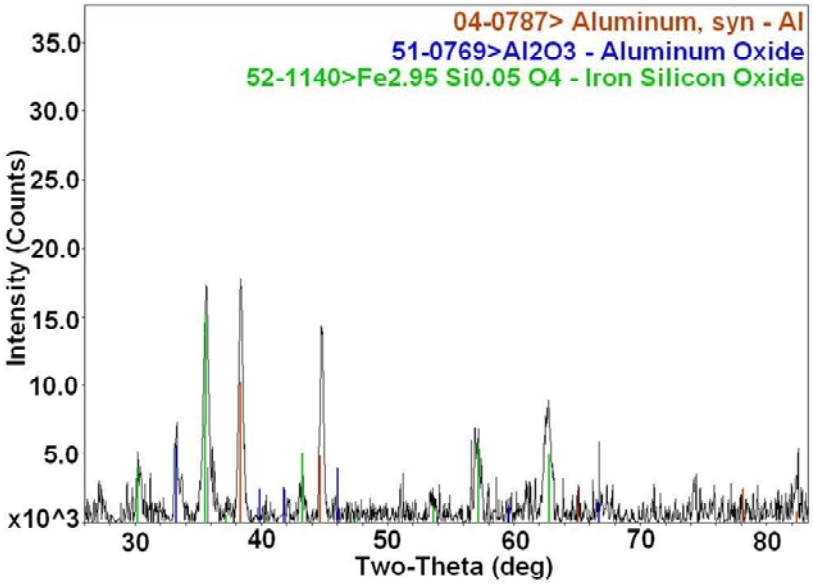

Figure 4.9 XRD test for the char obtained in a 5%nano alumina+156 pph Triton composite.

When the composite is subjected to intense heat from dry band arcing as simulated by infrared laser heating, the impinged region undergoes thermal degradation. When this occurs, it is hypothesized that since the micro-nanofilled composite has twice the number of silanol groups (in a 20%m+2.5%nfs+14 pph T composite); the interactions are presumably caused by hydrogen bonding between the silanol groups of the filler surface and the siloxane linkages in the polymer matrix. This interaction could create a stronger interface between the polymer and the filler making it more resistant to pyrolysis.

4.8 Thermal Conductivity (TC) of Composites

The TC was obtained from the heating and cooling profiles (decay profile) measured with the infrared camera and fitted according to the methodology described in Section 2.5.2. The variation in thermal conductivity for all the evaluated composites is shown in Figure 4.10; a baseline is also plotted to compare the TC of the SiR matrix.

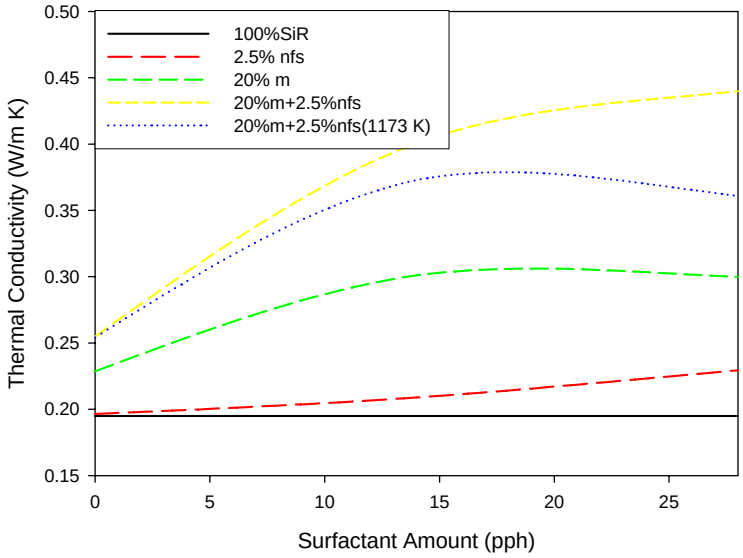

Figure 4.10 Variation in thermal conductivity with the amount of surfactant.

A comparison of the TC based on the ASTM D5470 standard, theoretical models, proposed models, and the values obtained from the decay profile is shown in Table 4.2. From the theoretical and proposed models it is not possible to determine the TC values when surfactant is added in the composite. Also the interactions between the filler, surfactant, and polymer matrix are not included due to limitations in these models. However, with the decay profile methodology it was possible to calculate the TC of the composites.

Table 4.2 Thermal conductivity of composites with different amounts of surfactant including the decay profile method.

Formulation	Thermal conductivity (W/m K)						
	Calculated			Measured	Calculated from Decay Profile		
	Rule of Mixtures	Lewis and Nielsen	Proposed Model	ASTM D5470	Surfactant (pph)		
					0	14	28
2.5%nfs	0.217	0.202	0.202	0.220	0.197	0.209	0.229
20%m	0.309	0.234	0.233	0.280	0.229	0.301	0.300
20%m+2.5%nfs	0.336	*	0.246	0.329	0.255	0.401	0.440
20%m+2.5%nfs+14 pph T	*	*	*	0.330	-	-	-
20%m+2.5%nfs+28 pph T	*	*	*	0.350	-	-	-
20%m+2.5%nfs (1173 K)	*	*	*	**	0.254	0.373	0.361

Notes: * No calculation possible

** Not determined

In all the composites, after the addition of surfactant, the TC measured from the decay profiles increased. This increment in TC is attributed to better dispersion of the filler as determined by the SEM measurements; as suggested in the literature, two different magnifications were used to analyse the filler distribution on macroscopic and microscopic scales. The increase in TC is up to 72% when surfactant is used in composites with micro and nanofillers. If the composite contains only nanofiller and surfactant is added, the increment reached up to 16%. The lower increment in TC for composites with only nanofiller can be due to the weight percentage of nanofiller in the formulation. In theory and according to

Rothon [87], usually 10 to 30% in volume of filler is required to achieve percolation; albeit this depends upon the type, particle size, shape, and the level of dispersion. This could be the reason why the composites with micro and nanofiller reached a higher value of TC.

Chapter 5

Conclusions and Suggestions for Future Work

5.1 Conclusions

In polluted environments, polymeric insulation is prone to surface degradation by tracking and erosion, which lead to failure. Micro fillers are used extensively in polymeric insulation materials for overhead applications to impart erosion resistance under conditions of dry band arcing. Until now, only micro-sized fillers have been used in commercial materials. In contrast, the applications of nanofillers have expanded over the last few years in research fields and some insulating materials have been reinforced; however, the use of nanofillers is not yet widespread. Considerable effort has been expended by many researchers to find a successful way to incorporate nanofillers into outdoor insulation applications.

From a range of studies on nanofiller applications, the main problem encountered in mixing nanoparticle fillers with organic materials is their dispersion. Most researchers agree that uniform mixing and particle dispersion are critical in the development of nanocomposites; otherwise, the properties of the composites are not consistent and their advantage becomes controversial. Also, little research has been done to elucidate the action mechanism of nanofillers in organic matrices. This work has focused on improving the dry band arcing erosion resistance of nanofilled silicone dielectrics, and how nanofillers impart this important characteristic.

The results in this thesis show that surface treatment of nanofillers with a surfactant can be used to improve the dispersion of the nanoparticles in a silicone rubber matrix. Scanning

electron microscopy analysis is used to show how the agglomeration of the nanofiller is diminished, although it is not possible to eliminate all the agglomerates. The reinforcement of organic material with nano fumed silica in a micro-filled composite yields a micro-nanocomposite with significantly improved resistance to heat ablation over compositions with only one or the other filler, particularly when the surfactant Triton is used to disperse the nanofiller. The evaluation of this micro-nanocomposite is done with one non-standard test and two standard tests. In the standard salt fog and inclined plane tests, electrical discharges cause thermal and chemical decomposition of the composite under test. In the non-standard test, a laser simulates the dry band arcing by heating the surface of the composite to around 970 K. All three tests complement each other in evaluating such composites and show improved resistance to heat ablation stemming from (originating from) dry band arcing.

Among the fillers selected for this work, fumed silica is shown to impart greater heat ablation resistance than either natural silica or alumina. There is some difference in the erosion resistance of natural silica- or alumina-filled compositions. However, the selection of the nanofiller and the appropriate surface treatment method is important in terms of compatibility with the host material, in this case silicone rubber.

According to one of the major manufacturers of fumed silica and several published studies, the interactions between the surface of silica and the SiR matrix occur mainly through hydrogen bonding. On this basis, it is shown that nano fumed silica, having 7.5 times more silanol groups than micro silica, a large number of interactions are presumably created between the polymer matrix and the filler. Although this physical interaction is not considered as strong as a chemical bonding, their large number compensates for their lower

strength. The thermal stability of the nanocomposite is likewise weakened as the number of silanol groups on the silica surface is reduced through thermal treatment.

A mechanism is suggested in this thesis by which nanofillers contribute to the erosion resistance of silicone rubber nanocomposites in dry band arcing due to increased thermal conductivity of the composite and to increased thermal stability as a result of the physical interactions between the filler and the matrix. The thermal model developed using COMSOL yielded a temperature distribution in the modelled nanocomposites which is comparable to the temperature distribution measured with an infrared camera under laser heating. A lower temperature in the heating profile is obtained when the composite contains both micro and nanofillers.

In this research SEM, EDAX, and XRD analysis techniques are used to analyze the silicone thermally decomposed after laser heating. The results suggest that one possible protective mechanism for the nanofillers is the formation of a silica layer on the surface that acts as a thermal barrier to protect the underlying material from further decomposition.

Hydrophobicity is the best advantage of SiR insulators to avoid complete wetting, leakage current, and dry band arcing on the surface of the insulation. So, for nanofilled composites including surfactant, hydrophobicity is also a desirable characteristic. Static contact angle measurements on the micro-nano composites show a slight reduction with surfactant, but this is not considered to affect the hydrophobic properties of the composites in the long term, as evident from the improved resistance to erosion. The low level of surfactant necessary for improved filler dispersion is also shown to be insufficient to affect the tensile and hardness properties of the filled composites. In contrast, excessive amounts of surfactant have a negative impact on the mechanical properties.

In summary, the surface treatment of nanofillers with surfactant is a very effective means of improving the dispersion of nanofillers in silicone composites. The reinforcement of a microfilled composite with nanofillers results in a composite more resistant to erosion from dry band arcing. From a commercial point of view, this option adds very little to the cost of the composite for a significant improvement in performance.

5.2 Suggestions for Future Work

It is seen that the dispersion of nanofillers is the key aspect of nanocomposites for improved properties. One type of surface treatment is successfully applied in this thesis but there may be other options for improving dispersion. Uniform dispersion is not easy to quantify, so a methodology to determine the degree of dispersion needs to be further investigated. SEM imaging is used to ascertain the dispersion of fillers qualitatively, but computational algorithms could serve to quantify the degree of dispersion more precisely. This is considered necessary as a tool in order to determine if other options can further improve nanofiller dispersion.

There is a wide variety of surfactants that may further improve dispersion, and there is merit in studying these compositions, for example the Brij surfactants which have a longer alkyl chain. The understanding of the action mechanism of many silicone surfactants still requires investigation, and a study of these surfactants may contribute further to improved nanofiller dispersion.

The understanding, control, and characterization of the nanofiller-matrix interface are the important aspects in nanocomposites, and XPS technique may be able to characterize the composites. By controlling the interface, tailor-made composite materials may be produced.

CHAPTER 5. CONCLUSIONS AND SUGGESTIONS FOR FUTURE WORK

Modelling of the interface between the filler and the insulating matrix should give more accurate values of thermal conductivity, and this may also suggest how to reduce the thermal barrier between the phases. Also, such improved modelling should also allow for a better prediction of the thermal, mechanical, and electrical properties of nanocomposites.

The field evaluation of the developed composites, in the form of actual insulators and at a polluted site, is also necessary to fully demonstrate the advantages of these new micro-nano composites. Finally, there is a need to apply this methodology in an industrial process for other types of materials, for example for heat cured silicone rubber, which is the commonly used material for outdoor insulators, which is indeed a significant challenge.

References

[1] Y. Fukushima and S. Inagaki, “Synthesis of an intercalated compound of montmorillonite and 6-polyamide”, J. Inclusion Phenomena, Vol. 5, pp. 473-482, 1987.

[2] T. J. Lewis, “Interfaces are the dominant feature of dielectrics at the nanometric level”, IEEE Trans. Dielectr. Electr. Insul., Vol. 11, pp. 739-753, 2004.

[3] G. H. Vaillancourt, S. Carignan, and C. Jean, “Experience with the detection of faulty composite insulators on high-voltage power lines by the electric field measurement method”, IEEE Transactions on Power Delivery, Vol. 13, No. 2, pp. 661-666, April 1998.

[4] W. Lynch, *Handbook of Silicone Rubber Fabrication*, Van Nostrand Reinhold, 1978.

[5] ASTM Standard D1418-05, “Standard practice for rubber and rubber latices nomenclature”, Vol. 9-01, pp. 274-276, 2005.

[6] J. P. Reynders, I. R. Jandrell, and S. M. Reynders, “Review of aging and recovery of silicone rubber insulation for outdoor use”, IEEE Transactions on Dielectrics and Electrical Insulation Vol. 6, No. 5, pp. 620-631, October 1999.

[7] R. Hackam, “Outdoor HV composite polymeric insulators”, IEEE Transactions on Dielectrics and Electrical Insulation Vol. 6, No. 5, pp. 557-585, October 1999.

[8] H. Janssen, A. Herden, and H. C. Karner, "The loss and recovery of hydrophobicity on silicone rubber surfaces", Intern. Sympos. High Voltage Eng., (ISH), Montreal, pp. 145-148, 1997.

[9] L. H. Meyer, E. A. Cherney, and S. H. Jayaram, “The role of inorganic fillers in silicone rubber for outdoor insulation-alumina tri-hydrate or silica”, IEEE Electrical Insulation Magazine, Vol. 20, No. 4, pp. 13-21, July/August 2004.

[10] T. Tanaka, “Dielectric nanocomposites with insulating properties”, IEEE Transactions on Dielectrics and Electrical Insulation, Vol. 12, No. 5, pp. 914-928, October 2005.

[11] S. Rätzke and J. Kindersberger, “Erosion behaviour of nanofilled silicone elastomers”, XIVth International Symposium on High Voltage Engineering, Tsinghua University, Beijing, China, pp C-09 1-6, 2005.

[12] L. Lei, W. Xishan, and C. Dengke, “Corona aging tests of RTV and RTV nanocomposite materials”, International Conference on Solid Dielectrics, Toulouse, France, pp. 804-807, 2004.

[13] C. Dengke, Y. J. Hui, W. Xishan, and L. Lei, “Research on characterization of RTV silicone rubber/LS(layered silicate) electrical insulation nanocomposites”, International Conference on Solid Dielectrics, Toulouse, France, Vol. 2, pp. 796-799, 2004.

[14] C. Dengke, W. Xishan, L. Lei, and Y. J. Hui, “Study on RTV silicone rubber/SiO_2 electrical insulation nanocomposites”, International Conference on Solid Dielectrics, Toulouse, France, Vol. 2, pp. 800-803, 2004.

[15] A. H. El-Hag, L. C. Simon, S. H. Jayaram, and E. A. Cherney,, “Erosion resistance of nano-filled silicone rubber”, IEEE Transactions on Dielectrics and Electrical Insulation, Vol. 13, No. 1, pp. 122-128, February 2006.

[16] L. H. Meyer, S. H. L. Cabral, E. Araújo, G. Cardoso, and N. Liesenfeld, “Use of nano-silica in silicone rubber for ceramic insulators coatings in coastal areas”, IEEE International Symposium on Electrical Insulation (ISEI), pp. 474-477, 2006.

[17] P. C. Irwin, Y. Cao, A. Bansal, and L. S. Schadle, “Thermal and mechanical properties of polyimide nanocomposites”, IEEE Conference on Electrical Insulation and Dielectric Phenomena (CEIDP), pp. 120-123, 2003.

[18] N. Fuse, M. Kozako, T. Tanaka, and Y. Ohki, “Effects of mica fillers on dielectric properties of polyamide nanocomposites”, IEEE Conference on Electrical Insulation and Dielectric Phenomena (CEIDP), pp. 148-151, 2005.

[19] T. Imai, F. Sawa, T. Nakano, T. Ozaki, T. Shimizu, M. Kozako, and T. Tanaka, “Effects of nano- and micro-filler mixture on electrical insulation properties of epoxy based composites”, IEEE Trans. Dielectrics and Electrical Insulation, Vol. 13, pp. 319-326, 2006.

[20] T. Imai, G. Komiya, K. Murayama, T. Ozaki, F. Sawa, T. Shimizu, M. Harada, M. Ochi, Y. Ohki, T. Tanaka, "Improving epoxy-based insulating materials with nano-fillers toward practical application", IEEE Conference International Symposium on Electrical Insulation, pp. 201-204, 2008.

[21] M. Roy, J. K. Nelson, L. S. Schadler, C. Zou, and J. C. Fothergill, "The influence of physical and chemical linkage on the properties of nanocomposites", IEEE Conference on Electrical Insulation and Dielectric Phenomena (CEIDP), pp. 183-186, 2005.

[22] S. Singha and M. Joy Thomas "Polymer composite/nanocomposite processing and its effect on the electrical properties", IEEE Conference on Electrical Insulation and Dielectric Phenomena (CEIDP), pp. 557-560, 2006.

[23] D. Wei, R. Dave, and R. Pfeffer, "Mixing and characterization of nanosized powders: an assessment of different techniques", Journal of Nanoparticle Research Vol. 4, pp. 21–41, 2002.

[24] M. Z. Rong, M. Q. Zhang, and W. H. Ruan, "Surface modification of nanoscale fillers for improving properties of polymer nanocomposites: a review", Materials Science and Technology Vol. 22, No. 7, pp. 787-796, 2006.

[25] M. J. Rosen, *Surfactants and Interfacial Phenomena*, Third Edition, Wiley-Interscience, 2004.

[26] K. Holmberg, B. Jönsson, B. Kronberg, and B. Lindman, *Surfactants and Polymers in Aqueous Solution*, John Wiley & Sons, Ltd. 2002.

[27] E. W. Flick, *Industrial Surfactants*, Noyes Publications, Second Edition, 1993.

[28] R. P. Bagwe, L. R. Hilliard, and W. Tan, "Surface modification of silica nanoparticles to reduce aggregation and nonspecific binding", American Chemical Society Vol.22, No. 9, pp. 4357-4362, 2006.

[29] A. Lazzeri, S. M. Zebarjad, M. Pracella, K. Cavalier, and R. Rosa, "Filler toughening of plastics. Part 1 - The effect of surface interactions on physico-mechanical properties and rheological behaviour of ultrafine $CaCO_3$/HDPE nanocomposites", Polymer Vol. 46, pp. 827–844, 2005.

[30] Z. Li, and Y. Zhu, "Surface-modification of SiO_2 nanoparticles with oleic acid", Applied Surface Science. Vol. 211, Issues 1-4, pp. 315–320, April 2003.

[31] S. H. Ahn, S. H. Kim, and S. G. Lee, "Surface-modified silica nanoparticle-reinforced poly(ethylene 2,6-naphthalate)", Journal of Applied Polymer Science, Vol. 94, pp. 812-818, 2004.

[32] W. W. Kubiak, and E. Niewiara, “Influence of the electrolyte on Triton X-100 adsorption on fumed silica”, Electroanalysis, No. 17, pp. 1169-1175, Wiley-VCH, 2002.

[33] L. T. Zhuravlev, “The surface chemistry of amorphous silica. Zhuravlev model”, Colloids and Surfaces A: Physico chemical and Engineering Aspects Vol. 173, No. 1, pp. 1–38, 2000.

[34] H. Barthel, L. Roesch, J. Weis, “Fumed silica - production, properties, and applications”, Publisher: VCH, Organosilicon Chemistry II: From Molecules to Materials, pp. 761-778, Munich, 1994.

[35] G. Wypych, *Handbook of Fillers*, 2nd Edition, ChemTec Publishing, 2000.

[36] T. Imai, F. Sawa, T. Nakano, T. Ozaki, T. Shimizu, M. Kozako, and T. Tanaka, “Effects of nano- and micro-filler mixture on electrical insulation properties of epoxy based composites”, IEEE Transactions on Dielectrics and Electrical Insulation Vol. 13, No. 1; pp. 319-326, February 2006.

[37] M. F. Fréchette and C. W. Reed, “The emerging field of nanodielectrics: an annotated appreciation”, IEEE International Symposium on Electrical Insulation, pp. 458-465, 2006.

[38] Degussa, “Successful use of Aerosil® fumed silica in liquid systems”, Technical Information No. 1279, March 2006.

[39] H. E. Bergna and W. O. Roberts, *Colloidal Silica Fundamentals and Applications*, Surfactant Science Series Volume 131, 2006.

[40] ASTM Standard D2303, ‘‘Standard test method for liquid-contaminant, inclined plane tracking and erosion of insulating materials’’, 2004.

[41] L. H. Meyer, S. Jayaram, and E. A.Cherney, “A novel technique to evaluate the erosion resistance of silicone rubber composites for high voltage outdoor insulation using infrared laser erosion”, IEEE Transactions on Dielectrics and Electrical Insulation Vol. 12, No. 6 pp. 1201-1208, December 2005.

[42] L. H. Meyer, S. Jayaram, and E. A. Cherney, “Thermal conductivity of filled silicone rubber and its relationship to erosion resistance in the inclined plane test”, IEEE Transactions on Dielectrics and Electrical Insulation Vol. 11, No. 4 pp. 620-630, August 2004.

[43] E. A. Cherney, “Silicone rubber dielectrics modified by inorganic fillers for outdoor high voltage insulation applications”, IEEE Transactions on Dielectrics and Electrical Insulation, Vol. 12, No. 6, pp. 1108-1115, December 2005.

[44] M. J. Billings, L. Warren, and R. Wilkins, “Thermal erosion of electrical insulating materials”, IEEE Transactions on Electrical Insulation, Vol. 6 pp. 82-90, 1971.

[45] IEC 60507, “Artificial pollution tests on high-voltage insulators to be used on a.c. Systems”, Second Edition 04-1991.

[46] IEC 61109, “Composite insulators for a.c. overhead lines with a nominal voltage greater than 1000 V - Definitions, test methods and acceptance criteria”, Edition 1.0 , March 1992.

[47] J. Seo, L. P. Lee, “Effects on wettability by surfactant accumulation/depletion in bulk polydimethylsiloxane (PDMS)”, Elsevier B. V., Sensors and Actuators B 119, pp 192–198, 2006.

[48] ASTM D1708-06a, “Standard test method for tensile properties of plastics by use of microtensile specimens”, 2006.

[49] ASTM D2240-05, “Standard test method for rubber property - durometer hardness”, 2005.

[50] Y. Kimata, S. Nakagawa and H. Kato, “Measurement of concentration of silanol group”, Japan Kokai Tokyo Koho JP 2001208683, 5 pp., 2001 (in Japanese).

[51] ASTM D5470 “Standard test method for thermal transmission properties of thermally conductive electrical insulation materials”, 2006.

[52] E. A. Cherney, "Silicone rubber dielectrics modified by inorganic fillers for outdoor high voltage insulation applications," , IEEE Transactions on Dielectrics and Electrical Insulation, Vol. 12, No. 6, pp. 1108-1115, Dec. 2005.

[53] R. C. Progelhof, J. L. Throne and R. R. Ruetsch, “Methods for predicting the thermal conductivity of composite systems: a review”, Polymer Engineering and Science, Vol. 16, pp. 615-625, 1976.

[54] P. Karayacoubian, M. M. Yovanovich, J. R. Culham, "Thermal resistance-based bounds for the effective conductivity of composite thermal interface materials," IEEE Twenty-Second Annual Semiconductor Thermal Measurement and Management Symposium, pp. 28-36, 2006.

[55] N. Araki, D. W. Tang, A. Makino, M. Hashimoto, T. Sano, "Transient characteristics of thermal conduction in dispersed composites", International Journal of Thermophysics, Vol. 19, No. 4, pp. 1239-1251, July 1998.

[56] COMSOL Multiphysics^{TM}, "User's guide of the heat transfer module", Version 3.4, October 2007.

[57] L. S. Mayboudi, A. M. Birk, G. Zak, and P. J. Bates, "Laser transmission welding of a lap-joint: thermal imaging observations and three–dimensional finite element modeling", Journal of Heat Transfer, Vol. 129, pp. 1177-1186, September 2007.

[58] M. F. Fréchette, R. Y. Larocque, M. Trudeau, R. Veillette, R. Rioux, S. Pélissou, S. Besner, M. Javan, K. Cole, M.-T. Ton That, D. Desgagnés, J. Castellon, S. Agnel, A. Toureille, and G. Platbrood, "Nanostructured polymer microcomposites: a distinct class of insulating materials", IEEE Transactions on Dielectrics and Electrical Insulation Vol. 15, No. 1, pp. 90-105, February 2008.

[59] T. Kashiwagi, J. W. Gilman, K. M. Butler, R. H. Harris, J. R. Shields, and A. Asano, "Flame retardant mechanism of silica gel/silica", Fire and Materials Vol. 24, pp. 277-289, 2000.

[60] G. Camino, S. M. Lomakin, and M. Lazzari, "Polydimethylsiloxane thermal degradation Part 1. Kinetic aspects", Polymer, Vol. 42, pp. 2395–2402, 2001.

[61] G. Camino, S. M. Lomakin, M. Lageard, "Thermal polydimethylsiloxane degradation. Part 2. The degradation mechanisms", Polymer 43, pp. 2011–2015, 2002.

[62] E. Papirer, Editor, *Adsorption on Silica Surfaces*, Surfactant Science Series, Vol. 90, 2000.

[63] L. Dewimille, B. Bresson and L. Bokobza, "Synthesis, structure and morphology of poly(dimethylsiloxane) networks filled with in situ generated silica particles", Polymer, Vol. 46, pp 4135–4143, 2005.

[64] E. F. Vansant, P. V. D. Voort, and K. C. Vrancken, "Characterization and chemical modification of the silica surface", Elsevier Science, Vol. 93, pp. 65-94, 1995.

[65] R. S. Pandurangi, M. S. Seehra, B. L. Razzaboni, and P. Bolsaitis, "Surface and bulk infrared modes of crystalline and amorphous silica particles: a study of the relation of surface structure to cytotoxicity of respirable silica", Environmental Health Perspectives Vol. 86, pp. 327-336, 1990.

[66] B. C. Smith, *Quantitative Spectroscopy: Theory and Practice*, Academic Press 2002.

[67] J. P. Cohen, L. Dujourdy, "Silica concentration dependence of the kinetics of polydimethylsiloxane adsorption on aggregates", Polymer Bulletin 41, pp. 253–260, Springer-Verlag 1998.

[68] J. K. Nelson and Y Hu, "Nanocomposite dielectrics-properties and implications", Journal of Physics D: Applied Physics Vol. 38, pp. 213-222, 2005.

[69] G. B. Sohoni and J. E. Mark, "Thermal stability of in situ filled siloxane elastomers", J. Appl. Polymer Sci., Vol. 45, pp. 1763-1765, 1992.

[70] J. E. Mark, Editor, *Physical Properties of Polymers Handbook*, 2007.

[71] J. S. Smith, O. Borodin, G. D. Smith, E. M. Kober, "A molecular dynamics simulation and quantum chemistry study of poly(dimethylsiloxane)–silica nanoparticle interactions", Journal of Polymer Science: Part B: Polymer Physics, Volume 45, pp. 1599–1615, 2007.

[72] S. Selimovic, S. M. Maynard, and Y. Hu, "Aging effects of precipitated silica in poly(dimethylsiloxane)", Journal of Rheology Vol. 51, No. 3, pp. 325-340, May/June 2007.

[73] D. M. Nevskaia, M. L. Rojas C., A. Guerrero R., and J. de D. López G., "Interaction of Triton X-100 on silica: a relationship between surface characteristics and adsorption Isotherms", J. Chem. Tech. Biotechnol. Vol. 63, pp. 249-256, 1995.

[74] H. Barthel, K. Nikitina, "Interactions and chemical reactions of polydimethylsiloxanes with fumed silica fillers", American Chemical Society, Rubber Expo 2001, pp. 2028-2065, Cleveland, OH, United States, 2001.

[75] P. B. Leng, H. M. Akil, and O. H. Lin, "Thermal properties of microsilica and nanosilica filled polypropylene composite with epoxy as dispersing aid", Journal of Reinforced Plastics and Composites, Vol. 26, No. 8, pp. 761-770, 2007.

[76] Cohen J. *Statistical Power Analysis for the Behavioural Sciences*", 2nd edition, Hillsdale, N. J., Erlbaum, 1988.

[77] J. P. Cohen-Addad, C. Roby, and M. Sauviat, "Characterization of chain binding to filler in silicone-silica systems", Polymer Vol. 26, pp. 1231-1233, August 1985.

[78] J. K. Nelson and J. C. Fothergill, "Internal charge behaviour of nanocomposites", Institute of Physics Publishing, Nanotechnology, Vol. 15 pp. 586-595, 2004.

[79] G. Tsagaropoulos and A. Eisenberg, "Dynamic mechanical study of the factors affecting the two glass transition behavior of filled polymers. Similarities and differences with random ionomers", Macromolecules, Vol. 28, pp. 6067-6077, August 1, 1995.

[80] M. Bartholmai and B. Schartel, "Layered silicate polymer nanocomposites: new approach or illusion for fire retardancy: investigations of the potentials and the tasks using a model system", Polym. Adv. Technol., Vol. 15, pp. 355–364, 2004.

[81] *Encyclopedia of Polymer Science and Technology*, John Wiley&Sons, Inc. 2005.

[82] K. Hayashida, S. Tsuge, H. Ohtani, "Flame retardant mechanism of polydimethylsiloxane material containing platinum compound studied by analytical pyrolysis techniques and alkaline hydrolysis gas chromatography", Polymer Vol. 44, pp. 5611–5616, 2003.

[83] C. D. Blasi, "Modelling and simulation of combustion processes of charring and non-charring solid fuels", Prog. Energy Combust. Sci., Vol. 19, pp. 71-104, 1993.

[84] J. Mansouri, R. P. Burford, Y. B. Cheng, "Pyrolysis behaviour of silicone-based ceramifying composites", Materials Science and Engineering A425, pp. 7–14, 2006.

[85] M. Kozako, N. Fuse, Y. Ohki, T. Okamoto and T. Tanaka, "Surface degradation of polyamide nanocomposites caused by partial discharges using IEC (b) electrodes", IEEE Transactions on Dielectrics and Electrical Insulation Vol. 11, No. 5, pp. 833-839, October 2004.

[86] B. Schartel, M. Bartholmai, and U. Knoll, "Some comments on the main fire retardancy mechanisms in polymer nanocomposites", Polym. Adv. Technol. Vol. 17, pp. 772–777, 2006.

[87] Roger N. Rothon, Editor, *Particulate-Filled Polymer Composites*, 1st Edition, Rapra Technology Limited, 2003.

Appendix A

Influence of Amount of Surfactant in a Improved Dispersion

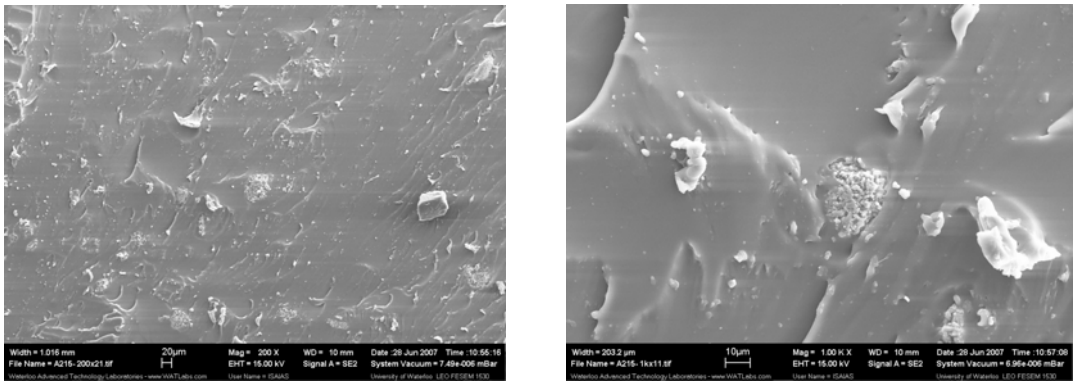

Figure A.1 Effect of Triton surfactant in composites containing 2.5% by weight nano Al_2O_3 + 97.5% SiR + 0 pph of Triton (magnification 200 x and 1000 x accordingly).

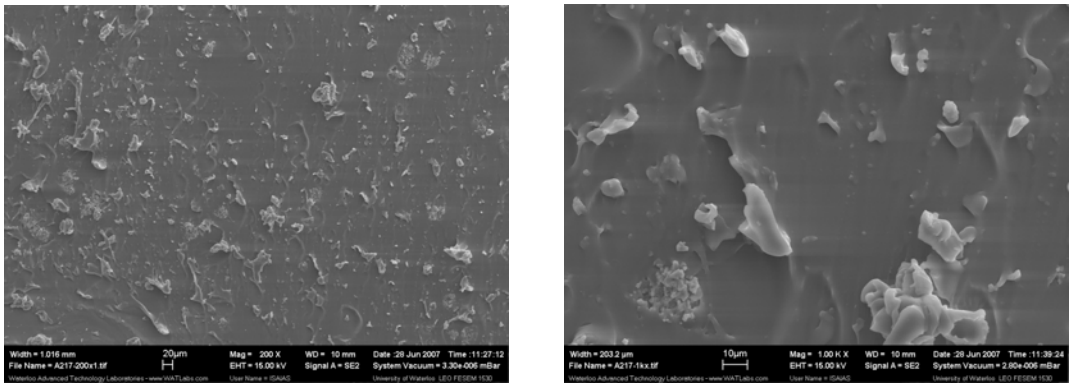

Figure A.2 Effect of Triton surfactant in composites containing 2.5% by weight nano Al_2O_3 + 97.5% SiR + 14 pph of Triton (magnification 200 x and 1000 x accordingly).

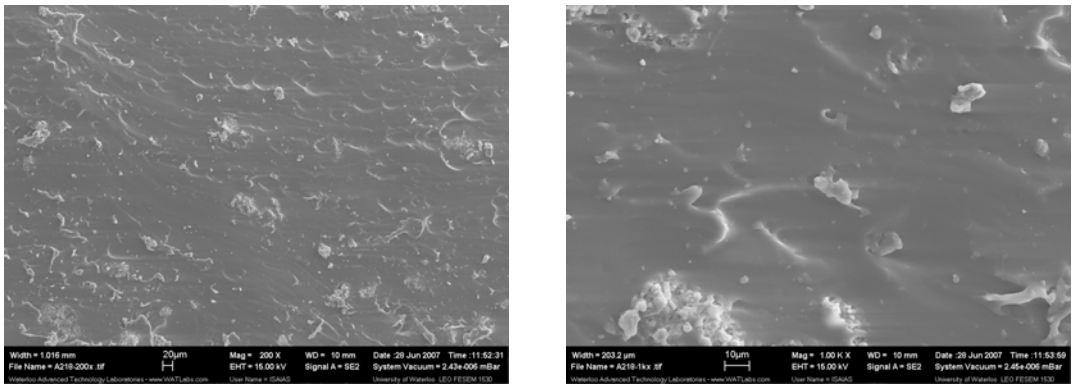

Figure A.3 Effect of Triton surfactant in composites containing 2.5% by weight nano Al_2O_3 + 97.5% SiR + 21 pph of Triton (magnification 200 x and 1000 x accordingly).

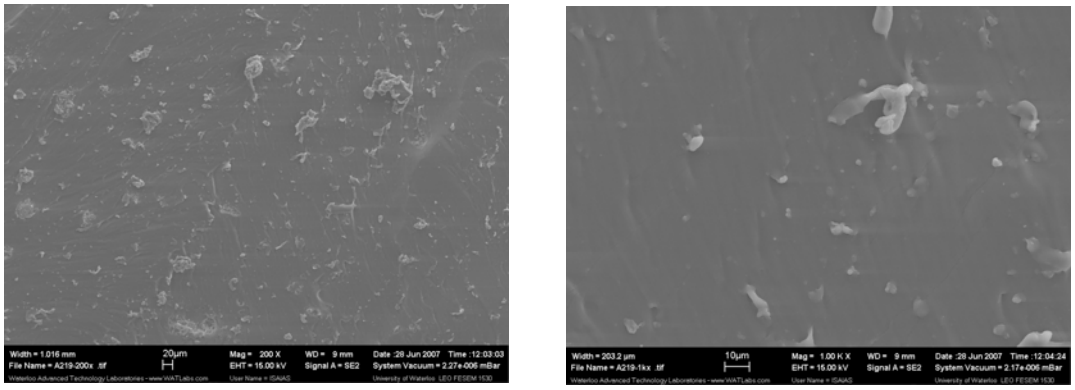

Figure A.4 Effect of Triton surfactant in composites containing 2.5% by weight nano Al_2O_3 + 97.5% SiR + 27 pph of Triton (magnification 200 x and 1000 x accordingly).

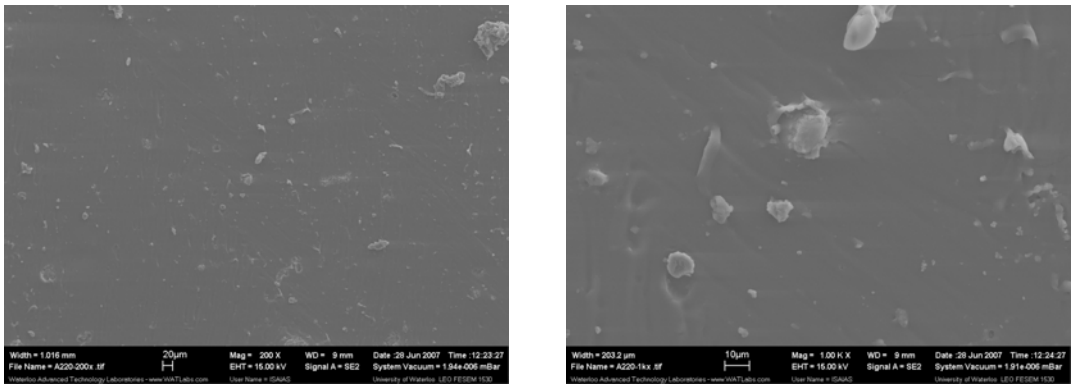

Figure A.5 Effect of Triton surfactant in composites containing 2.5% by weight nano Al_2O_3 + 97.5% SiR + 33 pph of Triton (magnification 200 x and 1000 x accordingly).

APPENDIX A

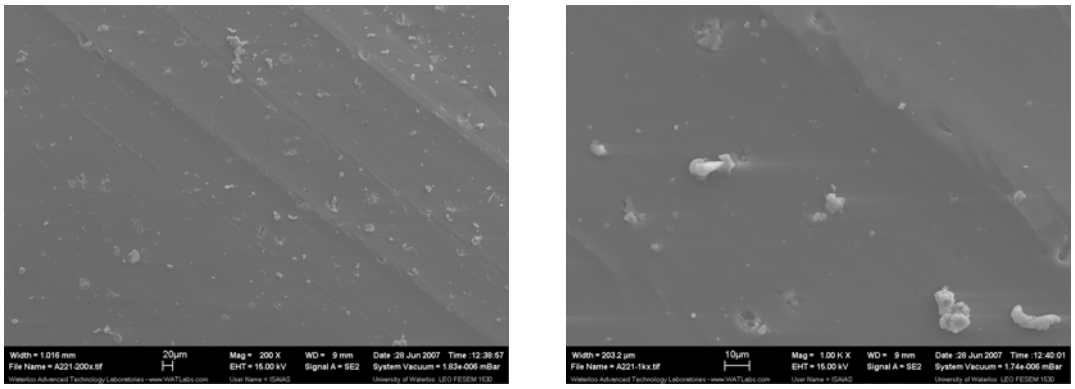

Figure A.6 Effect of Triton surfactant in composites containing 2.5% by weight nano Al_2O_3 + 97.5% SiR + 51 pph of Triton (magnification 200 x and 1000 x accordingly).

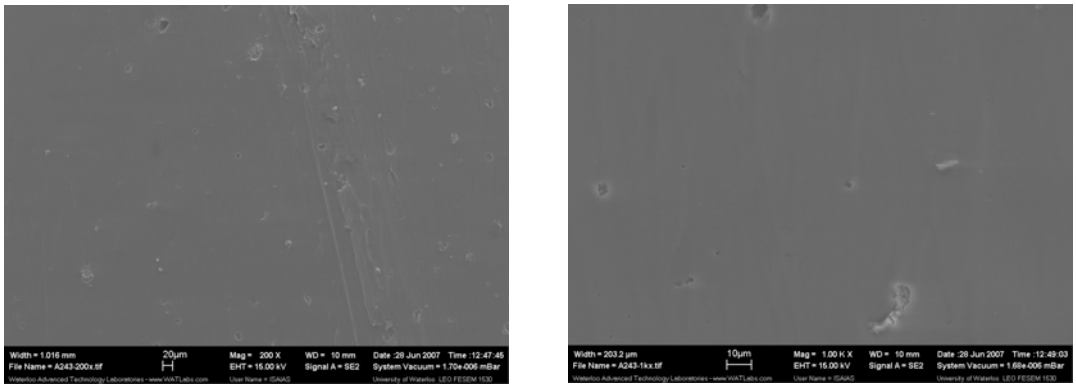

Figure A.7 Effect of Triton surfactant in composites containing 2.5% by weight nano Al_2O_3 + 97.5% SiR + 79 pph of Triton (magnification 200 x and 1000 x accordingly).

Appendix B

Experimental TC based on Temperature Profile Measurements with Infrared Camera

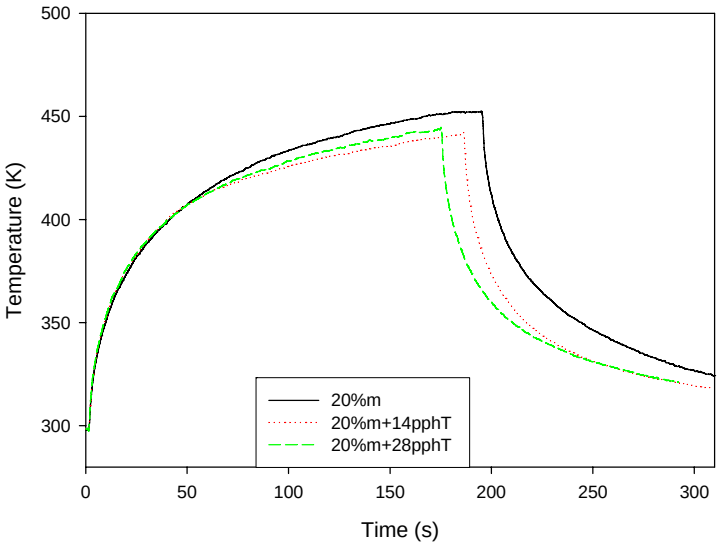

Figure B.1 Temperature profile during laser test for composites 20%m with 14 pph and 28 pph of surfactant.

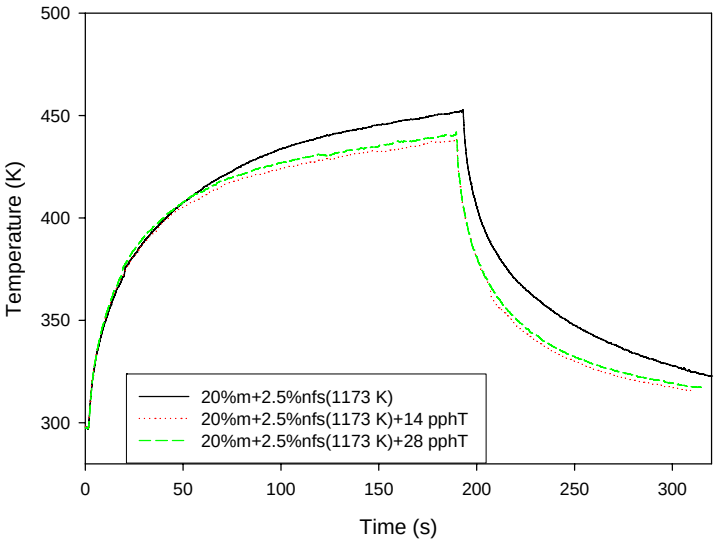

Figure B.2 Temperature profile during laser test for composites 20%m+2.5%nfs (1173 K) with 14 pph and 28 pph of surfactant.

APPENDIX B

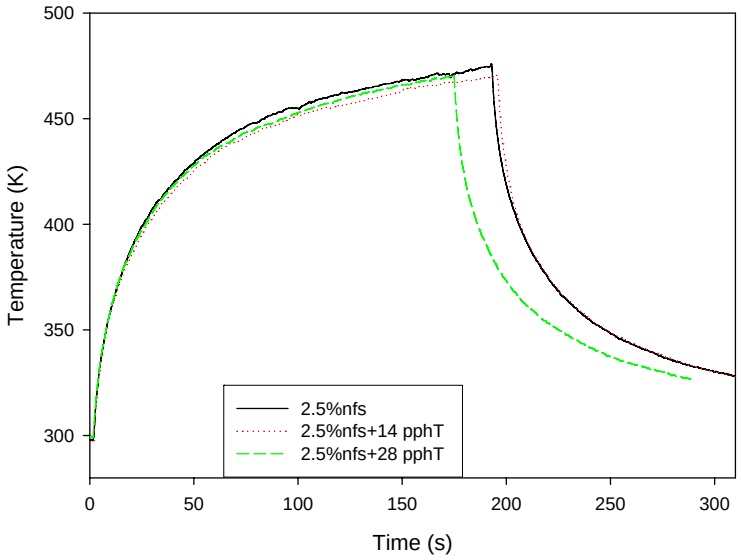

Figure B.3 Temperature profile during laser test for composites 2.5%nfs with 14 pph and 28 pph of surfactant.

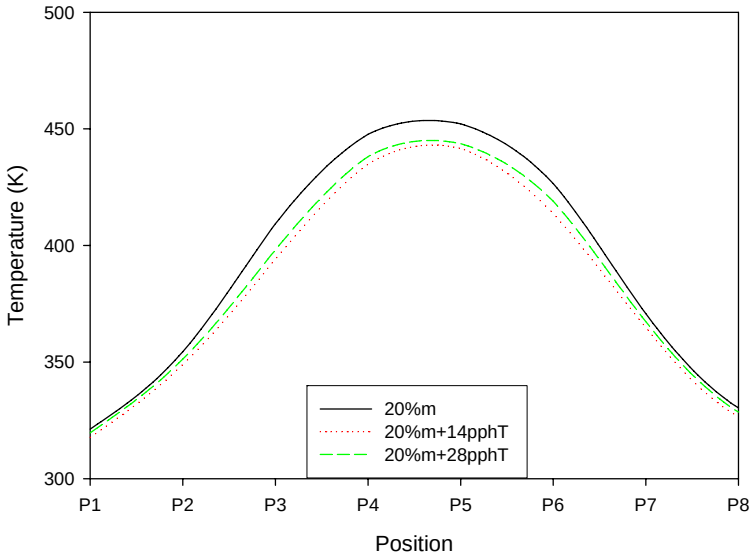

Figure B.4 Maximum temperature across a line passing through the center of the composites 20%m without and with 2 different amounts of surfactant.

APPENDIX B

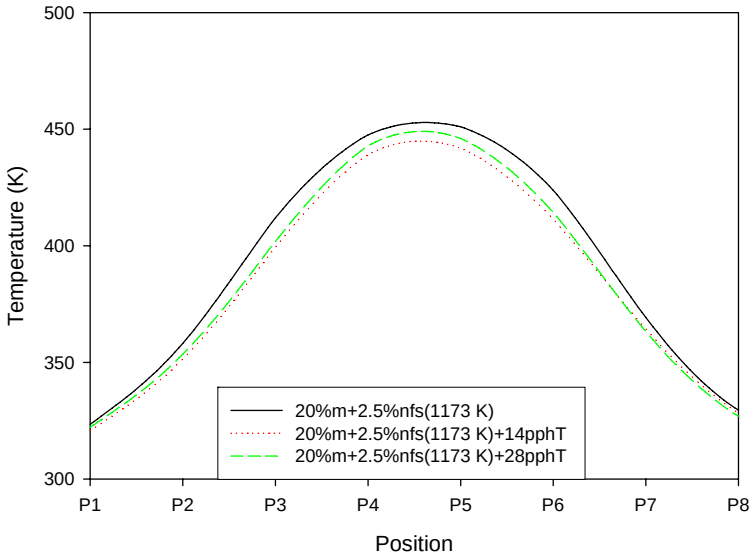

Figure B.5 Maximum temperature across a line passing through the center of the composites 20%m+2.5%nfs(1173 K) without and with 2 different amounts of surfactant.

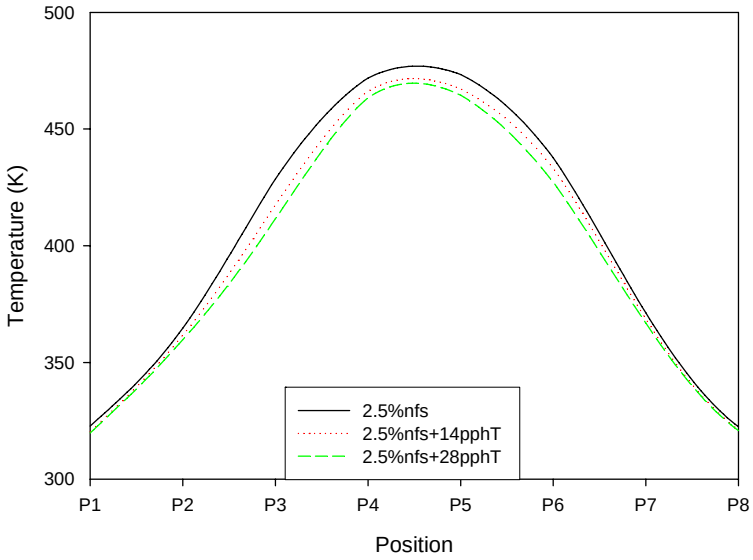

Figure B.6 Maximum temperature across a line passing through the center of the composites 2.5%nfs without and with 2 different amounts of surfactant.